Reviews

Normal Alkanes, Multialkane Synthetic Model Mixtures, and Real Petroleum Waxes: Crystallographic Structures, Thermodynamic Properties, and Crystallization

Michel Dirand,* Mohammed Bouroukba, Virginie Chevallier, and Dominique Petitjean

Laboratoire de Thermodynamique des Milieux Polyphasés EA n° 3099, Ecole Nationale Supérieure des Industries Chimiques, Institut National Polytechnique de Lorraine, 1, rue Grandville, BP 451, F-54001 Nancy Cedex, France

Emmanuel Behar and Véronique Ruffier-Meray

Institut Français du Pétrole, 1 et 4 avenue de Bois Préau, BP 311, F-92506 Rueil-Malmaison, France

A general review is presented concerning jointly the crystallographic structures and the solid−solid and solid−liquid transition temperatures and enthalpies in the pure normal alkanes, as well as the structural and thermodynamic behavior of their synthetic binary, ternary, and multinary model mixtures and of real petroleum waxes. A major part of the structural and thermodynamic data of the literature, relative to the pure *n*-alkanes, are listed from methane up to the alkane with carbon atom number equal to 390. Variation relationships of the crystallographic long *c*-parameter that corresponds to the periodicity of the molecule layer packing along their axis, melting temperatures, and transition enthalpies are given as a function of the carbon atom number. The study of the literature on the *n*-alkane mixtures highlights the existence of isostructural binary, ternary, and multinary intermediate solid solutions which can be likened to a single pseudocomponent. This intermediate solid solution is equivalent to a hypothetical pure *n*-alkane whose carbon atom number is equal to the average carbon atom number of the mixtures. As a result, the solubility of these multinary solid solutions or real multiparaffinic waxes in linear, cyclic, or aromatic light solvents is identical to that of the pure *n*-alkanes: pseudobinary eutectic crystallization of the model or real wax as a single pseudocomponent on one hand and the light solvent on the other hand.

1. Introduction

The formation of solid deposits in the fluids of crude oils and of the middle distillate fuels poses a constantly recurring problem in the petroleum industry (extraction, transportation through the pipelines, refining process, etc). Solid deposits, which block pipelines and filters, are a major issue in the damages of industrial equipment and of diesel motors in the very cold regions.

To solve these problems, it is essential to represent and predict the thermodynamic behavior of phases of crude oils, especially that of the solid deposits.

As a result, the understanding and knowledge of the structural behavior, the thermodynamic properties, the solid−solid and solid−liquid equilibria of pure normal alkanes as well as their binary, ternary, and multinary mixtures, and their solubilities in organic solvents are necessary to characterize the state of these solid deposits, which consist of high molecular weight saturated hydrocarbons, predominantly consecutive paraffins.

The structure of the pure normal alkanes (hereafter denoted by C_n) has been the subject of several articles in the literature.[1−86] In the solid state, the stable configuration of the molecules corresponds to the *all-trans* conformation of the *zigzag* type.[1−5] This description was made possible thanks to the structural studies of Müller and Saville[5] and Müller,[6] who were the first to determine the structure of C_n's, particularly that of C_{29}:[7] these authors[5,8] also highlighted the C_n polymorphism as a function of temperature.

Since then, the crystalline structures,[10−86] as well as the thermodynamic data of pure C_n's[87−140] and of the synthetic model mixtures consisting of two, three, four or five C_n's,[26,41,42,44,59,66,123,133,141−196] have been the subject of numerous publications. The literature results, obtained before 1960, have been reviewed by Mnyukh,[3] an exhaustive bibliography of the papers previous to 1971 has been presented by Turner,[53] the structural parameters of pure C_n's have been given by Heyding et al.,[24] and the monograph of Srivastava et al.[54] concerns more particularly the C_n polymorphism.

As the crystallization of normal paraffin hydrocarbons in the middle distillate fuels and in petroleum cuts is of significant interest in petroleum technologies, studies have been carried out on the solubilities of pure C_n's and of their

* Corresponding author. Telephone: 03.83.17.50.07. Fax: 03.83.17.50.76. E-mail: mdirand@ensic.u-nancy.fr.

10.1021/je0100084 CCC: $22.00
Published on Web 01/15/2002

synthetic mixtures in organic solvents[121,168,197−216] and on the structural and thermodynamic properties of model and real multicomponent paraffin waxes in order to seek adequate thermodynamic models to represent the behavior of petroleum cuts.[23,76,77,217−248]

The aim of this review is to summarize current findings in the literature and to give complementary results obtained in recent years.

2. Pure *n*-Alkanes

(A) Crystalline Structures at Low Temperatures. The ordered crystalline structures at *"low temperatures"* are described (authors, purity, origin, X-ray method, space group, and crystalline parameters) in Appendix 1 in the Supporting Information. Craig et al.[29] determined the unit-cell crystallographic parameters of the homologous series C_{13}−C_{60} which were derived from high-resolution synchrotron X-ray powder diffraction, and they propose the following classification with the *key structures* defined by Nyburg and Potworowski:[73]

odd-numbered C_{2p+1}'s:

$13 \leq 2p + 1 \leq 41$: "C_{23}−*Pbcm*" orthorhombic structure described by Smith[13,143]

even-numbered C_{2p}'s:

$14 \leq 2p \leq 26$: "C_{18}−$P\bar{1}$" triclinic structure described by Müller and Lonsdale[9] and Nyburg et al.[20,73]

$28 \leq 2p \leq 36$: "C_{36}−$P2_1/a$" monoclinic structure, described by Shearer and Vand[15]

$2p = 38$, 40, and 44: *Pbca* orthorhombic structure determined by Boistelle et al.[22]

$2p = 46$, 50, and 60: "C_{36}−$Pca2_1$" orthorhombic structure determined by Shearer and Vand[15] and Teare[17]

According to Boistelle et al.[22] and Craig et al.,[29] the *Pbca* orthorhombic structure corresponds to a stacking of alternate monoclinic layers, related one to the other by a 2-fold axis perpendicular to the (*00l*) planes.

The layouts of molecules in the crystalline unit-cells of the *key structures* C_{18}−$P\bar{1}$, C_{23}−*Pbcm*, and C_{36}−$Pca2_1$ defined by Nyburg and Potworowski[73] are shown in Figures 1−3, respectively.

Pbcm, $P\bar{1}$, $P2_1/a$, *Pbca*, and $Pca2_1$ correspond to space group notations of the *International Tables for Crystallography*.[249]

(B) Correlations between the Crystalline Long c-Parameter and the Number of Carbon Atoms of Pure n-Alkanes. Müller and Saville[5] observed that the experimental first X-ray long spacing, that corresponds to the higher values of the crystallographic plane equidistances, increases linearly as a function of the n_c carbon atom number: the numerical value of this increase is close to 1.3 Å per carbon atom. From the results of Bunn,[1] Müller,[6] Hengstenberg,[11] Kohlhaas,[12] and his own experiments, Teare[17] gave the value of 1.270 ± 0.01 Å for this increase, which corresponds to the carbon−carbon distance projected onto the chain axis.

Then Broadhurst[19] analyzed the solid phase behavior of C_n's and established a relationship between the crystalline *c*-parameters of the orthorhombic structures of the C_n's and their n_c carbon atom numbers (Table 1).

Later, Nyburg and Potworowski[73] predicted laws of linear variation of the *c*-parameter (Table 1) from *Z* coordinates of carbon atoms in "key structures".

(1) Pbcm Orthorhombic Structures of Odd-Numbered n-Alkanes. From the accurate and self-consistent data of Craig et al.,[29] Chevallier et al.[75] have established linear equations (Table 1) of the variation of *c*-parameters as a function of the n_c carbon atom number by linear least-squares fitting, particularly for the orthorhombic C_{2p+1}'s, in the range C_{13}−C_{41}, crystallizing with the C_{23}−*Pbcm key structure*[29] with an excellent factor of correlation $R^2 = 1$ (Figure 4):

$$(c/\text{Å})/2 = 1.2724n_c + 1.8752$$

or

$$c/\text{Å} = 2.5448n_c + 3.7504$$

This expression for the *c*-parameter fully verifies the predictions of Nyburg and Potworowski[73] for the C_{2p+1} *Pbcm* structures (Table 1).

The *c*/2 value of the orthorhombic unit-cell which corresponds to the *d*(002) experimental first X-ray long spacing represents the sum of the chain lengths of the carbon atoms and of the gaps between the planes of end methyl group (−CH_3) carbon atoms of two consecutive molecule layers (Figure 2). The slope of the linear equation represents the chain length increase per carbon atom, and it is equal to the average carbon−carbon distance projected onto the chain axis according to Teare.[17] For a chain with a n_c carbon atom number, there are (n_c − 1) carbon−carbon distances and it is possible to write the previous *c*/2 equation as follows:

$$(c/\text{Å})/2 = 1.2724(n_c - 1) + 3.1476$$

with

(i) 1.2724(n_c − 1): chain length/Å of n_c carbon atoms

and

(ii) 3.1476 Å: gap value between the planes of end methyl group carbon atoms of two consecutive molecule layers

Moreover, the gap can be calculated from the *Z* coordinates of the end group carbon atoms of two consecutive chains, which are respectively equal to 1.573 and −1.573 Å in the C_{23} *Pbcm key structure*, as determined by Smith[13] and Nyburg and Potworowski:[73] for this structure, the gap is equal to 3.146 Å. This value is very close to the one obtained from the previous equation.

The other higher C_{2p+1}'s (C_{31}, C_{37}, C_{45}, C_{61}, and C_{69}) also crystallize in the C_{23}−*Pbcm key structure* according to ref 64.

(2) Triclinic, Monoclinic, and Orthorhombic Structures of Even-Numbered n-Alkanes. For the triclinic ($P\bar{1}$: $n_c \leqslant 26$), monoclinic ($P2_1/a$: $28 \leqslant n_c \leqslant 36$), and orthorhombic (*Pbca*: n_c = 38, 40, and 44) structures of C_{2p}'s[29] the experimental first X-ray long spacing has a lower value than that in the *Pbcm* orthorhombic structure of C_{2p+1}'s because of the incline of the molecules (Figure 1). This value varies linearly as a function of the carbon atom n_c number (Figure 4) on lines situated below the line representing the variations of the *c*/2 parameter or d(002)

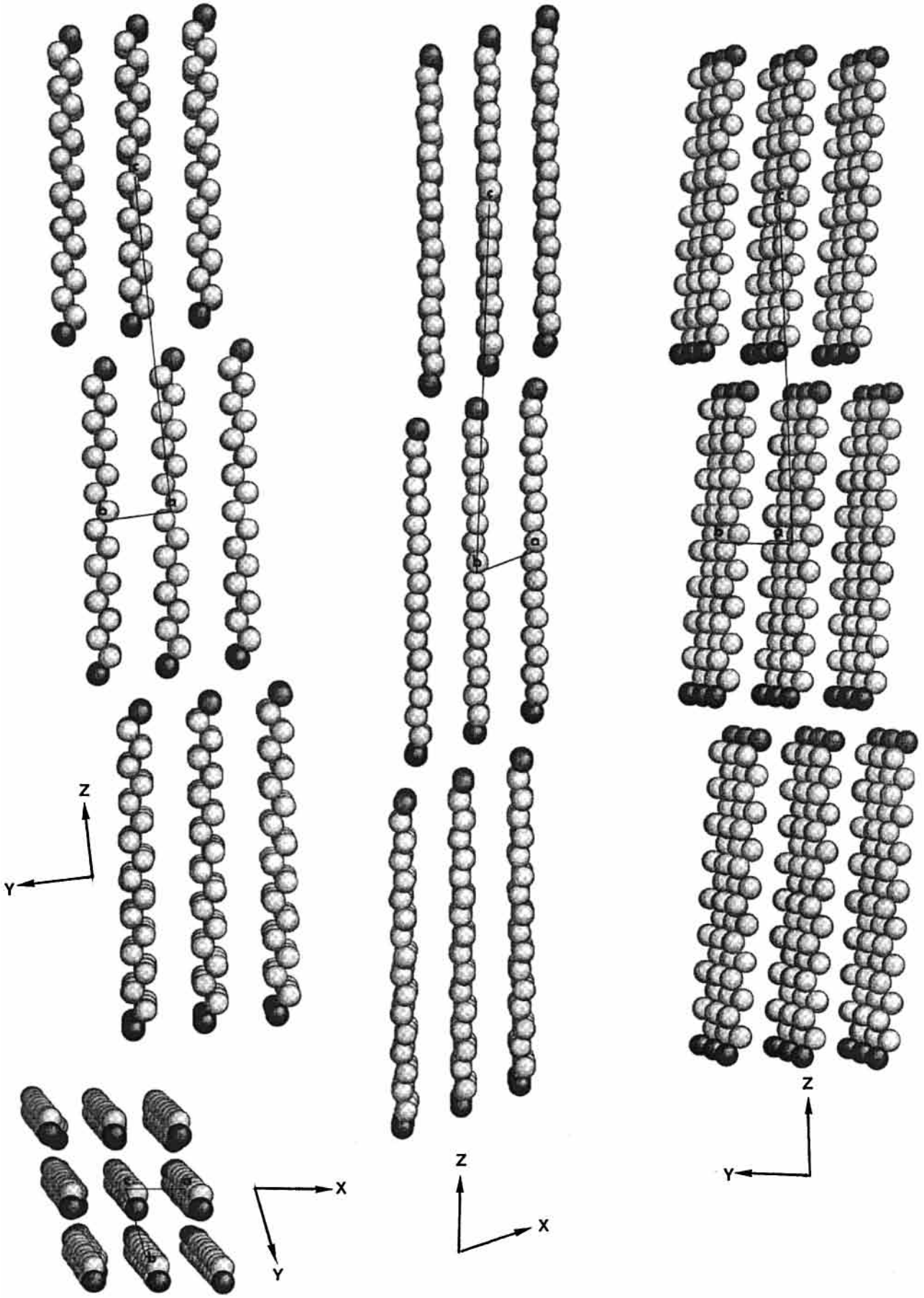

Figure 1. "$C_{18}-P\bar{1}$" key structure of even-numbered C_{2p}'s ($6 \leq 2p \leq 26$) according to the crystallographic data of Nyburg et al.[20,73]

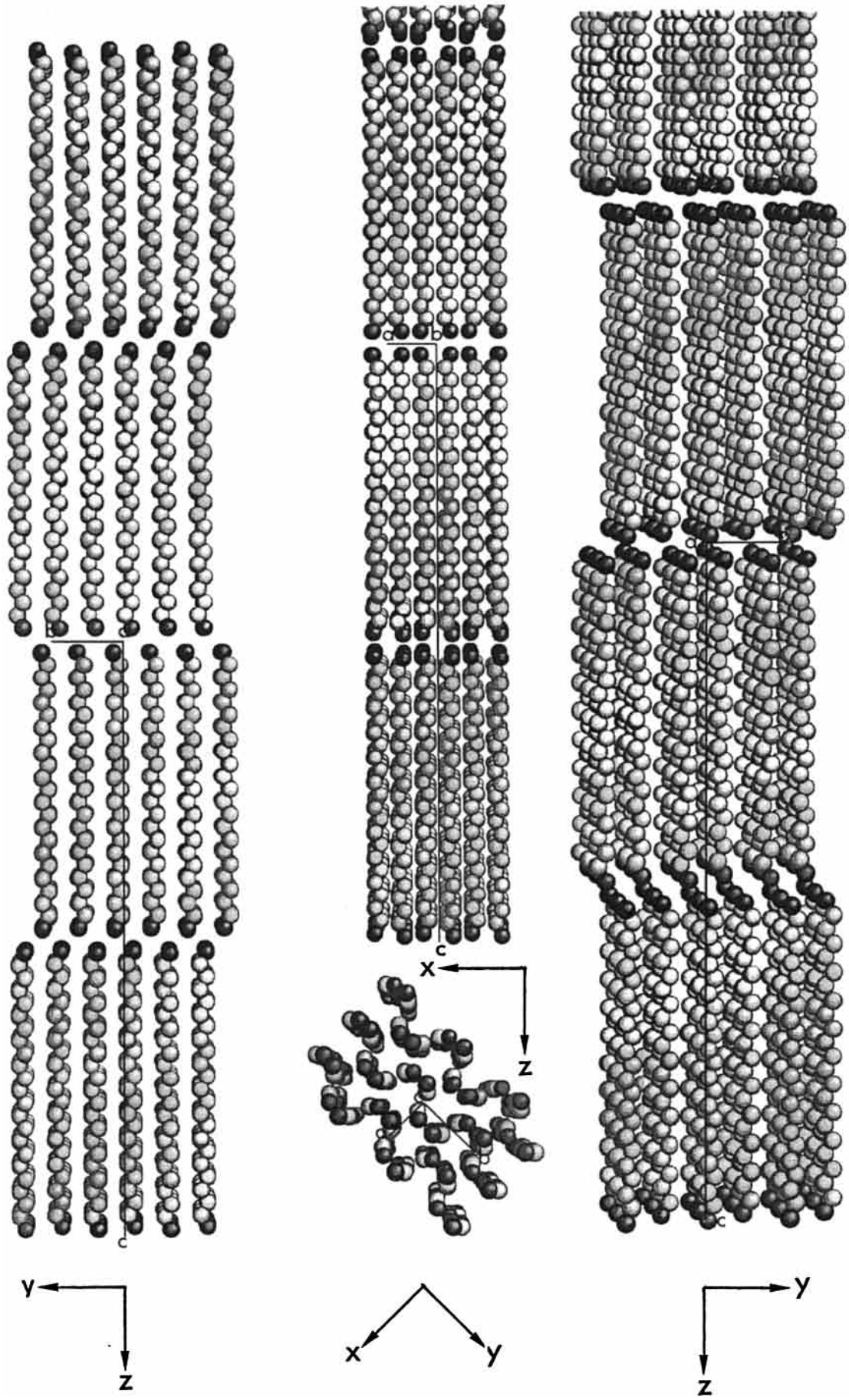

Figure 2. "C_{23}−*Pbcm*" key structure of odd-numbered C_{2p+1}'s ($11 \leq 2p + 1 \leq 41$) according to the crystallographic data of Smith[13] and Nyburg and Potworowski.[73]

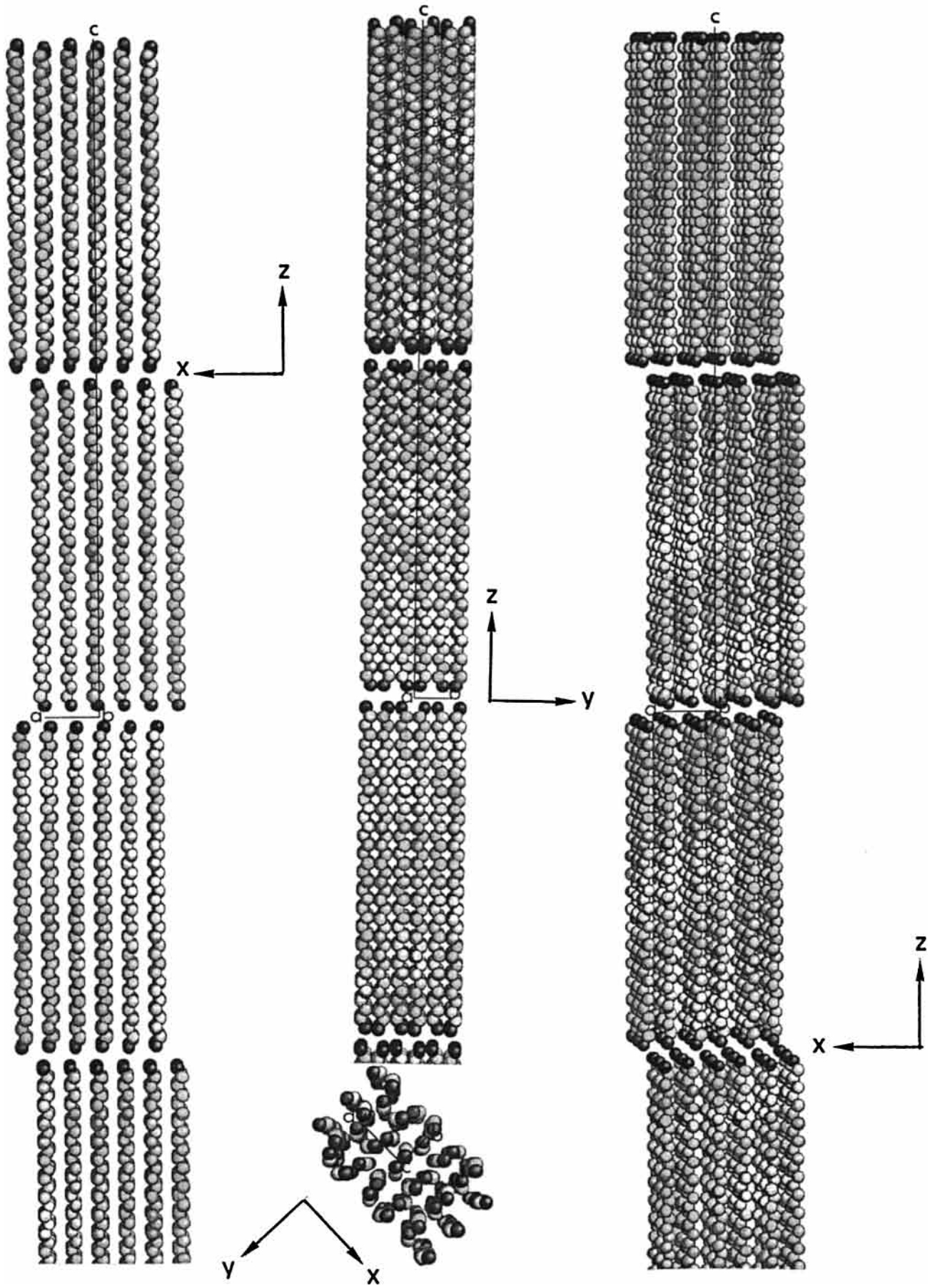

Figure 3. "C_{36}–*Pca*2_1" key structure of C_{46}, C_{50} and C_{60}.

Table 1. Linear Relationships of Crystalline *c*-Parameter Variations versus n_c Carbon Atom Number in C_n Structures

C_n structure	*c*/Å orthorhombic	(*c*/2)/Å orthorhombic or *c*/Å triclinic and monoclinic	(chain length + gap)/Å
Broadhurst[19]	$2.54n_c + 3.96$	$1.27n_c + 1.98$	$1.27(n_c - 1) + 3.25$
key structure *Pbcm*−C_{23} Nyburg and Potworowski[73]	$2.546n_c + 3.75$	$1.273n_c + 1.875$	$1.273(n_c - 1) + 3.148$
Pbcm $13 \le 2p + 1 \le 41$ Chevallier et al.[75]	$2.5448n_c + 3.7504$	$1.2724n_c + 1.8752$[a] $R^2 = 1$	$1.2724(n_c - 1) + 3.1476$
key structure *Pca*2_1−C_{36} Nyburg and Potworowski[73]	$2.54n_c + 3.693$	$1.27n_c + 1.8465$	$1.27(n_c - 1) + 3.1165$
triclinic *P*1−C_{2p}		$1.265n_c + 2.156$[b]	
$6 \le 2p \le 36$		$R^2 = 1$	
$14 \le 2p \le 26$		$1.1169n_c + 4.876$[a] $R^2 = 0.9977$	
monoclinic $P2_1/a$−C_{2p}		$1.2746n_c + 2.49$[b]	
$26 \le 2p \le 38$		$R^2 = 1$	
$28 \le 2p \le 36$		$0.9615n_c + 11.367$[a] $R^2 = 1$	

[a] Relationships determined by optimization from the data of Craig et al.[29] [b] Relationships determined by optimization from the data of Nyburg and Potworowski.[73]

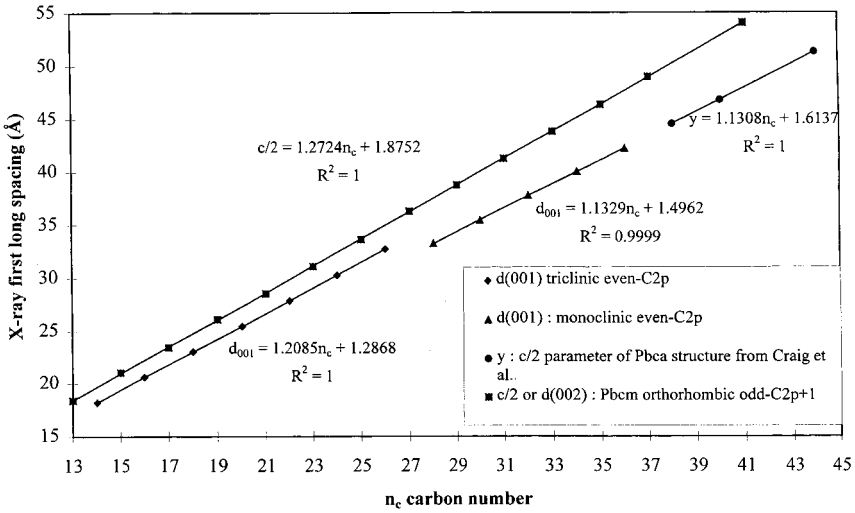

Figure 4. Plot of the variations of the experimental first X-ray long-spacing as a function of n_c, the carbon atom number: (■) d(002) of the *Pbcm* orthorhombic structures of odd-numbered C_{2p+1}'s; (◆ and ▲) d(001) of the triclinic and monoclinic structures of even-numbered C_{2p}'s; (●) the *c*/2 *Pbca* orthorhombic values. All the values have been determined from the data of Craig et al.[29]

of the *Pbcm* orthorhombic unit-cells (Figure 4). The variation line of the monoclinic first long spacing, d(001), is below that of the d(001) triclinic spacing, because the molecule axis is more inclined: (i) about 27° relative to the normal to the (001) plane in the C_{36} monoclinic structure[22] and (ii) nearly 19° in the C_{18} triclinic structure.[20,73] Moreover, the ratio of the slope, obtained for the monoclinic or triclinic structures, with the one of the *Pbcm* orthorhombic structure corresponds to the cosine of the mean incline angle of the molecule chains relative to their stacking planes. The following values, 27° and 18.23° obtained for the monoclinic and triclinic structures, respectively, agree with those previously mentioned.

It appears that the *c*/2 parameter values of the *Pbca* orthorhombic structures of C_{38}, C_{40}, and C_{44}, determined by Craig et al.,[29] are brought into alignment with the d(001) values of the monoclinic structures of C_{28}, C_{30}, C_{32}, C_{34}, and C_{36} (Figure 4). This observation confirms the depiction of Boistelle et al.[22] and Craig et al.[29] about the *Pbca* orthorhombic structure of C_{2p}'s: this orthorhombic structure is a stacking of alternate monoclinic layers, related one to the other by a 2-fold axis perpendicular to the (001) plane. The molecule tilt angle in the *Pbca* orthorhombic structure with a monoclinic subcell is certainly identical to that of molecules in the $P2_1/a$ monoclinic structure.

In the triclinic and monoclinic structures, the crystalline *c*-axis is tilted in relation to the normal to the molecule stacking layers, but it is not parallel to the alkane chain axis[73] because the slopes of the corresponding lines (Figure 5 and Table 1) are not equal to the average increase (1.2724 Å) of the chain length, determined from the *Pbcm* orthorhombic structure data.[29] Indeed, as the *all-trans* conformation of the C_n molecule is preserved whatever the structure of lower temperature, this increase must be identical in all *n*-alkane structures (for instance, it is found equal to the following mean values: 1.272 Å in C_{18} (ref 20) and 1.279 Å in C_{36} (ref 22)).

According to the atom coordinates of the literature[20,73,74] and the values of the first long spacing, that corresponds to the thickness of a molecule layer, the average gap between the planes of the end methyl group carbon atoms of two consecutive molecule layers is equal to 2.74 Å in triclinic C_{12}, C_{14}, C_{16}, and C_{18} and 2.98 Å in monoclinic C_{36}, respectively.

The other higher C_{2p}'s have the $Pca2_1$ orthorhombic structure[64] in which the chains are parallel to the *c*-axis[29] (Figure 3). Polytipic modifications are observed in C_{24} and C_{26} by Gerson et al.,[25] in C_{28} and C_{36} by Boistelle et al.,[22] in C_{44} and C_{94} by Sullivan and Weeks.[30]

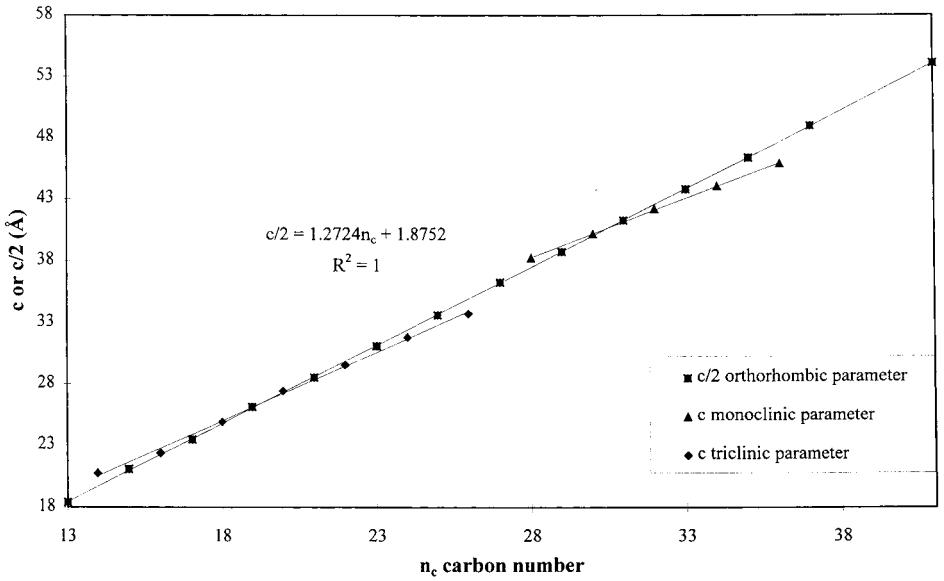

Figure 5. Comparison between the *c*/2 *Pbcm* orthorhombic values and the triclinic and monoclinic *c*-parameters (from the data of Craig et al.[29]).

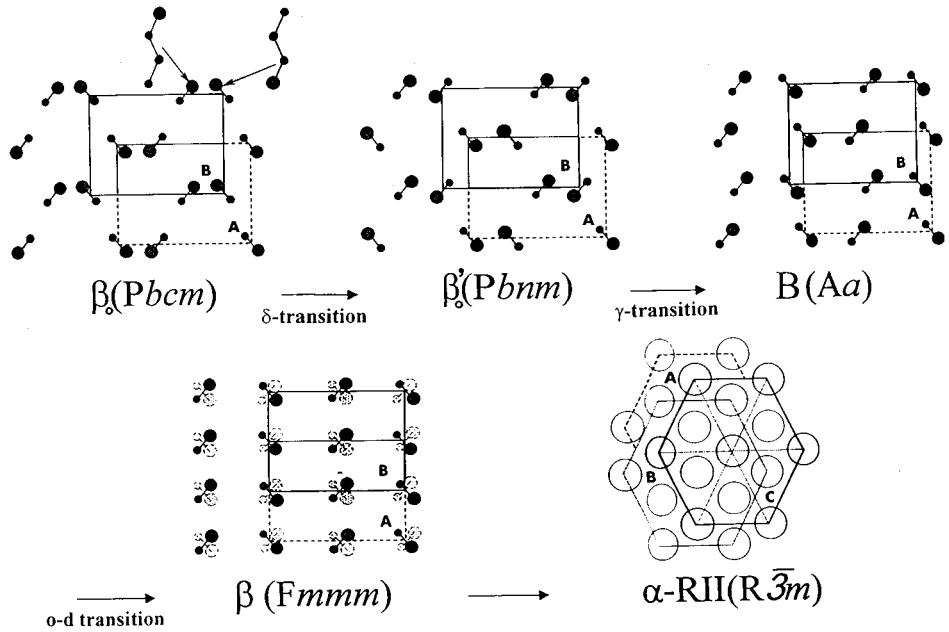

Figure 6. Stacking mode of the molecule layers into the structure of β_0(*Pbcm*), β'_0(*Pbnm*), B(*Aa*) (according to Nozaki et al.[46]), β(*Fmmm*), and α-RII($R\bar{3}m$) (according Ungar[33] and Doucet et al.[32,35]).

(C) C_n Structural Behavior versus Temperature. Müller[7,8] was the first to observe the existence of solid−solid transitions by X-ray diffraction, when the temperature increases, with the appeareance of disordered *rotator phases* below the melting points of C_n's (n = 18−44). Since then, the C_n structural behavior versus temperature has been the subject of numerous publications.[21,30−70,86]

(1) Definition and Classification of the Solid−Solid Transitions. For the pure C_n's, it is possible to distinguish two categories of polymorphous phases: (i) the *ordered phases* of *low temperatures*, also called crystal phases, and the *disordered phases* of *high temperatures*, denoted rotator phases or plastic phases.

The order−disorder solid−solid transition (hereafter named the *o−d transition*) is characterized by the higher thermal effect (Appendix 2 in the Supporting Information) observed at the solid state below the melting point. Other solid−solid transitions, with which lower thermal effects are associated, appear in each category, especially for the odd-numbered C_{2p+1}'s.

(2) Crystal ↔ Crystal Transitions below the o−d Transition. (i) δ-Transition. This transition has been highlighted by differential scanning calorimetry (DSC) in the odd-numbered C_{2p+1}'s from C_{23} up to C_{29} by Ungar,[33] Roblès et al.,[40] Snyder et al.,[43] and Hasnaoui et al.[65] It is called the *δ-transition* by Snyder et al.[43] and leads to a new phase, called β'_0 by Hasnaoui et al.[65] or V by Snyder et al.,[43] whose *Pbnm* orthorhombic structure has been suggested by Nozaki et al.[66] (Figure 6).

(ii) γ-Transition. A second crystal ↔ crystal transition, denoted the *γ-transition* by Snyder et al.,[43] is observed for C_{25} by Ungar,[33] Roblès et al.,[40] and Nozaki et al.,[66] for C_{27} by Roblès et al.[40] and Snyder et al.,[43,45] for C_{29} by Snyder et al.[43] and Nozaki et al.,[66] for C_{31} and C_{33} by Piesczek et al.,[21] and for C_{37} by Freund et al.[47] with the appearance of a monoclinic phase (Figure 6), called B by Piesczek et al.,[21]

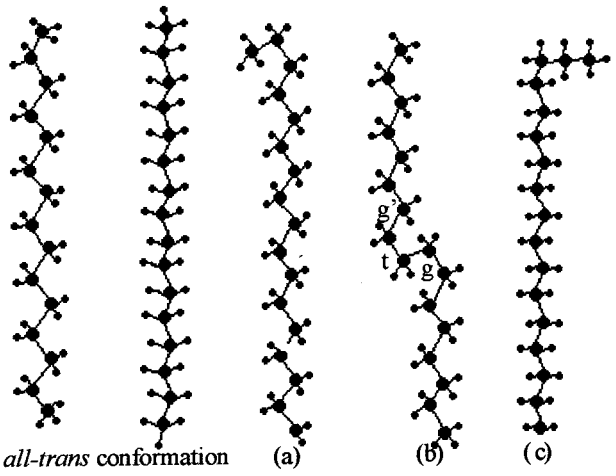

Figure 7. Molecule conformation defects: (a) "end-gauche" defect (...tg); (b) "kink defect" (...gtg′...) especially observed in α-RII and RIV "rotator" phases; (c) double "end-gauche" defect.

IV by Snyder et al.,[43,45] and M by Roblès et al.[40] The monoclinic space group, *Aa*, of the third ordered phase of *low temperatures* has been determined by Piesczek et al.,[21] Strobl et al.,[48] Ewen et al.,[49,50] and Sullivan and Weeks[30] and hereafter called B(*Aa*).

(iii) β-Transition. A third crystal ↔ crystal transition is observed for the odd-numbered C_{2p+1}'s from C_{31} up to C_{69}.[21,34,43,66,64,128,129] It is named the *β-transition* by Snyder et al.[43] and leads to the monoclinic phase, which has the *A*2 space group according to Piesczek et al.[21] This monoclinic phase is denoted C(*A*2) by Piesczek et al.,[21] Strobl et al.,[48] and Ewen et al.[49,50] or III by Snyder et al.[43,44] and Nozaki et al.[66] More structural details about this C(*A*2) phase are given by Takamizawa et al.[64] and by Sullivan and Weeks.[30]

All these crystal ↔ crystal transitions lead to ordered phases whose crystalline structures display differences in the stacking modes of molecule layers along the long crystalline *c*-axis (Figure 6) and molecule conformation defects, especially of the *end-gauch* type (..*tg*)[43] (Figure 7a); but any important modification of the molecule orientation around the *c*-axis is not observed in these *ordered phases* of odd-numbered C_{2p+1}'s.

The $\gamma(P\bar{1})$ triclinic and $\delta(P21/a)$ monoclinic *ordered phases* of even-numbered C_{2p}'s ($2p < 30$) do not have these types of crystal ↔ crystal transitions: their stability is certainly higher than that of the *Pbcm* orthorhombic ordered phase of odd-numbered C_{2p+1}'s.

(3) Order−Disorder Transition (o−d Transition). This solid−solid *o−d transition* is characterized by important modifications of the molecule orientation around the crystalline *c*-axis. This phenomenon is accompanied by the creation of many defects[43,44] in the molecular chains (Figure 7) that lead to nonplanar conformers.[43,116]

The *o−d transition* corresponds to the appearance following disordered phases:

(i) Orthorhombic β(Fmmm)[32−35,250] for the Odd-Numbered C_{2p+1} Series from C_9 up to C_{25}. In this structure, the stacking mode of the molecule layers along the long *c*-axis corresponds to the orthorhombic (or hexagonal) *ABAB* sequence (Figure 6) of (00*l*) crystalline planes; but the molecules orientate themselves in a disorderly manner around their long axis according to the two positions defined in the ordered structures (Figure 6), so that all molecule occupancies become equivalent in *A* and *B* crystallographic planes by this "disorder of the molecule orientation" and lead to the *Fmmm* centered face space group.

(ii) Rhombohedral α-RII ($R\bar{3}m$) for the Even Numbered C_{2p} from C_{22} up to C_{26}.[32−35] In this structure, the stacking mode of the (00*l*) molecule layers corresponds to the *ABC* rhombohedral sequence (Figure 6)[32−35] in which the molecules would most probably be in rotation around their axis according to McClure[63] and Mnyukh.[86] In addition to this movement, defects appear in the molecular chains that lead to *nonplanar* conformers (Figure 7) observed by infrared and Raman spectrometries by Piesczek et al.,[21] Zerbi et al.,[31] Ungar,[33] Snyder et al.,[43,44] Strobl et al.,[48] Ewen et al.,[49,50] and Maroncelli et al.[102] These *nonplanar* defects are also present in the RIII triclinic and RIV monoclinic disorder phases.

(iii) Triclinic RIII for the Odd-Numbered C_{27}, C_{29}, C_{31}, C_{33}, and C_{37} and the Even-Numbered C_{2p} from C_{28} to C_{40} and C_{44}. The depiction of the triclinic *R*III phase is given in the literature by Doucet et al.,[35] Sirota et al.,[38,51,52] Roblès et al.,[40] and Srivastava et al.[54]

(4) Disorder ↔ Disorder Transitions. Above of the *o−d transition* temperature, the C_n's can undergo other transitions of disorder−disorder type:

(i) β(Fmmm) ⇒ β-RI (Fmmm). Concerning the X-ray diffraction experiments, the occurrence of the *β*(*Fmmm*) phase in the course of the *o−d transition* is accompanied by (i) the disappearance of all the diffraction peaks (*hkl*) whose indices do not have the same parity,[19−22,24,25,27,60,242] which thus leads to the *Fmmm* centered face space group, and (ii) an important shift of the (020) diffraction toward small Bragg angles, that corresponds to an increase of the crystallographic *b* parameter and of the unit-cell base area (a,b) (Figure 8c−e) in relation to the orientation disorder appearance of the molecules around their axis.

First, the *β*(*Fmmm*) phase does not undergo any crystalline parameter evolution in a small temperature range; then, the crystallographic parameter *b*/*a* ratio of this phase increases progressively. The beginning of this phenomenon is observed by X-ray diffraction when the (020) line moves toward the (111) diffraction peak (Figure 8f−h); however, the X-ray diffraction line intensities do not change significantly. This transition, which is observed in pure C_{2p+1}'s with varying temperature and which is accompanied by an abnormal and continuous enthalpy consumption without any change in the space group (*Fmmm*) of the crystallographic structure (Figure 9), does not obey the phase law of Gibbs concerning first-order transitions; it probably corresponds to a second-order transition, which characterizes the RI rotator state of this *β*(*Fmmm*) phase. From the experimental observations by infrared and Raman spectroscopy of Piesczek et al.,[21] Snyder et al.,[43,45,50] Strobl et al.,[48] Ewen et al.,[49,50] and McClure,[86] it is very likely that, in this *β*-RI state of the *β*(*Fmmm*) phase, the molecules undergo a movement of oscillation around the molecule axis, whose amplitude progressively increases as a function of the temperature; this phenomenon leads to the progressive increase of the area of the unit-cell base (a,b) of the *β*(*Fmmm*) phase.

(ii) β-RI(Fmmm) → α-RII($R\bar{3}m$). When the two (020) and (111) diffraction lines coincide (Figure 8i), the symmetry of the unit-cell base (a,b) becomes hexagonal ($b/a = \sqrt{3}$) and the pure C_n's undergo a further weak first-order transition into the rhombohedral α-RII rotator phase whose space group $R\bar{3}m$ has been determined by Ungar:[33] The stacking mode of the chains along the crystallographic long *c*-axis corresponds to the rhombohedral *ABCABC* sequence of crystalline planes instead of the orthorhombic (or

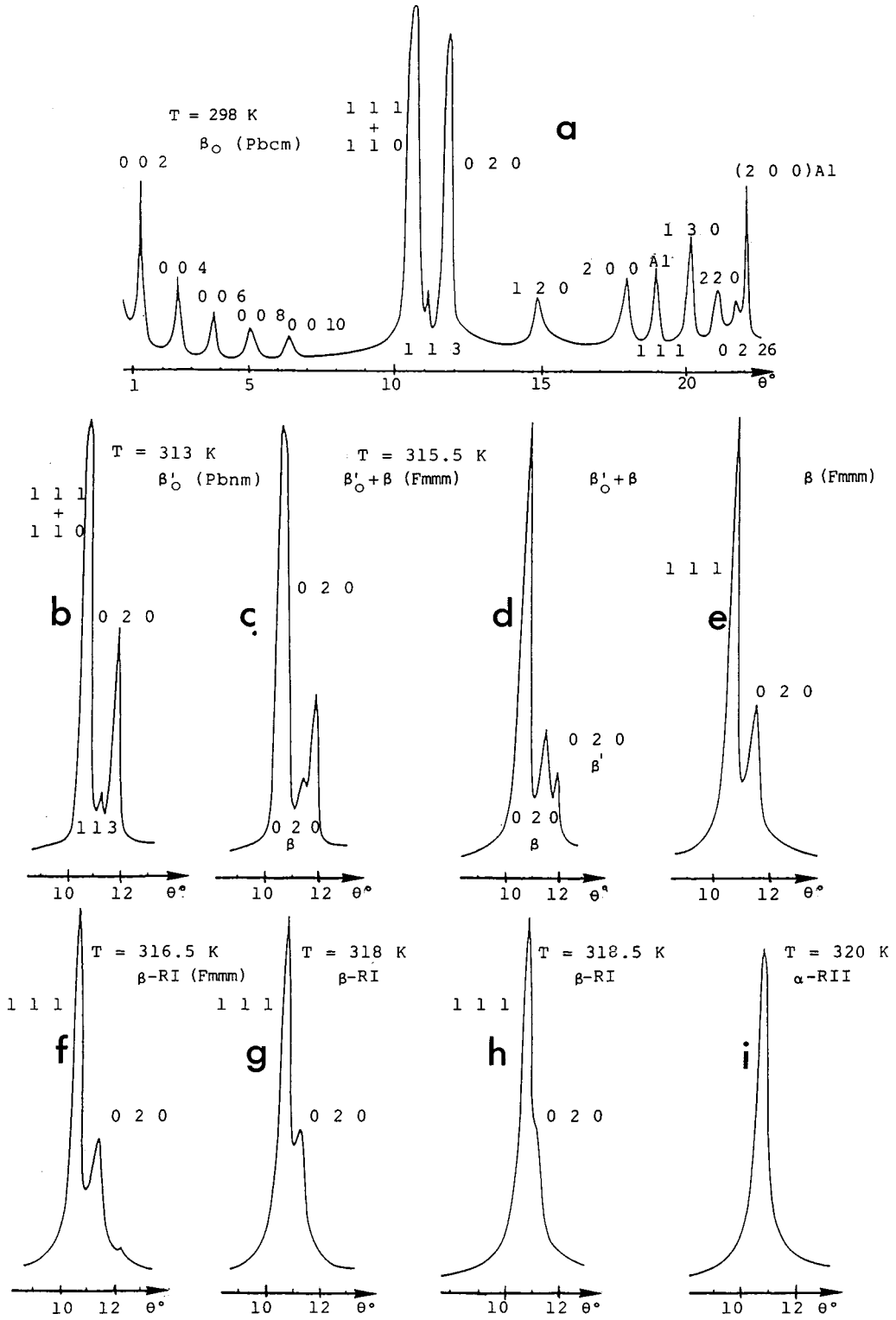

Figure 8. Structural evolutions of C_{23} from the $\beta_0(Pbcm)$ phase up to the α-RII ($R\bar{3}m$) rotator phase when the temperature increases ($\lambda_{Cu\ K\alpha}$): (a) $\beta_0(Pbcm)$ ordered phase; (b) $\beta'_0(Pbnm)$ ordered phase observed above the δ-transition; (c, d, and e) o−d transition $\beta'_0(Pbnm) \rightarrow \beta(Fmmm)$; (f, g, and h) second- or higher-order transitions of rotator RI in the $\beta(Fmmm)$ disordered phase; (i) α-RII rotator disordered phase.

hexagonal) *ABABAB* sequence as in the orthorhombic β-($Fmmm$) structure.[32−35] In the α-RII ($R\bar{3}m$) phase rotator state, the molecules would most probably be in rotation around their axes according to Mnyukh[63] and McClure[86].

(iii) RIII → RIV. This transition has been highlighted by Sirota et al.[38] in C_{27}, C_{28}, C_{29}, and C_{30}.

To sum up, the phase succession, when the temperature increases, is shown in Chart 1.

Reminder. According to the phase equilibrium law of Gibbs:

(i) The pure components or compounds undergo the solid−solid and solid−liquid first-order equilibrium transi-

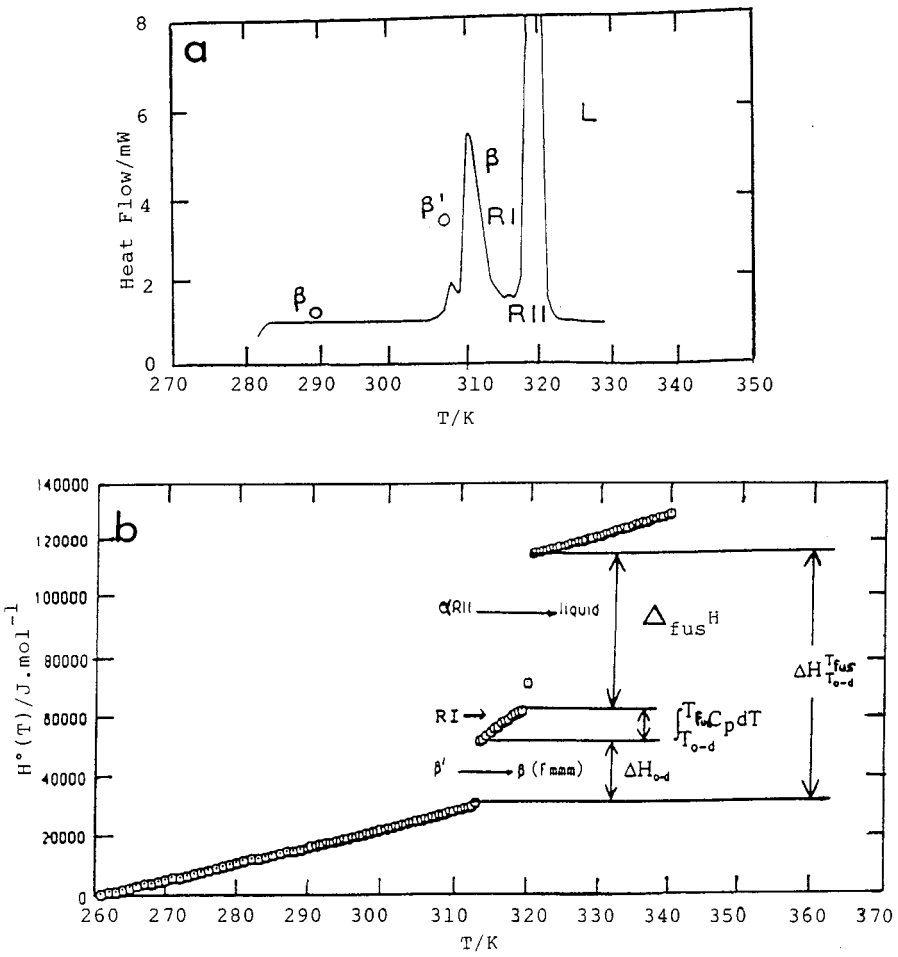

Figure 9. Differential scanning calorimetry (a) and enthalpy variation (b) curves of C_{23}.

Chart 1. Phase Succession When the Temperature Increases[a]

odd-numbered C_{2p+1}

9 to 21	β_o (Pbcm)	$\xrightarrow{o\text{-}d}$ β(Fmmm)⇒β-RI(Fmmm)		→liquid
23	β_o (Pbcm) $\xrightarrow{\delta}$ β'_o (Pbnm)	$\xrightarrow{o\text{-}d}$ β(Fmmm)⇒β-RI(Fmmm)→αRII ($R\bar{3}m$)		→liquid
25	β_o (Pbcm) $\xrightarrow{\delta}$ β'_o(Pbnm) $\xrightarrow{\gamma}$ B(Aa)	$\xrightarrow{o\text{-}d}$ β(Fmmm)⇒β-RI(Fmmm)→α RII ($R\bar{3}m$)		→liquid
27-29	β_o (Pbcm) $\xrightarrow{\delta}$ β'_o(Pbnm) $\xrightarrow{\gamma}$ B(Aa)	$\xrightarrow{o\text{-}d}$ RIII → RIV		→liquid
31,33,37	β_o(Pbcm) $\xrightarrow{\gamma}$ B (Aa) $\xrightarrow{\beta}$ C(A2)	$\xrightarrow{o\text{-}d}$ RIII		→liquid
45	β_o(Pbcm) $\xrightarrow{\gamma}$ B (Aa) $\xrightarrow{\beta}$ C(A2)			→liquid
61,65,69	β_o(Pbcm) $\xrightarrow{\beta}$ C(A2)			→liquid

even-numbered C_{2p}

10 to 20	γ_o ($P\bar{1}$)			→liquid
22 to 26	γ_o ($P\bar{1}$)	$\xrightarrow{o\text{-}d}$	α-RII ($R\bar{3}m$)	→liquid
28,30	δ_o($P2_1/a$)	$\xrightarrow{o\text{-}d}$ RIII → RIV		→liquid
32→36	δ_o($P2_1/a$)	$\xrightarrow{o\text{-}d}$ RIII		→liquid
38→44	β_o(Pbca)	$\xrightarrow{o\text{-}d}$ RIII		→liquid
48,60	β_o($Pca2_1$) $\xrightarrow{\beta}$ C(A2)			→liquid

[a] The *o−d transition* disappears from C_{45}.[64,128,129] → corresponds to first-order transitions. ⇒ corresponds to second- or higher-order transitions.

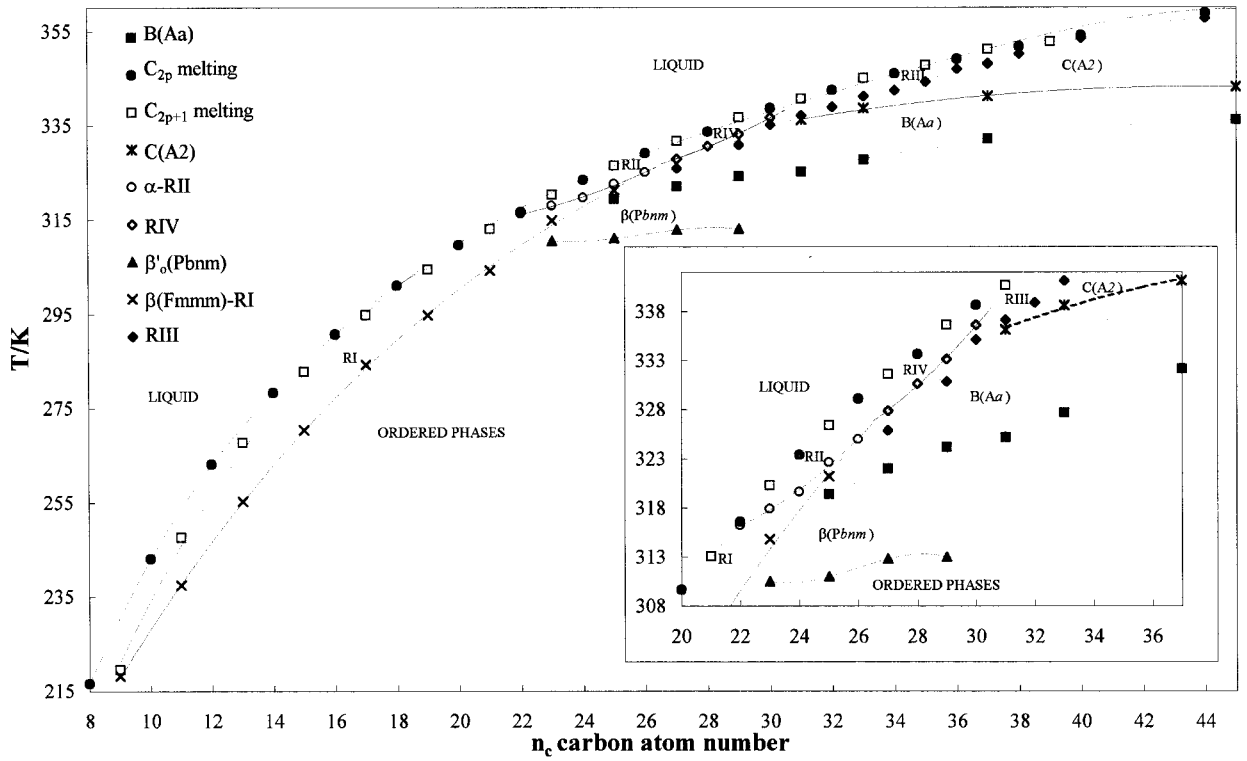

Figure 10. Sequence of the phases versus temperatures and evolution of solid−solid and solid−liquid transition temperatures of pure C_n's ($8 \le n_c \le 45$) versus the n_c carbon atom number.

tions (→) at constant temperature. The influence of the pressure can be negligible for this transition type, except at very high pressure, as observed by Lourdin et al.[119]

(ii) The physical constant of a solid phase is its crystalline structure and more particularly its space group which characterizes it. Thus a solid−solid first-order transition corresponds to a change of the space group. This is generally not the case for the solid−solid second- or higher-order transitions (⇒) which do not obey Gibbs's rule concerning the first-order equilibria. For instance, the rotator RI state of the $\beta(Fmmm)$ phase is observed at varying temperatures without change of the space group ($Fmmm$) and thus without change of the $\beta(Fmmm)$ phase. It is not recommended to change its notation.

The variations of temperatures of solid−solid transitions and fusion are reported as a function of n_c carbon atom number for the pure C_n's from n_c equals 9 to 45 in Figure 10.

(D) Thermodynamic Behavior. The mean values of the thermodynamic data, determined from the experimental values of Appendix 2 in the Supporting Information whose relative gaps are lower than ±0.5/K for the temperatures and 5% for the enthalpy values, are given in Table 2 (melting temperature (T_{fus} ± 0.5/K); melting enthalpy $\Delta_{fus}H$; o−d transition enthalpies ΔH_{o-d}; and o−d transition temperature (T_{o-d} ± 0.5/K)).

Although numerous data (Appendix 2 in the Supporting Information) about temperatures and enthalpies of solid−solid and solid−liquid transitions of C_n's are available in the literature,[87−140,250,251] only some authors[14,92,95,99,109,118,126,127] have carried out measurements of the variations of thermodynamic functions (heat capacities, enthalpies, entropies) versus temperatures from the ordered crystal phases of low temperatures above the melting point.

(1) Melting Temperatures. The average values (±0.5 K) of melting temperatures of pure C_n's are displayed in Tables 2 and 4 and in Figures 10−12. Broadhurst[130] proposed the following analytical expressions, $T_{fus} = f(n_c)$, for the orthorhombic C_n melting temperatures T_{fus}, as a function of the number of carbon atoms per molecule n_c:

first

$$T_{fus}/\mathrm{K} = T_0\frac{n_c + a}{n_c + b} \qquad \text{(1-model)}$$

with the following values of constants

$$T_0 = \lim_{n_c \to \infty} T_{fus}(n_c) = 414.3\ \mathrm{K}; \quad a = -1.5; \quad b = 5.0$$

then, taking into account the Flory and Vrij[131] model that describes the C_n melting thermodynamic equations

$$T_{fus}/\mathrm{K} = T_0\frac{n_c + a}{n_c + \ln n_c + b} \qquad \text{(2-model)}$$

with

$$T_0 = \lim_{n_c \to \infty} T_{fus}(n_c) = 418.5\ \mathrm{K}$$

Broadhurst[130] compared the values of T_0 constants with that of the melting temperature of polyethylene to infinite molecular weight, that is assessed between 416.65 and 418.65 K.

In this study, a new fitting is carried out based on the 67 values of melting points (Table 2; $1 \le n_c \le 390$). The optimization has been performed on different sets of data using the subroutine published by Byrd et al.[252] and Zhu et al.[253] This method is primarily based on the Broyden, Fletcher, Goldfarb, and Shanno (BFGS) quasi-Newton method mentioned by Fletcher.[254] This optimization method is very efficient and provides the optimized parameters without any noticeable difficulty. It is only necessary to

Table 2. Mean Values of Thermodynamic Data of Appendix 2 in the Supporting Information

n_c[a]	M[b]	T_{fus}[c]	$\Delta_{fus}H$[d]		T_{o-d}[e]	ΔH_{o-d}[f]	
		K	J·mol^{-1}	J·g^{-1}	K	J·mol^{-1}	J·g^{-1}
1	16.0426	90.7	940	58.6			
2	30.0694	90.1	2859	95.1			
3	44.0962	85.5	3527	80.0			
4	58.123	134.8	4661	80.2			
5	72.1498	143.4	8405	116.5			
6	86.1766	177.8	13124	152.3			
7	100.2034	182.5	14061	140.3			
8	114.2302	216.3	20707	181.3			
9	128.257	219.6	15465	120.6	217.2	6278	48.9
10	142.2838	243.5	28698	201.7			
11	156.3106	247.7	22225	142.2	236.6	6857	43.9
12	170.3374	263.6	36755	215.8			
13	184.3642	267.6	28485	154.5	255	7656	41.5
14	198.391	279	45030	227.0			
15	212.4178	283.1	34574	162.8	270.9	9162	43.1
16	226.4446	291.2	53332	235.5			
17	240.4714	294.9	40124	166.9	283.8	10935	45.5
18	254.4982	301.2	61306	240.9			
19	268.525	304.9	45580	169.7	295.5	13750	51.2
20	282.5518	309.5	69730	246.8			
21	296.5786	313.2	47697	160.8	305.6	16418	55.4
22	310.6054	316.8	48785	157.1	315.2	29020	93.4
23	324.6322	320.4	53127	163.7	315.6	21728	66.9
24	338.659	323.6	54396	160.6	320.7	31701	93.6
25	352.6858	326.3	57088	161.9	320.3	26676	75.6
26	366.7126	329.2	59973	163.5	326	33815	92.2
27	380.7394	331.7	61145	160.6	326.3	26791	70.4
28	394.7662	334.2	65137	165.0	330.5	35136	89.0
29	408.793	336.2	66107	161.7	330.8	30786	75.3
30	422.8198	338.2	68293	161.5	332.15	36986	87.5
31	436.8466	341.1			336.5		
32	450.8734	342.5	75758	168.0	337.15	40835	90.6
33	464.9002	344.3	79496	171.0	340.95	31178	67.1
34	478.927	345.6	79378	165.7	342.2	48032	100.3
35	492.9538	347.75	86346	175.2	344.2	41087	83.3
36	506.9806	348.95	87682	172.9	347	31071	61.3
37	521.0074	349.8			348.8		
38	535.0342	351.7	133223	249.0	350.2		
39	549.061	352.7					
40	563.0878	354	135547	240.7	353.5	14000	24.9
41	577.1146	354.85					
42	591.1414	356.5					
43	605.1682	356.95					
44	619.195	358.75	149641	241.7	357.7	18200	29.4
45	633.2218	360.15					
46	647.2486	360.7	175992	272.0			
48	675.3022	363.65					
50	703.3558	365.25	162434	230.9			
54	759.463	368.15					
58	815.5702	370.15					
60	843.6238	372.45	193228	230			
61	857.6506	373.45					
62	871.6774	373.65					
64	899.731	375.75					
65	913.7578	375.25					
69	1010.181	377.83					
70	983.8918	380.05					
80	1124.1598	385.15					
100	1404.6958	389.65					
102	1432.7494	388.9					
120	1685.2318	392.15					
140	1965.7678	394.15					
150	2106.0358	396.4					
198	2779.3222	399.8					
246	3452.6086	401.8					
294	4125.895	403.6					
390	5472.4678	405.2					

[a] Carbon atom number of the C_n. [b] Molar mass. [c] Melting point ± 0.5 K. [d] Melting enthalpy. [e] Order−disorder transition temperature ± 0.5 K. [f] Order−disorder transition enthalpy (relative error on enthalpies 5%).

provide the expression of the considered cost function J and of its gradient with respect to the parameters to be estimated.

The data which are treated by optimization can be classified according to different criteria: (i) either all data or only data concerning even- or odd-numbers of carbon atoms of the C_n chain; (ii) with the previous criterion, data concerning a number of carbon atoms larger than 2, thus excluding methane and ethane; (iii) the same criteria but with a number of carbon atoms larger than 16 [for these C_n's ($n_c > 16$), the alternation between the melting points of even- and odd-numbered C_n's disappears (Figures 10−12)].

The following cost function has been defined with respect to the experimental data (noted "exp") and the results from the model (noted "mod"):

$$J = \sum_i (T_{fus}^{exp} - T_{fus}^{mod})^2$$

where the models are 1- and 2-Broadhurst's[130] models, respectively.

Thus, the estimated parameters are T_0, a, and b.

The treatment concerning these data has been summarized in Table 3, where the optimal J values of the corresponding cost function are given. It clearly appears from the J values of the cost function that 1-Broadhurst's model is better than the 2-model, as the latter gives a better criterion in only one case, where odd C_{2p+1}'s larger than 17 are considered. The estimated parameters are given in Table 3. The parameter T_0 is the asymptotic value given by the 1- and 2-models when the number of carbon atoms tends toward infinity. It is better predicted in 1-Broadhurst's model than in the 2-model. The parameter a is very sensitive to the set of data while the parameter b is less sensitive, especially in 1-Broadhurst's model.

The lower J values of the cost function are obtained when the data are fitted with carbon atom numbers higher than 16 (Table 3):

(i) The T_0 parameter of 2-Broadhurst's model tends to the melting temperature of the polyethylene to infinite molecule weight;[130] nevertheless, the gap increases between the experimental melting points and the calculated values for the higher C_n's (Figure 12), whereas 2-Broadhurst's model has been planned to better predict the melting temperatures of high molecular weight C_n's by extrapolation. For the smaller C_n's ($n_c \leq 17$), the curve extrapolated from the 2-model tends to the odd-numbered C_{2p+1} melting temperatures (Figure 12) and deviates from those of the even-numbered C_{2p}'s.

(ii) The 1-Broadhurst's model gives better agreement for the melting temperatures of the higher C_n's (Figure 11). For the smaller C_n's ($n_c \leq 14$), the extrapolated corresponding curve tends to the even-numbered C_{2p} melting points and deviates from those of odd-numbered C_{2p+1}'s (Figure 11).

It should be stressed that it is not advisable to use a model with given coefficients outside the domain where it was designed, even if it seems to give acceptable results. For example, any model designed with all even alkanes with n_c larger than 16 shoud not be used when n_c is lower. Thus, comparisons between models are reasonable only when they concern the same domain.

(2) Enthalpy Variations. The mean values of melting and o−d transition enthalpies, determined from the data of Appendix 2 in the Supporting Information whose relative gaps are lower than 5%, appear in Table 2. As previously well-known in the literature, the melting enthalpies show

Table 3. T_0 and a and b Estimated Parameters for Broadhurst's Models in All Cases of Considered Data and Corresponding J Cost Function Values

type of data	1-Broadhurst's model				2-Broadhurst's model			
	T_0/K	a	b	J	T_0/K	a	b	J
all C_n	421.1	0.05778	7.740	4675	430.0	−0.3407	4.950	7237
all even C_{2p}	415.3	−0.3478	6.507	360.9	424.6	−0.8713	3.503	1023
all odd C_{2p+1}	430.0	0.3348	8.964	3439	430.0	−0.1628	5.422	5373
all C_n with $n_c \geq 3$	412.8	−1.320	4.992	552.3	422.7	−1.857	1.939	990.3
all even C_{2p} with $2p \geq 4$	412.7	−0.9887	5.353	58.2	420.2	−1.827	1.695	206.1
all odd C_{2p+1} with $2p + 1 \geq 3$	415.7	−1.411	5.169	166.7	430.0	−1.764	2.665	375
all C_n with $n_c \geq 17$	413.2	−0.7247	5.754	32.4	416.7	−3.776	−1.136	48.6
all C_{2p} with $2p \geq 16$	413.2	−0.7405	5.717	26.3	416.4	−3.985	−1.433	41.9
all C_{2p+1} with $2p + 1 \geq 17$	412.8	−0.7774	5.670	5.40	418.9	−2.985	0.05315	4.23

Table 4. Enthalpy Variations

		$\Delta H_{T_{o-d}}^{T_{fus}}$ [c]		$\Delta_{fus}H$ [d]		δ [e]		ΔH_{o-d} [f]		$\int_{T_{o-d}}^{T_{fus}} C_p\,dT$ [g]
n_c [a]	M [b]	J·mol^{-1}	J·g^{-1}	J·mol^{-1}	J·g^{-1}	J·mol^{-1}	J·g^{-1}	J·mol^{-1}	J·g^{-1}	J·mol^{-1}
1	16.0426	940	58.6	940	58.6					
2	30.0694	2859	95.1	2859	95.1					
3	44.0962	3527	80.0	3527	80.0					
4	58.123	4661	80.2	4661	80.2					
5	72.1498	8395	116.4	8395	116.3					
6	86.1766	13124	152.3	13124	152.3					
7	100.2034	14024	140.0	14024	140					
8	114.2302	20720	181.4	20720	181.4					
9	128.257	22380	174.5	15453	120.5	6927	54.0	6280	49	647
10	142.2838	28687	201.6	28687	201.6					
11	156.3106	32900	210.5	22158	141.7	10742	68.7	6858	44	3884
12	170.3374	36800	216.0	36800	216.0					
13	184.3642	41992	227.8	28474	154.4	13518	73.3	7661	41.6	5857
14	198.391	45027	227.0	45027	227.0					
15	212.4178	50900	239.6	34560	162.7	16340	76.9	9167	43	7173
16	226.4446	53307	235.4	53307	235.4					
17	240.4714	59452	247.2	40124	166.8	19328	80.4	10945	45.5	8383
18	254.4982	61573.5	241.9	61573	241.9					
19	268.525	65500	243.9	43750	162.9	21750	81.0	13780	51	7970
20	282.5518	69440.5	245.8	69440	245.8					
21	296.5786	72962.5	246.0	46851	158.0	26111	88.0	15992	54	10119
22	310.6054	77622	249.9	48959	157.6	28663	92.3	28204	91	459
23	324.6322	82506	254.2	53115	163.6	29391	90.5	21630	67	7761
24	338.659	88353.5	260.9	54450	160.8	33903	100.1	31400	93	2503
25	352.6858	90669.5	257.1	57248	162.3	33421	94.8	26285	75	7136
26	366.7126	97498.5	265.9	59752	162.9	37746	102.9	32861	90	4885
27	380.7394	96650	253.8	60417	158.7	36233	95.2	26568	69.8	9665
28	394.7662	102215	258.9	64643	163.7	37572	95.2	35438	89.8	2134
29	408.793	103805	253.9	66107	161.7	37698	92.2	29706	72.7	7992
30	422.8198	108909	257.6	66441	157.1	42468	100.4	36986	87.5	5482
				$36 \leq n_c \leq 60$ mean values of other literature data (Table 1)						
36	506.9806	134000	264.3	87682	172.9	46318	91.4	31071	61.3	15247
38	535.0342	133223	249.0							
40	563.0878	149547	265.6	135547	240.7	14000	24.9	14000	24.9	
44	619.195	167841	271	149641	241.5	18200	29.4	18200	29.4	
46	647.2486	175992	272.0	175992	272.0					
50	703.3558	171100	239.7	171100	239.7					
60	843.6238	193228	230.0	193228	230.0					

[a] Carbon atom number. For $5 \leq n_c \leq 18$, the values of Messerly et al.[92] are shown. For $18 \leq n_c \leq 25$, the mean values of the experimental data of Schaerer et al.[14,127] and Barbillon et al.[99] are shown. For $n_c = 26$, the mean values of the data of Schaerer et al.[14,127] and Barbillon et al.[99] and Andon et al.[118] are shown. For $27 \leq n_c \leq 29$, the data of Schaerer et al.[14,127] are shown. For $n_c = 30$, $\Delta H_{T_{o-d}}^{T_{fus}}$ is the value of Schaerer et al.[14,127] and $\Delta_{fus}H$ and ΔH_{o-d} are the mean values of the literature data. [b] Molecular mass. [c] Enthalpy variation from the order−disorder solid−solid transition temperature, T_{o-d}, up to the melting temperature, T_{fus} ($\Delta H_{T_{o-d}}^{T_{fus}} = \Delta H_{o-d} + \int_{T_{o-d}}^{T_{fus}} C_p\,dT + \Delta_{fus}H$). [d] Melting enthalpy. [e] Enthalpy difference between the enthalpy variation from T_{o-d} up to T_{fus} and the melting enthalpy $\Delta_{fus}H$ ($\delta = \Delta H_{T_{o-d}}^{T_{fus}} - \Delta_{fus}H$). [f] Order−disorder transition enthalpy. [g] Enthalpy variation in disordered phases ($\int_{T_{o-d}}^{T_{fus}} C_p\,dT = \delta - \Delta H_{o-d}$).

an alternation between the even-numbered and odd-numbered C_n's, particularly for numbers of carbon atoms n_c lower or equal to 20 carbon atoms: this alternation is observable in Table 2 column 5, in which the melting enthalpies are given in Joules per gram. For the odd-numbered C_{2p+1}'s with $13 \leq 2p + 1 \leq 35$ and the even-numbered C_{2p} with $22 \leq 2p \leq 36$, the average values of experimental melting enthalpies (disordered solid → liquid) converge to a mean value equal to 165 ± 8 J·g^{-1} (Tables 2 and 4).

The explanation of that alternation is due to the difference of the crystalline structure of the solid phase—stable just below the melting point—between the odd-numbered C_{2p+1}'s and the even-numbered C_{2p}'s ($2p \leq 20$). Indeed, according to the solid phase sequence when the temperature increases (cf. C_n Structural Behavior versus Temper-

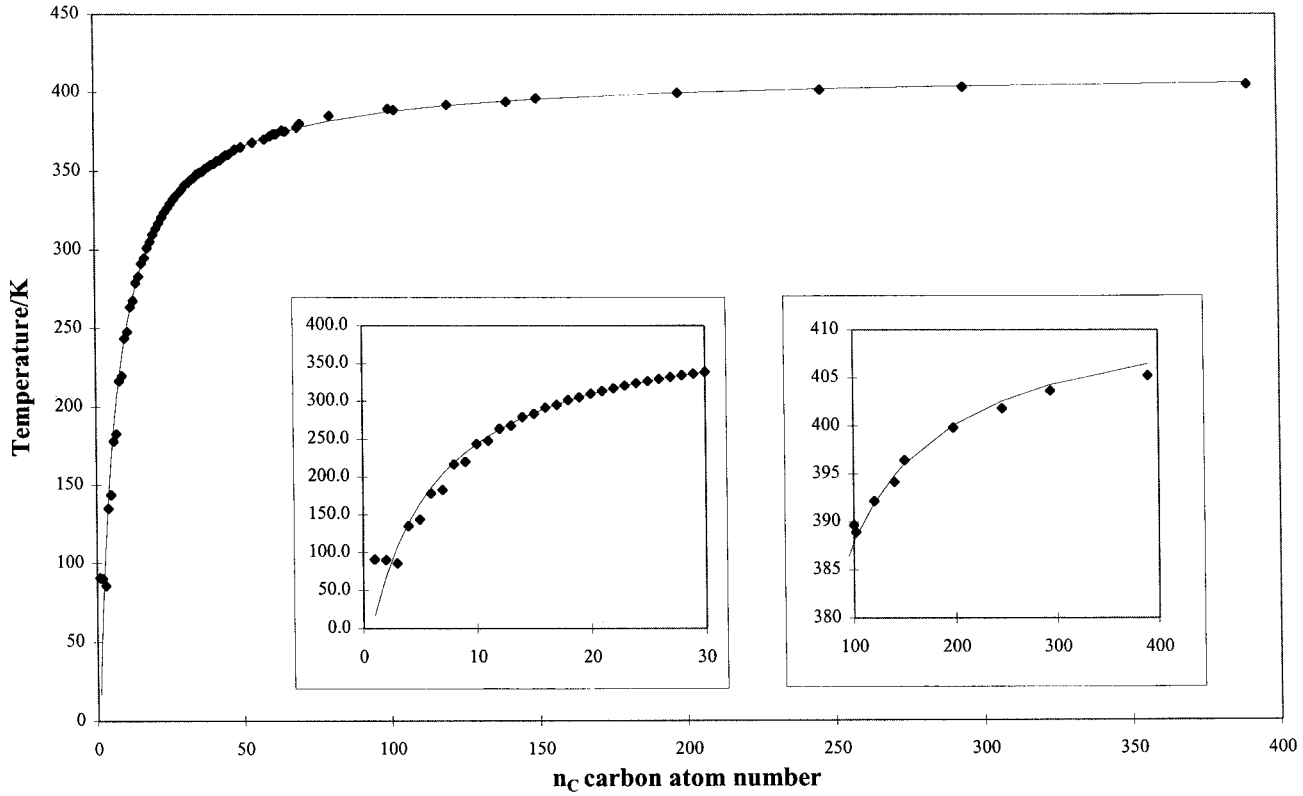

Figure 11. Melting points of pure C_n's: comparison between the mean values of the literature data (±0.5 K) and the calculated values from 1-Broadhurst's model[130] (all C_n; $n_c \geq 17$).

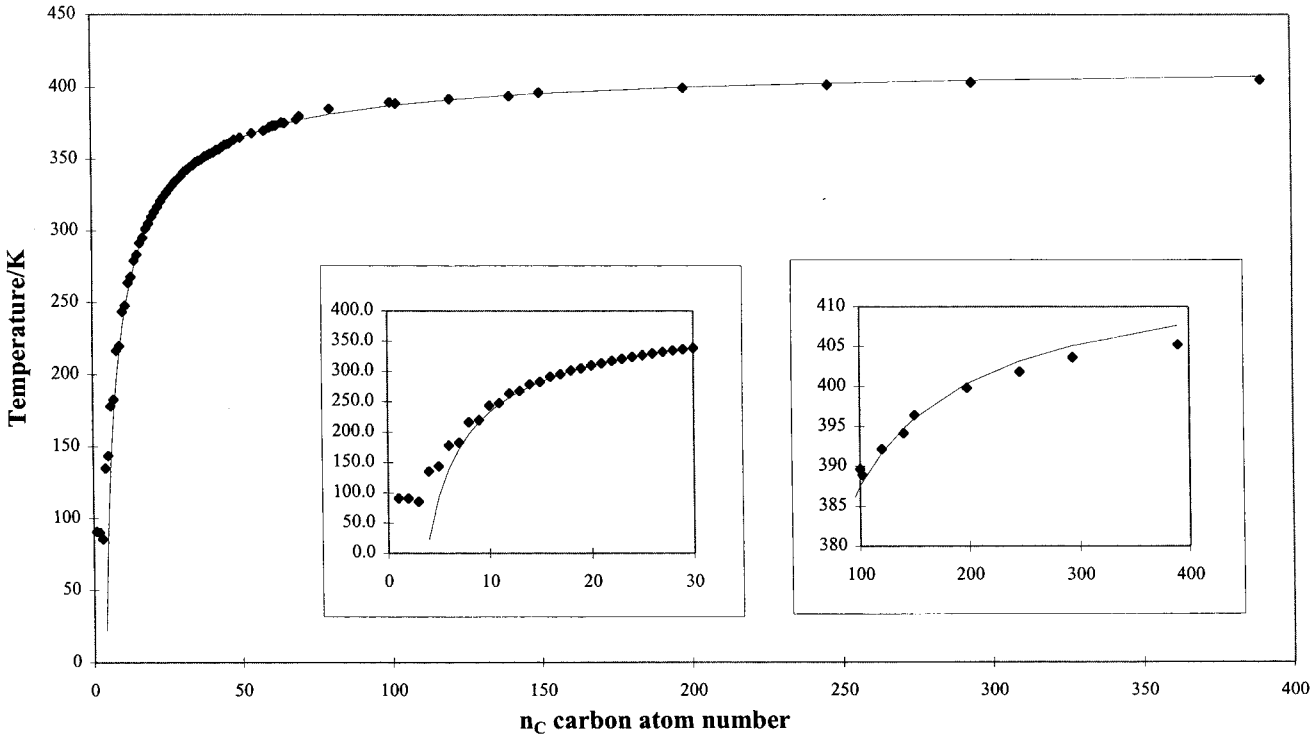

Figure 12. Melting points of pure C_n's: comparison between the mean values of the literature data (±0.5 K) and the calculated values of 2-Broadhurst's model[130] (all C_n's; $n_c \geq 17$).

ature and Figure 10), the solid−liquid equilibria are as follows: (i) for the even-numbered C_{2p} ($2p \leq 20$), $\gamma_0(C_{2p})$−$P\bar{1}$ triclinic ordered phase → liquid and (ii) for the odd-numbered C_{2p+1} ($9 \leq 2p + 1 \leq 19$), $\beta(Fmmm)$−RI orthorhombic disordered phase → liquid.

The o−d transition enthalpy and the consumption of the enthalpy, when the temperature increases in the $\beta(Fmmm)$ disordered phase—which moreover is seen to be in the rotator RI state—are certainly responsible for the alternation between the even- and odd-numbered C_n's ($n \leq 20$).

Thus, the study of the enthalpy variation (hereafter denoted $\Delta H_{T_{o-d}}^{T_{fus}}$) between the ordered phases and the liquid phase of pure C_n's is of major interest and most useful for

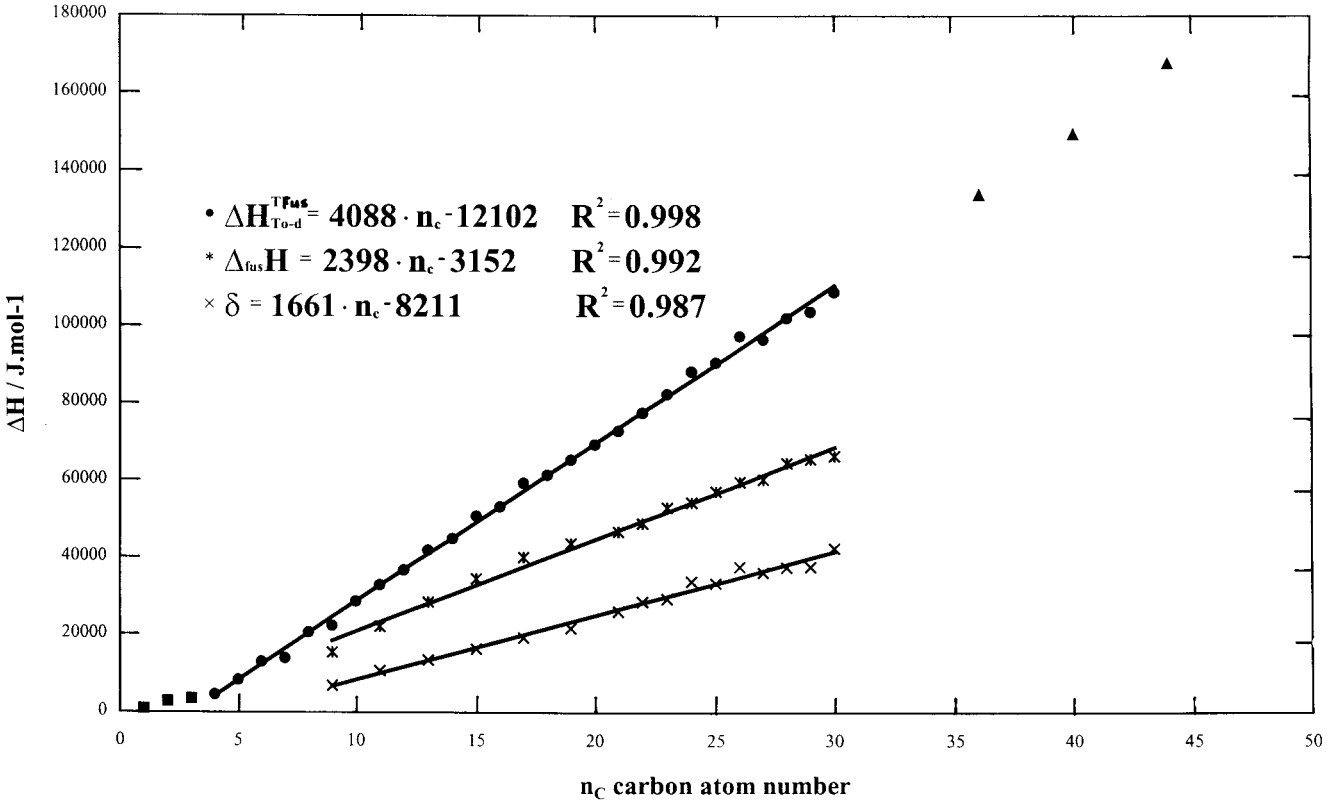

Figure 13. Enthalpy variation as a function of the n_c carbon atom number: $\Delta H^{T_{fus}}_{T_{o-d}}$, the enthalpy variation from the ordered phase at the o−d transition temperature up to the liquid at the melting temperature of pure C_n's (ordered phase → liquid) [The corresponding values of C_{36}, C_{40}, and C_{44} are brought into alignment with the variation line $\Delta H^{T_{fus}}_{T_{o-d}}$ versus n_c. $\Delta H^{T_{fus}}_{T_{o-d}} = \Delta_{fus}H$ for $n_c = 2p \leq 20$ and $n_c = 2p + 1 \leq 7$]; (∗) $\Delta_{fus}H$, the melting enthalpy variation from the disordered phase (disordered phase → liquid); (×) $\delta = \Delta H^{T_{fus}}_{T_{o-d}} - \Delta_{fus}H$, corresponding to the sum of the ΔH_{o-d} o−d transition enthalpy and the enthalpy variation in the range of the disordered phases ($\int_{T_{o-d}}^{T_{fus}} C_p \, dT$).

the modeling of the thermodynamic behavior of the C_n mixtures.

The ($\Delta_{fus}H + \Delta H_{o-d}$) sum often appears in the literature. However, this sum does not have any physical meaning, because the enthalpy variation $\int_{T_{o-d}}^{T_{fus}} C_p \, dT$ in the temperature range of disordered phases between T_{o-d} and T_{fus} is not taken into account; nevertheless, that variation is important especially for the odd-numbered C_{2p+1}'s whose $\beta(Fmmm)$ disordered phase undergoes the rotator-RI second- or higher-order transition with enthalpy consumption and the disorder−disorder transition $\beta(Fmmm) \rightarrow \alpha(R\bar{3}m)$ (Figure 9 and Table 4).

The $\Delta H^{T_{fus}}_{T_{o-d}}$ enthalpy variations of Table 4 and Figure 13 are determined from (i) the self-consistent data of Messerly et al.,[92] for the C_n's whose n_c carbon atom numbers are in the 5−18 range, (ii) the mean values of the experimental data of Schaerer et al.[14,127] and Barbillon et al.[99] for $19 \leq n_c \leq 25$ and of Andon et al.,[118] Schaerer et al.,[14,127] and Barbillon et al.[99] for $n_c = 26$, and (iii) the data of Schaerer et al.[127] for $n_c = 27$, 28, 29, and 30.

$\Delta H^{T_{fus}}_{T_{o-d}}$ corresponds to the enthalpy variation between the ordered phase which is in equilibrium at the o−d transition temperature and the liquid at the melting point:

$$\Delta H^{T_{fus}}_{T_{o-d}} = \Delta H_{o-d} + \int_{T_{o-d}}^{T_{fus}} C_p \, dT + \Delta_{fus}H$$

For the even-numbered C_{2p}'s with $2p \leq 20$ and the odd-numbered C_{2p+1}'s with $2p + 1 \leq 7$, $\Delta H^{T_{fus}}_{T_{o-d}} = \Delta_{fus}H$, because the ordered phases of low temperatures are stable up to the melting point and the disordered phases do not appear in these C_n's.

The value of the $\Delta H^{T_{fus}}_{T_{o-d}}$ enthalpy increases linearly with respect to the n_c carbon atom number from $n_c = 4$ to 30 in an independent manner of the n_c parity (Figure 13). The same behavior occurs for the melting enthalpy values $\Delta_{fus}H$ when the fusion corresponds to the state change: disordered phase → liquid (Figure 13). The difference δ between the $\Delta H^{T_{fus}}_{T_{o-d}}$ and $\Delta_{fus}H$ values, when the o−d transition is observed, corresponds to the sum of the o−d transition enthalpy and the enthalpy variation in the disordered solid phases as a function of the temperature from the o−d transition temperature up to the melting point; this δ value also varies linearly with respect to the n_c carbon atom number (Figure 13).

The linear equations ($\Delta H = an_c + b$) of the variations of enthalpies as a function of the n_c atom carbon number are established by least-squares fitting, and the results are as follows:

(i) for $4 \leq n_c \leq 30$

$$\Delta H^{T_{fus}}_{T_{o-d}}/\mathrm{J \cdot mol^{-1}} = 4088 n_c - 12102$$

$$R^2 = 0.9982 \text{ (ordered solid} \rightarrow \text{liquid)}$$

for $n_c = 2p \leq 20$ and $n_c = 2p + 1 \leq 7$

$$\Delta H^{T_{fus}}_{T_{o-d}} = \Delta_{fus}H$$

(ii) for $9 \le n_c = 2p + 1 \le 29$ and $22 \le n_c = 2p \le 30$

$$\Delta_{fus}H/J\cdot mol^{-1} = 2398n_c - 3152$$
$$R^2 = 0.9916 \text{ (disordered solid} \rightarrow \text{liquid)}$$

and

$$\delta/J\cdot mol^{-1} = \Delta H_{o-d} + \int_{T_{o-d}}^{T_{fus}} C_p \, dT = 1661n_c - 8211$$
$$R^2 = 0.9869$$

For $n_c \ge 4$, the slopes of the three linear equations correspond to the increases of enthalpies per CH_2 group, respectively, for a signification level equal to $\alpha = 0.05$:

(4088 ± 60) J·mol^{-1}·(CH$_2$)$^{-1}$ for the $\Delta H_{T_{o-d}}^{T_{fus}}$ enthalpy variation from the ordered phase at T_{o-d} to the liquid at T_{fus} ($4 \le n_c \le 30$; $n_c = 2p \le 20$ and $n_c = 2p + 1 \le 7$; $\Delta H_{T_{o-d}}^{T_{fus}} = \Delta_{fus}H$)

(2398 ± 100) J·mol^{-1}·(CH$_2$)$^{-1}$ for the $\Delta_{fus}H$ melting enthalpy from the disordered solid phases ($22 \le n_c = 2p \le 30$ and $9 \le n_c = 2p + 1 \le 29$)

(1661 ± 90) J·mol^{-1}·(CH$_2$)$^{-1}$ for the δ sum of the ΔH_{o-d} order−disorder transition enthalpy and of the enthalpy variation in disordered solid phases

The b value on the ΔH axis at n_c equal to zero does not have any physical meaning, because for $n_c \le 4$ a breaking of the slope is observed in the $\Delta_{fus}H$ variations from butane for methane, ethane, and propane, whose $\Delta_{fus}H$ extrapolated values tend toward 0 for $n_c = 0$ ($n_c \le 4$; $\Delta_{fus}H = 1177n_c$) (Figure 13).

Rajabalee et al.[174,175] determined a relationship between the order−disorder transition enthalpy and the atom carbon number for the odd-numbered C_{2p+1}'s ($13 \le 2p + 1 \le 29$), as follows:

$$\Delta H_{o-d}/J\cdot mol^{-1} = 5441.8 - 462.273(2p + 1) + 46.18507(2p + 1)^2$$

Table 5 gives the average values of temperature and enthalpy data concerning the other solid−solid transitions of C_n's ($23 \le n \le 45$), respectively (i) the order−order transitions in the crystal phases of low temperatures (δ-transition, γ-transition, and β-transition) and (ii) the rotator−rotator transitions of the disordered phases of high temperatures.

Schaerer et al.,[14] Dreisbach et al.,[87] Company et al.,[104] Templin et al.,[111] Kern et al.,[116] Josefiak et al.,[120] and Jin et al.[126] (Appendix 2 in the Supporting Information) have highlighted by thermal analysis a solid−solid transition just below the o−d transition of C_{36} (T_{o-d} = 347 K) respectively at $T = 344.9 \pm 0.6$ K with an enthalpy equal to 9916 J·mol^{-1} (ref 14), 9916 J·mol^{-1} (ref 87), and 15 300 J·mol^{-1} (ref 126).

Takamizawa et al.[64] have carried out thermal and structural analyses on pure C_n's, obtained by synthesis processes (n_c = 48, 60, 61, 65, 69); at room temperature, their structure is orthorhombic with the $Pca2_1$ space group for the even-numbered C_{48} and the $Pbcm$ space group for the odd-numbered C_{61}, C_{65}, and C_{69}. They observed in these C_n's a solid−solid transition which leads to the appearance of the C monoclinic phase with the $A2$ space group, also denoted M_{101} in ref 30. The transitions occur at the following temperatures: 337.25 K for C_{48}, 355.05 K for C_{60}, 357.15 K for C_{61}, 360.65 K for C_{65}, and 362.55 K for C_{69}.

To sum up: (i) for the melting points of C_n's (T_{fus}), see Table 3; (ii) the C_n ($17 \le n_c \le 30$) enthalpy variations ($\Delta H_{T_{o-d}}^{T_{fus}}$) are 253.7 ± 10 J·g^{-1} for the ordered phase → liquid transition and $\Delta_{fus}H$ for n_c = 18 and 20; and (iii) the C_{2p+1} ($13 \le 2p + 1 \le 35$) and C_{2p} ($22 \le 2p \le 36$) melting enthalpies ($\Delta_{fus}H$) for the disordered phases → liquid transition are 165 ± 8 J·g^{-1}.

3. Model *n*-Alkane Mixtures

The term "model *n*-alkane mixtures" is applied to the synthetic mixtures, obtained from pure C_n's by the melting process; these mixtures are real molecular alloys with a thermodynamic behavior similar to those of metallic alloys and other organic component mixtures as described by Haget.[177]

The behavior of mixtures of C_n's obeys the laws of thermodynamics:

(i) Phase Stability. Intermediate solid solutions of mixture components appear if their Gibbs's energies are lower than those of the pure components. For instance, this rule has been applied to the binary mixtures of C_n's by Asbach and Killian.[146]

(ii) Miscibility in the Solid State. In the solid state, the components of mixtures can form a continuous homogeneous solid solution if they display the same crystalline solid phase; that means that the solid phases of the pure components must have the same crystalline structure and more particularly the same space group. Kitajgorodskij[55] applied this rule to the binary mixtures of C_n's. Reciprocally, if the components of a mixture do not have the same crystalline structure, characterized by the same space group, they cannot form a continuous homogeneous solid solution in the whole range of the concentrations, according to Gibbs's law of phases.

(iii) Size of Molecules. To that law is added a criterion concerning the difference between the lengths of C_n molecules, defined by Kravchenko[142] for their binary mixtures.

(iv) Thermodynamic Representation of Phase Equilibria. The phase equilibria of the first-order transitions in the multicomponent systems are described in the phase equilibrium diagrams which must respect the rule of adjacent equilibrium domains of Palatnik and Landau;[184] this rule is a consequence of the phase law of Gibbs.

In the literature, many phase diagrams appear which do not respect these elementary laws of the first-order thermodynamic equilibria of all pure or multicomponent physical systems. Moreover, the name of a solid phase does not change when this phase undergoes a second- or higher-order transition: For instance, the face centered cubic phase of nickel is always denoted α on both sides of Curie's temperature, and it is the same for the α body centered cubic phase of iron on both sides of the magnetic transition, because the group space of these phases does not change. In both cases, as far as the thermodynamics is concerned, these transitions do not correspond to phase changes of the first-order, and thus, the phase whose space group does not change keeps the same notation in order not to confuse the first-order transitions with the second- or higher-order transitions.

(A) Binary Systems of Consecutive C_n's ($\Delta n_c \le 2$). The first studies concerning the binary systems of C_n's were carried out by Piper et al.,[10,80] Kravchenko,[142] Kitajgorodskij,[55] and Smith[143] ($18 < n < 36$, particularly C_{24}/C_{26}). From the difference factor of the molecule lengths, Kravchenko[142] predicted (Table 6) the type of probable equilibria in the binary systems of C_n's. However, for mixtures which do not display a continuous solid solution according to Kravchenko's predictions ($\Delta n_c/n_c > 0.06$, Table 6), Kitajgorodskij[55] shows that, for low concentrations close

Table 5. Mean Values of the Literature Data of the Enthalpies (Relative Error 5%) and the Temperatures (±0.5 K) of Ordered−Ordered and Disordered−Disordered Phase Transitions

n_c	ref		δ−transition	γ−transition	β−transition	RI → RII	RIII → RIV
23	33	T/K	309.1			317.8	
	40	ΔH/J·mol^{-1}	320			320	
25	33	T/K	310.8	319.6		322	
	40						
	43	ΔH/J·mol^{-1}	350	350		350≤	
27	14	T/K	310.85	321			328.2
	24						
	38						
	43						
	78						
	102						
	109						
	123	ΔH/J·mol^{-1}	281	2370			
28	38	T/K					330.65
29	14	T/K	310.9	322.4			333.15
	38	ΔH/J·mol^{-1}	293	2594			
30	38	T/K					337.55
31	38	T/K		324.3	335.1		
	129						
33	28	T/K		327.15	338.1		
	38						
	43						
	48						
	49	ΔH/J·mol^{-1}		2092	4602		
37	64	T/K		330	339.6		
	129						
45	64	T/K		335.15	342.05		
	129						

Table 6. Miscibility of Binary *n*-Alkanes Mixtures (C_n/$C_{n'}$) versus Number Difference of Carbon Atoms in the Solid State at "Room Temperature" According to Kravchenko's Predictions[142]

$\Delta n_c = n_c - n'_c$	total miscibility	partial miscibility	no miscibility
1	$n_c > 16$[a]	$17 > n_c > 7$	$n_c < 8$
2	$n_c > 33$	$34 > n_c > 13$	$n_c < 14$
4	$n_c > 67$	$68 > n_c > 27$	$n_c < 28$

[a] In this case, if the two consecutive C_{2p} and C_{2p+1} do not have the same crystalline structure, they cannot form a continuous solid solution.

to pure C_n's, the binary mixtures, which consist of C_{18}, C_{19}, or C_{20}, form terminal solid solutions with a limited solubility which retain the structure of pure C_n's; moreover, Smith[143] highlighted the existence of orthorhombic intermediate solid solutions in these same binary systems of C_n's ($18 < n < 36$). Particularly in (C_{24}/C_{26}) mixtures with composition ratios 1/1 and 2/1, the structure of the pure C_{24} and C_{26} crystalline phase is triclinic according to Craig et al.[29] (Appendix 1 in the Supporting Information). From the observations and many results about the binary mixtures of C_n's, quoted in his monograph, Turner[53] suggested binary phase diagrams as a function of the parity and the Δn_c gap between n_c carbon atom numbers of chains of the two C_n's; however, these depictions proved incomplete afterward.

(1) Binary Mixtures of Consecutive C_n's ($\Delta n_c \leq 2$). The binary mixtures of C_n's have been the subject of numerous articles.[26,55,65,133,141−195,237,256,257] Many phase diagrams have been presented with an orthorhombic continuous solid solution at room temperature even if the two pure C_n's displayed a $(n_c - n_{c'})/n_c$ relative gap between the chain lengths of molecules which was too high, according to Kravchenko's rule (Table 6), and/or a triclinic or monoclinic phase not compatible with Palatnik and Landau's rule: for instance, (C_{18}/C_{20}; C_{19}/C_{21}; C_{21}/C_{23}; C_{22}/C_{23}; C_{22}/C_{24}; C_{24}/C_{26}; C_{30}/C_{35}; C_{35}/C_{36}),[144] (C_{21}/C_{23}),[255] (C_{19}/C_{21}),[170] (C_{24}/C_{28}).[194]

In 1974, Lüth et al.[145] published the (C_{20}/C_{22}) phase diagram and established the existence of (i) two limited terminal solid solutions with the triclinic structures of pure γ(C_{20}) and γ(C_{22}) and (ii) three orthorhombic intermediate solid solutions, two of which are indistinguishable by X-ray diffraction on both sides of the third, situated near the central region of the phase diagram.

Then Hasnaoui et al.[65] also highlighted three orthorhombic intermediate phases in the (C_{22}/C_{24}) system; Achour et al.[149,150,152] showed the similarity between the (C_{20}/C_{22}) phase diagram of Lüth et al.[65] and those of both of the (C_{22}/C_{24})[149,150,152] and (C_{24}/C_{26}) systems determined by Achour-Boudjema et al.[154,157] At the same time, Gerson and Nyburg[24] determined the structure of one of these intermediate phases of the C_{24}/C_{26} system: orthorhombic space group $Bb2_1m$

From the structural observations of Smith[143] and Gerson and Nyburg[26] and the phase diagrams determined by Lüth et al.[145] (C_{20}/C_{22}), by Achour et al.[149,150] (C_{22}/C_{24} and C_{24}/C_{26}),[154,157] by Denicolo et al.[168] and Nouar et al.[165] (C_{22}/C_{23}), by Nouar et al.[164] (C_{23}/C_{24}), and by Jouti et al.[155,156,162,163] (C_{21}/C_{23} and C_{23}/C_{25}), Dirand et al.[159,160] established a generalization of the thermodynamic and structural behavior of the binary mixtures of consecutive C_n's ($\Delta n_c \leq 2$) ($20 \leq n_c \leq 26$) as follows.

(i) At room temperature, limited terminal solid solutions with the pure C_n crystalline structure exist for the concentrations close to two pure C_n's, and two ($\Delta n_c = 1$) or three orthorhombic intermediate solid solutions ($\Delta n_c = 2$) appear when the concentration varies; these intermediate phases are respectively denoted β'_{1or2} and β''_{1or2}. In all the binary systems, the β' phases are indistinguishable and thus they are isostructural. It is the same for all the β'' phases. The index (1 or 2) corresponds to two isostructural phases of different stoichiometries on both sides of

Table 7. Sequences of the Solid Solution Domain versus the Concentration of the Longer C_n in the Binary Systems of Consecutive (Even/Odd), (Even/Even), and (Odd/Odd) C_n's at "Low Temperature"[a]

terminal solid solutions	intermediate solid solutions	terminal solid solutions
	$\Delta n_c = 1$; Even−Numbered and Odd-Numbered *n*-Alkanes	
$\gamma_0(C_{2p})$	/.../β'_1/.../β''_1/.../	$\beta'_0(C_{2p+1})$/.../$\beta'_0(C_{2p+1})$
n-$C_{2p}H_{4p+2}$	x(*n*-C_{2p+1})	*n*-$C_{2p+1}H_{4p+4}$
$\beta_0(C_{2p-1})$/.../$\beta'_0(C_{2p-1})$	/.../ β''_1/.../β'_1/.../	$\gamma_0(C_{2p})$
n-$C_{2p-1}H_{4p}$	x(*n*-C_{2p})	*n*-$C_{2p}H_{4p+2}$
	$\Delta n_c = 2$; Two Even−Numbered *n*-Alkanes	
$\gamma_0(C_{2p})$	/.../β'_1/.../β''_1/.../β'_2/.../	$\gamma_0(C_{2p+2})$
n-$C_{2p}H_{4p+2}$	x(*n*-C_{2p+2})	*n*-$C_{2p+2}H_{4p+6}$
	$\Delta n_c = 2$; Two Odd-Numbered *n*-Alkanes	
$\beta_0(C_{2p-1})$/.../$\beta'_0(C_{2p-1})$	/.../β''_1/.../β'_1/.../β''_2/.../	$\beta'_0(C_{2p+1})$/.../$\beta_0(C_{2p+1})$
n-$C_{2p-1}H_{4p}$	x(*n*-C_{2p+1})	*n*-$C_{2p+1}H_{4p+4}$
	For Instance	
n-$C_{22}H_{46}$	/.../β'_1/.../β''_1/.../	*n*-$C_{23}H_{48}$
n-$C_{23}H_{48}$	/.../β''_1/.../β'_1/.../	*n*-$C_{24}H_{50}$
n-$C_{22}H_{46}$	/.../β'_1/.../β''_1/.../β'_2/.../	*n*-$C_{24}H_{50}$
n-$C_{23}H_{48}$	/.../β''_1/.../β'_1/.../β''_2/.../	*n*-$C_{25}H_{52}$

[a] /.../ designates two-phase regions.

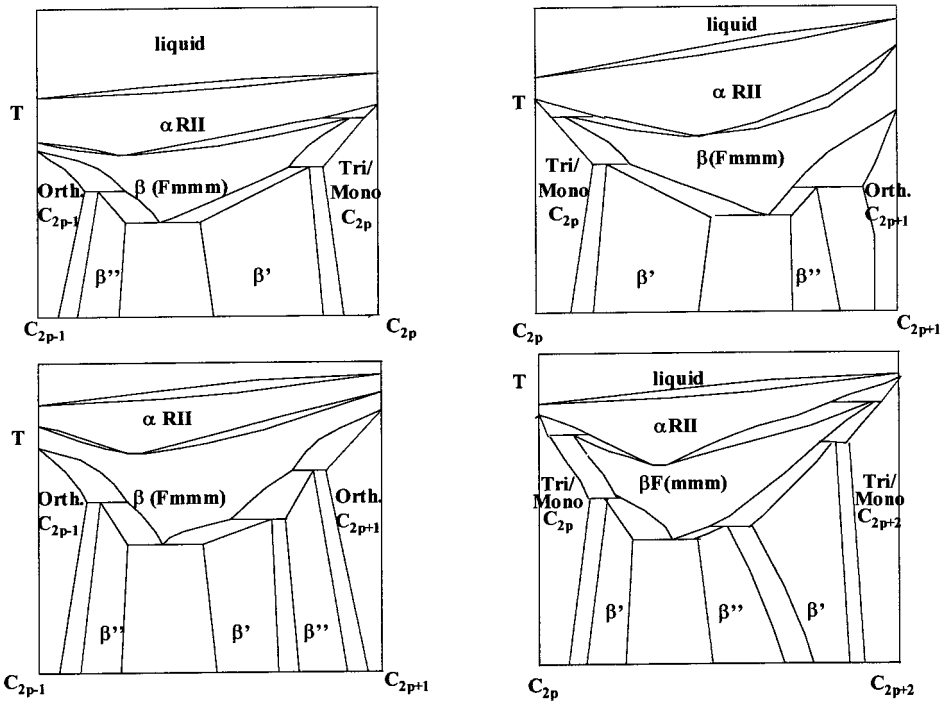

Figure 14. General behavior of binary diagrams of two-consecutive C_n's ($\Delta n_c \leq 2$).

the third in the same binary system (Table 7 and Figure 14).

All the previous results of the literature have allowed the latter authors, Dirand et al.,[158,160] to determine the following rules of the solid-phase sequences at "low temperature" when the second C_n concentration increases.

(i) from an even C_{2p}: $\gamma_0(C_{2p})$, β'_1, β''_1

(ii) from an odd C_{2p+1}: $\beta_0(C_{2p+1})$, $\beta'_0(C_{2p+1})$, β''_1, β'_1

(iii) On the one hand the structural behavior is "symetrical" on both sides of the last intermediate phase of the above sequences if the solute C_n has the same parity ($\Delta n_c = 2$) as the solid solvent (Table 7). This structural behavior is normal because the second C_n becomes the solvent beyond the last intermediate phase and the rule of the solid-phase sequences is applied in the inverse direction. For instance, in the system (C_{22}/C_{24})[149,150] (Table 7), this sequence is $\gamma_0(C_{22})$, β'_1, β''_1, β'_2, $\gamma_0(C_{24})$ when the C_{24} molar concentration increases. It is the same for the binary system (C_{24}/C_{26})[154,157] (Tables 6 and 7). In the system (C_{23}/C_{25}),[155,162] the sequence is $\beta_0(C_{23})$, $\beta'_0(C_{23})$, β''_1, β'_1, β''_2, $\beta_0(C_{25})$, $\Delta n_c = 2$ (Table 7).

On the other hand, if the two *n*-alkanes do not have the same parity ($\Delta n_c = 1$), the terminal solid solutions of the second C_n appear next to the last intermediate phase of the above sequences (Table 7). For example, in the system (C_{22}/C_{23}),[165] the sequence is $\gamma_0(C_{22})$, β'_1, β''_1, $\beta'_0(C_{23})$, $\beta_0(C_{23})$. In the system (C_{23}/C_{24}),[164] the sequence is $\beta_0(C_{23})$, $\beta'_0(C_{23})$, β''_1, β'_1, $\gamma_0(C_{24})$; this sequence is the opposite of the above sequence.

According to Palatnik and Landau's rule,[184] a two-phase domain is always adjacent to each single-phase domain,

characterized by its crystalline structure (Table 7 and Figure 14).

(ii) When the temperature increases, all the intermediate phases β'_n and β''_n undergo the same solid−solid transitions as the pure C_{23} above its transition δ up to their melting point. The solid-phase sequence from "low" to "high temperatures" for the β'_n or β''_n phases corresponds to the following diagram:

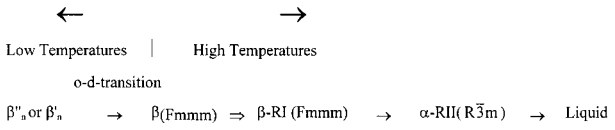

where → corresponds to the first-order transitions and ⇒ to second- or higher-order transitions.

Figure 14 shows the binary phase diagram types of (odd/even), (odd/odd), and (even/even) C_n's ($\Delta n_c \leq 2$). All the intermediate phases β'_n or β''_n undergo peritectoid decompositions when the temperature increases (Figure 14).

(i) The first intermediate phases which appear next to the terminal solid solutions undergo the following decompositions:

in the systems (even/even) or (even/odd)

$$\beta'_{1or2} = \gamma_0 + \beta(Fmmm)$$

in the systems (odd/odd) or (odd/even)

$$\beta''_{1or2} = \beta'_0 \text{ or } \beta_0 + \beta(Fmmm)$$

(ii) The second intermediate phases display the following transformations:

in the systems [even/even]

$$\beta''_1 = \beta'_2 + \beta(Fmmm)$$

in the systems [odd/odd]

$$\beta'_1 = \beta''_2 + \beta(Fmmm)$$

In the RI state of the $\beta(Fmmm)$ phase, the ratio of the parameters b/a increases with increasing temperature as in the odd-numbered pure C_{23} or C_{25}. Next, when the subcell is hexagonal ($b/a = \sqrt{3}$), the mixtures undergo a further weak first-order transition into the rotator phase α-RII ($R\bar{3}m$), just a few degrees below the solidus line. This transition extricates a very small enthalpy effect according to Achour et al.,[187] Jouti et al.,[188] and Srivastava et al.[189] and leads to a two-phase domain ($\beta(Fmmm)$ + α-RII); when the phase $\beta(Fmmm)$ does not exist in the pure C_n, the latter undergoes the following peritectoid decomposition (β-$(Fmmm)$ = terminal solid solution (C_n) + α-RII) or peritectic melting ($\beta(Fmmm)$ = liquid + α-RII). The binary mixtures can form continuous homogeneous disordered solution domains at "high temperature" below the solidus line, provided the same disordered phase ($\beta(Fmmm)$ or α-RII) exists in the two pure C_n's.

With decreasing temperature from the "low temperature" domain, the intermediate phases β'_n and β''_n may undergo eutectoid decompositions:

in the systems (even/even)[149,150,152,154,157]

$\beta'_{1or2} = \gamma_0 + \beta''_1$ then

$$\beta''_1 = \gamma_0(n - C_{2p}) + \gamma_0(n - C_{2p+2})$$

in the systems (odd/odd)[155,156,162,163]

$\beta''_{1or2} = \beta_0 + \beta'_1$ then

$$\beta'_1 = \beta_0(n - C_{2p-1}) + \beta_0(n - C_{2p+1})$$

All these solid−solid transitions of equilibrium are explained by solid-state diffusion, especially studied by Yamamoto and Nozaki[171] in the (C_{21}/C_{23}) system.

(B) Particular Observations. (i) The structural behaviors of the two phase diagrams (C_{2p-1}/C_{2p} and C_{2p}/C_{2p+1}) are "symetrical" in relation to the pure even-numbered C_{2p}'s (Figure 14).

(ii) The phase diagram of two consecutive even-numbered C_{2p}'s (C_{2p}/C_{2p+2}) or odd-numbered C_{2p+1}'s (C_{2p-1}/C_{2p+1}) has a "symetrical" behavior on both sides of the intermediate phase, β'' or β', respectively (Figure 14).

(iii) The phase diagram (C_{2p-1}/C_{2p+1}) (Figure 14) can be described as the addition of the two diagrams (C_{2p-1}/C_{2p}) + (C_{2p}/C_{2p+1}) when the terminal solid solutions of the even-numbered C_{2p}'s have been eliminated.

(iv) It is the same for the diagram (C_{2p}/C_{2p+2}) as for the two phase diagrams (C_{2p}/C_{2p+1}) + (C_{2p+1}/C_{2p+2}) with the deletion of the terminal solid solution of the odd-numbered C_{2p+1}'s.

Recently, these rules of the structural and thermodynamic behavior of the binary mixtures of consecutive C_n's ($\Delta n_c \leq 2$) established by Dirand et al.[158,160] have been confirmed by Metivaud et al.[176] (C_{21}/C_{22}) and by Rajabalee et al.[174,175] (C_{26}/C_{28} and C_{23}/C_{25}). These rules can be extended to other C_n binary systems ($\Delta n_c \leq 2$, $n_c < 20$, or $n_c > 28$) as Metivaud et al.[172] showed in (C_{18}/C_{19}) mixtures. All the latter authors[172−176] described in detail these complex binary phase diagrams, gave further details about the structures of the intermediate solid solutions, and suggested the following space groups: monoclinic *Aa* for β'_n (the crystalline parameters of this unit-cell, with the β angle almost equal to $\pi/2$, correspond to a orthorhombic unit-cell which would undergo a very low distortion) and orthorhombic $Pca2_1$ for β''_n.

Achour et al.[186,187] and Jouti et al.[188] measured the variations of thermodynamic functions versus temperature for various molar concentrations, respectively in (C_{24}/C_6) and (C_{23}/C_{25}) systems. Srivastava et al.[189] determined by differential scanning calorimetry the solid−solid and solid−liquid transition enthalpies of different binary mixtures of C_{24} with other C_n's.

(C) Other Binary ($\Delta n_c > 2$), Ternary, Quaternary, and Quinary Systems. (1) Binary ($\Delta n_c > 2$) Systems. One intermediate solid solution is still observed for binary mixtures of C_n's with $\Delta n_c = 4$, for instance, in C_{22}/C_{26} and C_{24}/C_{28} systems. When the difference of the C_n chain length is too high according to Kravchenko's rules (Table 6), the binary phase diagram displays partial miscibility or no miscibility with eutectic[55,181,189,190,232,256,257] or peritectic[192] solidification, as forseen by Turner.[53]

(2) Ternary, Quaternary, and Quinary Systems. Nouar et al.[193,258] showed that the same intermediate solid solutions β'_n and β''_n are also present in ternary molecular alloys of consecutive C_n's ($C_{22}/C_{23}/C_{24}$, Figure 15). As a function of the composition at room temperature, single-phase domains are adjacent to two-phase or three-phase regions (Figure 15).

Craig et al.[248] examined ternary, quaternary, and quinary mixtures of consecutive C_n's ($18 \leq n_c \leq 26$). They observed the existence of an only solid solution in the molecular alloys which they studied by high-resolution synchrotron X-ray powder diffraction. Orthorhombic (room

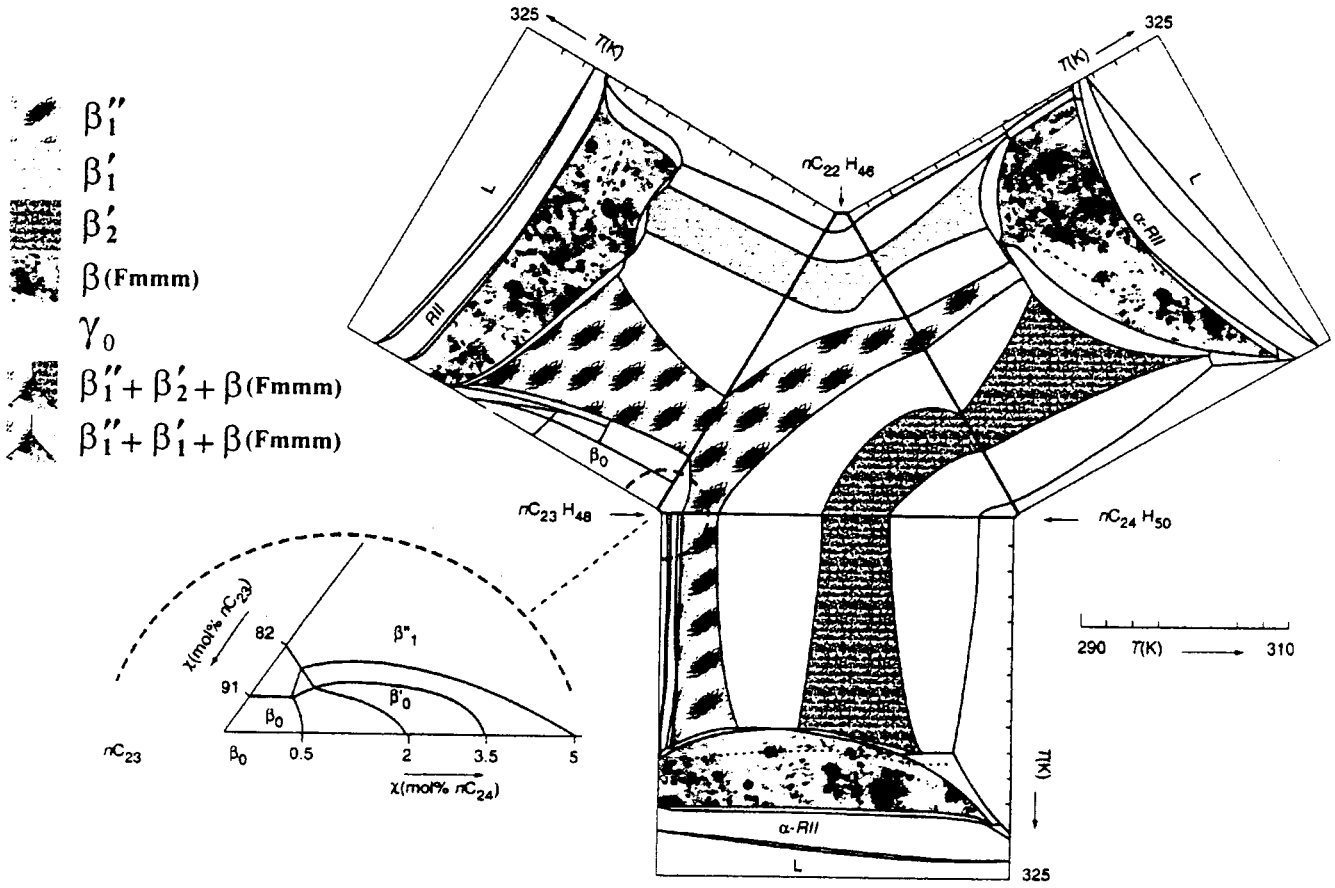

Figure 15. Ternary isothermal section at 298 K of the ($C_{22}/C_{23}/C_{24}$) system.

temperature) and hexagonal (high temperature) solid solutions were observed by Clavell-Graunbaum et al.[195] in several model waxes consisting of two, three, and four C_n's with chain length differences of four carbons between their components.

(3) Molecule Conformational Defects in Multicomponent Solid Solutions. Craig et al.[248] determined the crystalline parameters and the unit-cell volumes of molecular alloy solid solutions. They found that their unit-cell volume was higher than that of the pure C_n with a chain length close to the mean length of the mixture. Nouar et al.[193] and Dirand et al.[243] calculated the mean carbon atom number, n_c, of solid solutions from the measurements of the crystalline long *c*-parameter, using the relationship established by Chevallier et al.[76] for the orthorhombic (*Pbcm*) pure C_n's, and came to the following conclusion: the molecule packing identity *c*-period of solid solutions corresponds to that of a hypothetical pure C_n with n_c number of carbon atoms equal to the $\bar{n}$ average composition in carbon atoms of mixtures. n_c always displays an excess value in relation to $\bar{n}$:

$$n_c = \frac{(c/\text{Å}) - 3.7504}{2.5448}$$

$$\bar{n} = \sum_{n_{min}}^{n_{max}} n x_n$$

where x_n is the molar fraction of each C_n and n_{max} and n_{min} are the carbon atom numbers of the longest and smallest C_n chains, respectively, in the mixture.

The excess value (volume for Craig et al.[248] or n_c for Dirand et al.[243]) in relation to that for the pure C_n's is very likely due to the conformational disorder of chain packing in the binary, ternary, quaternary, or quinary crystalline solid solutions such as described by Kim et al.,[37] Maroncelli et al.,[170] and Clavell-Grunbaum et al.:[195] these are *end-gauch* type defects (...ttg or ...tgt; Figure 7a of Snyder et al.[43]) which especially modify the longer C_n's of mixtures; for instance all the chains of C_{21} or C_{50} for low concentrations in the C_{19}/C_{21} and C_{46}/C_{50} mixtures display at least one *gauch* connection (Kim et al.[37] and Maroncelli et al.[170]).

The β'_n and β''_n intermediate solid solutions of binary, ternary, quaternary, quinary, and ... mixtures of C_n's can be distinguished by a different sequencing of those conformational defect types.

(D) Solubility of Heavy Pure C_n's and Their Binary Model Mixtures in Organic Solvents. (1) Heavy Pure C_n and Light Solvent. Solubility studies of the heavy pure C_n's in light solvents were described in the literature, for instance by Couthino et al.,[197] Provost et al.,[198,199] Ghogomu et al.,[200−205] Chang et al.,[206] Arenosa et al.,[207] Domanska et al.,[208−210] Ksiazczak et al.,[108,121] Madsen and Boistelle,[211] Floter et al.,[212] Buchowski et al.,[213] and Mahmoud et al.[214,215] These binary systems of C_n's, which have a high difference of chain length between the *heavy solute* and *light solvent*, respect Kravchenko's rules about their solubility for the solid state and display phase diagrams with no miscibility in the solid phase and eutectic solidification[198,199,208,211] (Figure 16):

(i) The liquidus curve corresponds to the solubility limit variation in the liquid phase as a function of concentrations and temperatures.

(ii) The eutectic point is situated close to the light pure solvent.

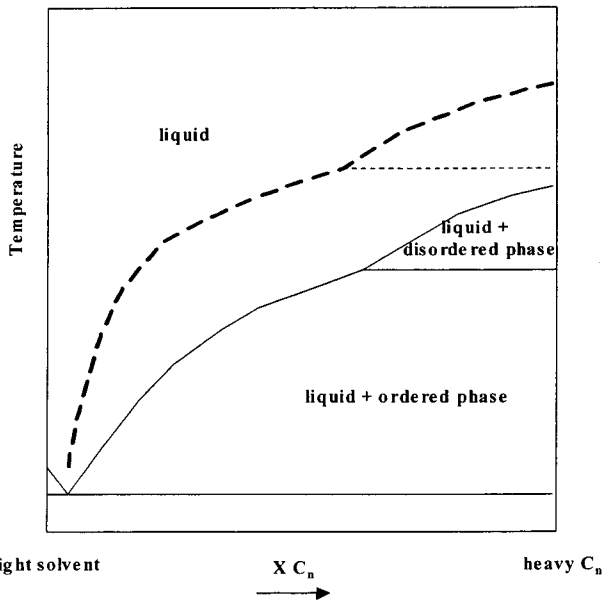

Figure 16. General behavior of solutions which consist of a light solvent (linear, cyclic, aromatic) and a pure heavy C_n (eutectic crystallization) or a binary, ternary, ..., or multinary intermediate solid solution of heavy C_n's ("pseudobinary" eutectic crystallization): In the same solvent, the solubility limit (- - -) of a higher C_n or a heavier intermediate solid solution decreases.

(2) Influence of the Solvent Concentration. Whatever the solvent or the heavy C_n, two behaviors are observed, depending on the solvent concentrations (Figure 16): (i) In the rich region of the heavy C_n, the solid, which forms the first deposit, is the disordered phase of the heavy pure C_n: at the solubility limit of the heavy C_n in the liquid on the liquidus curve, the equilibrium is (liquid + disordered solid phase). Then for these low light solvent concentrations, the o-d transition temperature, observed and measured by differential scanning calorimetry and simple thermal analysis with decreasing or increasing temperature is always equal to that of the heavy pure C_n according to Provost et al.[198] (Figure 16). That indicates that only the pure heavy C_n crystallizes.

(ii) When the concentration of the light solvent increases, the solid deposit corresponds to the triclinic $\gamma_0(C_{2p})$ or orthorhombic $\beta_0(C_{2p+1})$ "low temperatures" ordered phase of the pure even-numbered C_{2p} or odd-numbered C_{2p+1}, respectively. For the diluted solutions the solubility limit corresponds to the equilibrium (liquid + ordered phase) (Figure 16).

(3) Influence of the Chain Length. For the same light solvent, solubility decreases when the number of carbon atoms of the heavy C_n chain increases (Figure 16) according to Domanska and Rolinska[210] (C_{20}, C_{24}, C_{26}, and C_{28} in pure hydrocarbons), Provost et al.[198] (C_{23}, C_{25}, C_{26}, and C_{28} in C_7), and Madsen and Boistelle[211] (long-chain *n*-paraffins in C_5 and C_7).

(4) Influence of the Nature of the Solvent. Provost et al.[198,199] carried out solubility measurements for solutions of the same heavy C_n in one of three linear, aromatic, and cyclic solvents containing seven carbon atoms (heptane, toluene, and methylcyclohexane): their results indicate that the nature of the solvent has no major influence on the solubility, except for the very diluted solutions for which the liquidus curves are discriminated as a function of the difference of the melting points of solvents.

All these results[198,199,210] are in agreement with the research work of Chang et al.,[206] Arenosa et al.,[207] Domanska et al.,[208,209] Ksiazczak et al.,[101] Madsen et al.,[211] and Ghogomu et al.[202−205]

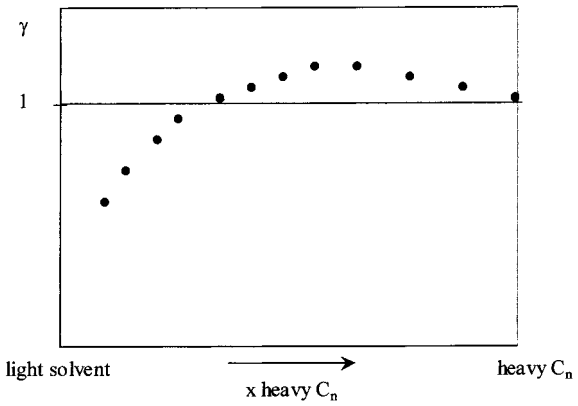

Figure 17. Variations of the γ activity coefficient of a heavy C_n in liquid solution in a light C_n versus molar concentration: (γ < 1) liquid + ordered phase of the heavy C_n equilibrium; (γ > 1) liquid + disordered phase of the heavy C_n equilibrium.

The liquidus curve (Figure 16) can be calculated by models: the use of the ideal solution model is not appropriate to represent the experimental results, whereas the application of the expression of Buchowski et al.,[213] for instance, gives good results for the binary systems C_{23}, C_{25}, C_{26}, or C_{28} in C_7.[199] Moreover, Provost et al.[198] have calculated the activity coefficients γ of C_{26} and C_{28}, in the liquid solution, for the binary systems C_{26}/C_7 and C_{28}/C_7, using the standard thermodynamic relationship for equilibrium between a pure solid component and a liquid.

$$\gamma = \frac{1}{x}\exp\left(-\frac{\Delta G(T)}{RT}\right)$$

where x = the molar composition of the liquid, T = the equilibrium temperature, $\Delta G(T)$ = the melting Gibbs energy, R = the universal gas constant.

The evolution of the activity coefficient versus composition for these system types is represented in Figure 17 and shows an atypical behavior: (i) γ < 1 for higher C_7 solvent concentrations which correspond to the equilibrium (liquid + ordered phase of the heavy C_n) and (ii) γ > 1 for low C_7 concentrations which correspond to the equilibrium (liquid + disordered phase of the heavy C_n). This phenomenon indicates a trend to association for low heavy C_n concentrations and to demixion for higher concentrations.

Similar phase diagrams with eutectic solidification were also determined for other binary systems by Ghogomu et al.[200] (C_{22}, C_{23}, or C_{24} + ethylbenzene) and by Mahmoud et al.[214,215] (C_{18}, C_{28}, C_{30}, C_{36}, or C_{50} + pyrene and C_{21}, C_{25}, C_{28}, or C_{36} + dibenzofurane or xanthene). An atypical behavior also leads to γ activity coefficients higher than 1 in these binary mixtures.[214,215]

(5) Binary Mixtures of Heavy C_n's and Light Solvent. The solubility of the binary model mixtures of heavy C_n's in light solvents was studied by Provost et al.[198] (C_{26}/C_{28} + C_7), Ghogomu et al.[200] (C_{22}/C_{24} and C_{23}/C_{24} + ethylbenzene), and Flöter et al.[212] (C_{22}/C_{24} + C_7).

The joint structural and thermodynamic study of an equimolar mixture of (C_{26}/C_{28}) in C_7, carried out by Provost et al.,[198] highlighted the following results:

(i) For the mixtures (C_{26}/C_{28} + solvent) which are poor in solvent, the solid deposit is the disordered phase, as for solutions with a single heavy pure C_n; then when the temperature decreases, the o−d transition is observed in the solid deposit.

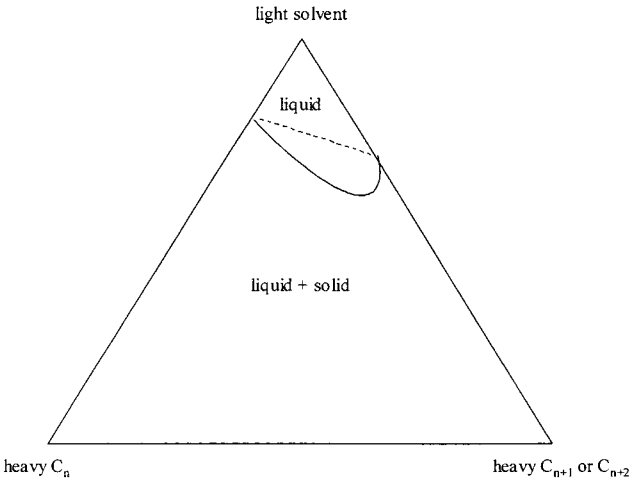

Figure 18. General behavior of the ternary system (binary mixture of two heavy consecutive C_n's ($\Delta n_c \leq 2$) + light solvent): the solubility limit (—) of the binary mixtures is higher than that (- - -) of corresponding hypothetical ideal mixtures.

(ii) With the concentration increase of C_7, the solid which crystallizes is a phase whose orthorhombic structure is different from the triclinic or monoclinic structure of pure C_{26} and C_{28}, respectively (Appendix 1 in the Supporting Information).

This phase, observed by X-ray diffraction in equilibrium with the liquid, is isostructural to the orthorhombic intermediate solid solution β''_1 of the consecutive C_n binary molecular alloys, especially in the (C_{26}/C_{28}) system:[42] the chemical analysis shows that the concentration of this β'' phase which forms the first deposits is greater in C_{28}.[198]

The crystallization of the β'' intermediate solid solution explains the following notable phenomenon, observed by Ghogomu et al.,[200,202] Provost et al.,[199] and Flöter et al.:[212] the addition of one long C_n ($0 < xC_n < 0.1$) to a short one (C_{n-1} or C_{n-2}) increases the solubility of the latter (C_{n-1} or C_{n-2}) in the solvents; thus, as shown by all these authors, the solubility of each binary heavy C_n mixture in a light solvent is greater than the solubility of the corresponding hypothetical ideal mixtures (Figure 18). The structural defects of the β'' binary phase, due to molecule conformation defects, favor its solubility in relation to that of the "ideal" structure of the pure heavy C_n's.

When the ternary system (binary heavy $C_n/C_{n'}$ ($\Delta n_c = 1$ or 2) + solvent) is in the solid state, X-ray diffraction also highlights the solid phase of the pure light solvent.

In this way, to sum up, as for the binary systems (pure heavy C_n + light solvent), the thermodynamic behavior of these ternary solutions (binary heavy $C_n/C_{n'}$ ($\Delta n_c = 1$ or 2) + light solvent) in the course of crystallization resembles pseudobinary eutectic solidification of the β'' binary intermediate solid solution of the two heavy C_n's as a single pseudocomponent on the one hand and of the light solvent on the other hand (as in Figure 16, in which it is possible to replace the pure C_n by the binary intermediate solid solution).

4. Real Multiparaffinic Waxes

(A) Preamble. The formation of solid deposits in crude oils and middle distillate fuels poses a constantly recurring problem in the petroleum industry (extraction, transportation through the pipelines, refining process, ...) and in very cold regions for the diesel-fuel consumers. The solid deposits, which block pipelines and filters, are a major issue in the deterioration of the industrial equipment.

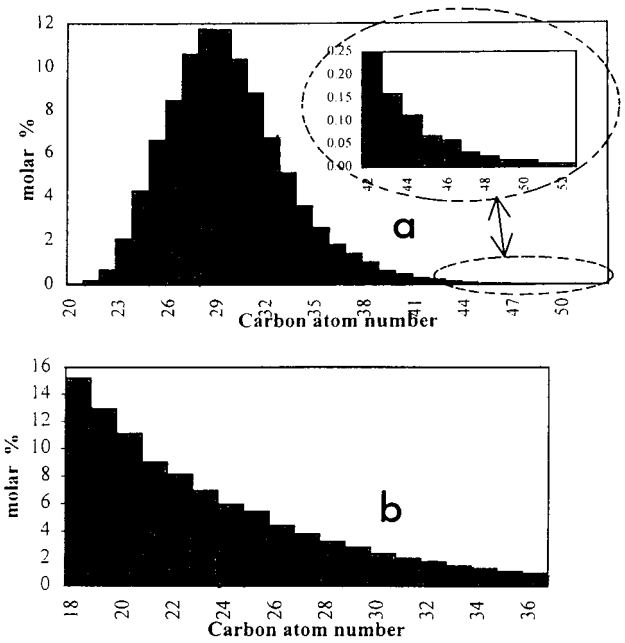

Figure 19. Distribution shapes of C_n molar concentrations of multi-C_n mixtures: (a) distribution of the *normal logarithmic* type; (b) distribution of the *exponential decreasing* type.

To find a remedy for these risks, it is necessary to be able to represent and predict the thermodynamic behavior of phases of crude oils, particularly that of the solid deposits. The development of adequate thermodynamic models[197,217−228] requires the characterization of the state of these solid deposits. According to Srivastava et al.,[54] the petroleum waxes are multicomponent mixtures of high molecular weight saturated hydrocarbons, predominantly consecutive paraffins, in the range C_{18} to C_{65}.

The industrial and commercial multi-C_n samples, which have been studied in the literature by Retief and Leroux,[23] Craig et al.,[248] Dirand et al.,[243] and Chevallier et al.,[76,77,244,245] can be classified in two categories, as a function of the distribution shape of C_n molar concentrations: (i) a *normal logarithmic* type distribution (Figure 19a) as in paraffinic Fischer−Tropsch waxes,[23] solid deposits of real diesel wax systems,[248] and commercial paraffinic waxes coming from the petroleum refining process[76,77,243−245] and (ii) a *decreasing exponential* type distribution (Figure 19b) as in the real petroleum fluids where the x_n molar concentrations of C_n are regularly decreasing, according to the recurrence relationship $x_{n+1} = \alpha x_n$ ($\alpha < 1$).[227,228,246]

(B) Multiparaffinic Mixtures with C_n Molar Concentration Distributions of the Normal Logarithmic Type. (1) Structural State at Room Temperature. X-ray diffraction patterns of plant waxes, composed of complicated mixtures of aliphatics, esters, ketones, paraffins, fatty acids, and fatty alcohols with undetermined compositions, were studied earlier in the literature.[229−236] Their structures are lamellar with a single molecule stacking spacing when the wax components have similar chain lengths; if not, several lamellar periodicities appear: McCrorie[241] has observed a single lamellar spacing in six dental modeling waxes whose main constituents were paraffin wax and bee wax. Recently, Dorset[237−240] has carried out studies on refined petroleum products and made the comparison between these paraffinic waxes and plant and insect waxes; but the accurate nature of the components and the composition of all these waxes have not been defined.

With regard to commercial multi-C_n waxes, which mainly consist of many consecutive C_n's (from 20 up to 33) with chain lengths between 20 and 52 carbon atoms whose molar concentrations display a distribution of *normal logarithmic* type, Dirand et al.[243] and Chevallier et al.[76,77,244−246] observed by X-ray diffraction (i) a single family of harmonic diffraction lines (00*l*) (these peaks define a single molecule packing identity *c*-parameter and thus the existence of a single crystalline phase) and (ii) other diffraction peaks which are characteristic of the β' orthorhombic intermediate solid solution, isostructural to that observed in binary, ternary, and ... C_n systems.

From the experimental values of the crystallographic *c*-parameter of the multi-C_n solid solution, they calculated the $\bar{n}_c$ mean number of carbon atoms per molecule from the relationship, established by Chevallier et al.[75] for the *Pbcm* odd-numbered pure C_{2p+1}'s,

$$\bar{n}_c = \frac{(c/\text{Å}) - 3.7504}{2.5448}$$

and compared it with the $\bar{n}$ mean composition of carbon atoms of multi-C_n mixtures that they determined by gas chromatography analysis, using the following relationship:

$$\bar{n} = \sum_{n_{\min}}^{n_{\max}} n x_n$$

where x_n is the molar fraction of each C_n and $n_{\max}$ and $n_{\min}$ are the carbon atom numbers of the longest and smallest C_n chains, respectively, in the multi-C_n mixture.

The conclusion of their studies[76,77,243−246] is as follows: the multi-C_n mixtures with *normal logarithmic* type distributions of C_n molar concentrations form a single solid solution, whose orthorhombic structure is isostructural to the β' ordered intermediate phase of C_n binary and ternary alloys (the single periodicity of the molecule layer stacking along the long crystallographic *c*-axis corresponds to that of a hypothetical orthorhombic pure C_n with the number of carbon atoms, n_c, equal to the mean composition $\bar{n}$ of carbon atoms of multi-C_n mixtures with an excess value close to one carbon atom in relation to the results of chromatographic analyses).

These results are in agreement with the experimental observations of Retief and Leroux[23] and Craig et al.,[248] who respectively studied paraffinic Fischer−Tropsch waxes and solid deposits of real diesel wax systems.

(2) Behavior with Increasing Temperature. Chevallier et al.[77] studied the structural and thermodynamic evolutions of the β' orthorhombic multi-C_n solid solution by X-ray diffraction and differential scanning calorimetry with increasing temperature. Mixtures, consisting of 23 ($19 < n_c < 43$) and 33 ($19 < n < 53$) C_n's, respectively, were analyzed. As in pure C_n's and the binary, ternary, and ... mixtures, the β' orthorhombic multi-C_n phase undergoes the *o−d transition* when the temperature increases below the solidus point: (i) for the light cut ($\bar{n} = 25.5$), consisting of 23 C_n's, through two two-phase domains, [first, a region with the β' ordered phase and $\beta(Fmmm)$ disordered phase and, then, a domain with the two $\beta(Fmmm)$-RI and $\alpha(R\bar{3}m)$-RII disordered phases and (ii) for the heavier cut ($\bar{n} = 27.15$), consisting of 33 C_n's, through a single two-phase domain ($\beta' + \alpha$-RII).

In the range between the final o−d transition temperature and the solidus temperature, these multi-C_n mixtures form a single solid solution which is the α-RII ($R\bar{3}m$) disordered phase in the rotator configuration.

(3) Crystallization of Multi-C_n Waxes in a Solvent. Thermodynamic and structural studies of the formation of solid deposits in solutions, which consist of a multi-C_n wax (23 C_n's: $19 < n_c < 43$) in C_{14}, used as solvent, were jointly carried out by X-ray diffraction as the temperature decreases from the liquid state, by chromatography analyses of (liquid and solid) phases separated at equilibrium, and by simple and differential scanning calorimetry.[227,228,244−246]

The experimental results of Chevallier et al.[244−246] show that *the solid deposits form a single multi-C_n solid solution* in the course of the crystallization of (wax + C_{14}) mixtures:

(i) The first deposits, observed just below the liquidus point, *consist of all the C_n's* from C_{20} to C_{42} and display an average number of carbon atoms higher (around 2 carbon atoms) than that for the initial wax.

(ii) As the temperature decreases, this average number of carbon atoms decreases as the ratio of smaller C_n's gradually increases in the β' multi-C_n solid solution.

(iii) As for the solutions of a heavy pure C_n or binary mixtures of heavy C_n's in light solvent, two behaviors are observed as a function of the concentrations. (1) For the mixtures (wax + C_{14}) which are poor in C_{14} solvent, the solid deposit is the α-RII ($R\bar{3}m$) disordered multi-C_n phase; then when the temperature decreases, the o−d transition is observed in the solid deposit (α-RII → β'). (2) When the concentration of C_{14} solvent increases, the solid which crystallizes is the β' orthorhombic ordered multi-C_n solid solution.

(iv) Whatever the wax and solvent concentrations, the final temperatures of the solidification of the mixtures are invariant. Below the invariant temperature, the solid mixture displays two phases: (β' multi-C_n solid solution + $\gamma(C_{14})$ triclinic pure C_{14}).

(v) These experimental observations of Chevallier et al.[244−246] clearly show that the (multi-C_n wax + C_{14}) system exhibits behavior which resembles *pseudobinary eutectic solidification* with the independent crystallization of the wax as a single pseudocomponent on one hand and of the C_{14} solvent on the other hand (Figure 16), in which it is possible to replace the pure C_n by the β' multi-C_n solid solution.

Similar behavior with a pseudobinary eutectic solidification was highlighted by Dorset[238] for the mixtures, consisting of a multi-C_n *Gulfwax* in naphthalene

Dirand et al.[243] observed analogous behavior with real heavy crude oil by X-ray diffraction: the deposit in equilibrium with the liquid in this heavy crude oil consists of an amorphous solid and a single orthorhombic crystalline multi-C_n solid solution whose carbon atom number, n_c, determined from the measurements of the single molecule packing identity *c*-period, is equal to 35.

The question which is raised about the development of an adequate thermodynamic model to represent the behavior of petroleum cuts concerns the presence of the amorphous solid which is probably composed of all the other heavy hydrocarbons that are not found in the multi-C_n crystalline solid solution: this amorphous solid must be taken into account in liquid−deposit equilibria to determine the total quantity of the solid deposit.

(C) Multi-C_n Synthetic Mixtures with C_n Molar Concentration Distributions of the Decreasing Exponential Type. In the real petroleum fluids, the x_n molar concentrations of C_n's are regularly decreasing (Figure 19b), according to the recurrence relationship: $x_{n+1} = \alpha x_n$ ($\alpha < 1$). Pauly et al.[227] and Dauphin et al.[228] carried out studies concerning the crystallization of synthetic multi-C_n mixtures (full series of C_n from C_{18} to C_{36} with $x_{n+1} = 0.858x_n$)

in C_{10} by chromatography analyses of phase fractions separated at liquid−solid equilibrium: the variation of the composition of the solid and liquid phases and the mass composition of the solid phase were characterized as a function of the temperature below the crystallization onset temperature.[227,228]

Chevallier et al.[246] characterized the thermodynamic and structural behavior of the same synthetic mixture (C_{18} to C_{36}, $\alpha = 0.858$; mean carbon atom number $\bar{n} = 23$). The structural and differential thermal analyses highlighted the successive appearance of three multi-C_n solid solutions in the course of the cooling from the liquid state: (i) first, just below the crystallization onset temperature, one β' multi-C_n solid solution with an average carbon atom number equal to 32.5 ± 0.5, (ii) then, a second multi-C_n solid solution in the α-RII($R\bar{3}m$) disordered phase with an average carbon atom number equal to 27.4 ± 0.4, and, (iii) finally, a third multi-C_n solid solution, whose structure corresponds to the β' intermediate solid solution, with an average carbon atom number equal to 30.0 ± 0.5.

When the temperature decreases down to room temperature, these average numbers of carbon atoms decrease as the ratio of smaller C_n's gradually increases in the three multi-C_n solid solutions: (i) from 32.5 to 31.6 for the first phase, (ii) from 27.4 to 20.8 for the second phase, and (iii) from 30 to 27.7 for the third phase. The first and third multi-C_n phases are always isostructural to the β' C_n binary intermediate solid solution whereas the second multi-C_n solid solution successively exhibits the α-RII ($R\bar{3}m$) disordered phase in the RII rotator configuration, then the β-($Fmmm$) disordered phase in the RI rotator configuration, and finally the β' ordered intermediate phase of the binary mixtures of C_n.

(D) Structural Difference between the Two Types of Distribution. The multi-C_n mixtures, which display C_n molar concentration distributions of the *normal logarithmic* type (Figure 19a), form a single multi-C_n solid solution isostructural to the β' ordered intermediate phase of binary C_n alloys; the *c*-periodicity of the molecule layer stacking corresponds to that of a hypothetical pure C_n whose n_c number of carbon atoms is equal to the $\bar{n}$ average number of carbon atoms of the multi-C_n mixtures with an excess value close to one carbon atom. In these kinds of mixtures, the crystalline structure and the corresponding molecular layer thickness of the single multi-C_n solid solution are imposed by the C_n's whose chain lengths have numbers of carbon atoms close to the $\bar{n}$ mean carbon atom number of the molar concentration distribution and which are in the majority. In this structure the higher chains can display many conformational defects (Figure 7) or bend to insert themselves between these crystalline planes and organize themselves to adjust the considerable difference of molecule chain lengths between the longer and smaller molecules or cross the interfacial gap between two successive layers of molecules, as described by Craig et al.,[248] Dirand et al.,[243] and Chevallier et al.[76]

At room temperature, the synthetic mixture with a concentration distribution of *decreasing exponential* type (Figure 19b) displays three different multi-C_n solid solutions. The smaller chains, which here are in the majority, do not succeed in making the longer chains bend, to form a single solid solution.

The accurate determination of the crystalline structure of the β' and β'' binary, ternary, ..., and multinary solid solutions of C_n mixtures is very difficult because of the crystalline long *c*-parameter which leads to uncertainties in (*hkl*) crystalline plane indexing of powder pattern diffraction-X lines. The suggestions of structures are as follows:

(i) Lüth et al.[145] determined the orthorhombic $Bb2_1m$, $Bb2b$, $Bbm2$, or $Bba2$ structure for the β'' intermediate solid solution of C_{20}/C_{22} mixtures by X-diffraction from single crystals.

(ii) Gerson and Nyburg[26] specified the orthorhombic $Bb2_1m$ structure for the same β'' intermediate solid solution of C_{24}/C_{26} mixtures by X-ray diffraction from single crystals.

(iii) Metivaud et al.[176] suggested the monoclinic Aa structure for the β' intermediate solid solution and the orthorhombic $Pca2_1$ structure for the β'' intermediate phase of C_{23}/C_{25} mixtures; but their experiments were carried out by powder X-ray diffraction.

(iv) Moreover, Dorset[240] proposed the same orthorhombic structure as Lüth et al.[145] and Gerson and Nyburg[26] for the multi-C_n solid solution with the $A2_1am$ space group, which is the same group as $Bb2_1m$ when the ($\vec{a}$) and ($\vec{b}$) axes are reversed; this result was obtained by single-crystal electron diffraction.

5. Conclusion

Knowledge of the thermodynamic and structural data of the pure C_n's allows us to better understand the behavior of their binary, ternary, ..., and multinary synthetic mixtures on the one hand and of real multi-C_n waxes on the other hand.

The synthetic mixtures and real multi-C_n waxes can generally behave as real pseudocomponents and form only a binary, ternary, ..., or multi-C_n solid solution equivalent to that for a hypothetical pure C_n whose n_c number of carbon atoms is equal to the $\bar{n}$ average number of carbon atoms of the mixtures.

As a result, identical phenomena are observed in pure C_n's, their synthetic mixtures, and real multi-C_n waxes: (i) the appearance of the disordered solid state below the solidus point with increasing temperature and (ii) pseudo-binary eutectic crystallization in solutions with other linear, aromatic, or cyclic pure hydrocarbons.

All these experimental observations predict the state of the phases in the liquid−solid and solid−solid equilibria of these complicated systems and will allow us to propose adequate thermodynamic models in order to represent correctly the thermodynamic behavior of petroleum cuts.

Acknowledgment

We are indebted to Mr. Geoffrey Sockett, native speaker of English, and Mrs. Myriane Pastore, Professors of English at Ecole Nationale Supérieure des Industries Chimiques, for the correction of this manuscript.

Supporting Information Available:

Tables of structural data by X-ray diffraction and thermodynamic data. This material is available free of charge via the Internet at http://pubs.acs.org.

Notations of Crystallographic Structure

β = orthorhombic phases
δ = monoclinic phases
γ = triclinic phases

Ordered Phases at "Room Temperature"

index 0 = pure alkanes and terminal solid solution
$\beta_0(C_{2p+1})$ = orthorhombic phase *Pbcm* of odd-numbered C_{2p+1} ($n_c = 2p + 1$).
$\delta_0(C_{2p})$ = monoclinic phases of even-numbered C_{2p} ($n_c = 2p$)
$\gamma_0(C_{2p})$ = triclinic phase $P\bar{1}$ of even-numbered C_{2p} ($n_c = 2p$)

β'_n and β''_n = orthorhombic intermediate solid solutions with the index $n = 1$ or 2 to identify isostructural phases of different stoichiometries on both sides of the middle intermediate solid solution in the same binary or ternary systems

Disordered Phases at "High Temperature"

$\beta(Fmmm)$ = orthorhombic phase; this phase presents the "rotator" state, called β-RI

α-RII = rhombohedral rotator phase ($R\bar{3}m$)

RIII = triclinic disorder phase

RIV = monoclinic disorder phase

Notations of Thermodynamic Data

T_{o-d}, ΔH_{o-d} = temperature and enthalpy of the order−disorder transition (o−d transition)

T_{fus}, $\Delta_{fus}H$ = temperature and enthalpy of the melting

$\Delta H_{T_{o-d}}^{T_{fus}}$ = enthalpy variation from the order−disorder transition temperature (T_{o-d}) to the melting temperature (T_{fus})

$\delta = \Delta H_{T_{o-d}}^{T_{fus}} - \Delta_{fus}H = \Delta H_{od} + \int_{T_{o-d}}^{T_{fus}} C_p \, dT$

Literature Cited

(1) Bunn, C. W. Crystal structure of long-chain normal paraffin hydrocarbons, "Shape" of the methylene group. *Trans. Faraday Soc.* **1939**, *35*, 482−491.

(2) Kobayashi, M. Lattice dynamical investigation of the rotator phase of the n-paraffins. *J. Chem. Phys.* **1978**, *68*, 145−151.

(3) Mnyukh, Y. V. The structure of normal paraffins and of their solid solutions. *J. Struct. Chem.* **1960**, *1*, 346−365.

(4) Bondi, A. Packing density of polymer melts near the glass-transition temperature, van der Waals, Volumes and Radii. *J. Phys. Chem.* **1964**, *48*, 441−451.

(5) Müller, A.; Saville, W. B. Further X-ray measurements on long-chain compounds (n- hydrocarbons). *J. Chem. Soc.* **1925**, *127*, 599−663.

(6) Müller, A. Further X-ray investigation of long chain compounds (n-hydrocarbon). *Proc. R. Soc. London* **1928**, *A120*, 437−459.

(7) Müller, A. Crystal structure of the normal paraffins at temperatures ranging from that of liquid air to the melting point. *Proc. R. Soc. London* **1930**, *A127*, 417−430.

(8) Müller, A. An X-ray investigation of normal paraffins near their melting points. *Proc. R. Soc. London* **1932**, *A138*, 514−530.

(9) Müller, A.; Lonsdale, K. The low-temperature form of $C_{18}H_{38}$. *Acta Crystallogr.* **1948**, *1*, 129−134.

(10) Piper, S. H.; Brown, D.; Dyments, S. X-rays and the constitution of the hydrocarbons from paraffin wax. *J. Chem. Soc.* **1925**, *127*, 2194−2200.

(11) Hengstenberg, J. X-ray investigation of the structure of the carbon chains in hydrocarbons. *Z. Kristallogr.* **1928**, *67*, 583−594.

(12) Kohlhaas, R.; Soremba, K. H. The structure of crystallized aliphatic compounds. the structure of triacontane. *Z. Kristallogr.* **1938**, *100*, 47−57.

(13) Smith, A. E. The crystal structure of the normal paraffin hydrocarbons. *J. Chem. Phys.* **1953**, *21*, 2229−2231.

(14) Schaerer, A.; Busso, C. J.; Smith, A. E.; Skinner, L. B. Properties of pure normal alkanes in the C_{17} to C_{36} range. *J. Am. Chem. Soc.* **1955**, *77*, 2017−2019.

(15) Shearer, H. M. M.; Vand, V. The crystal structure of the monoclinic form of n-hexatriacontane. *Acta Crystallogr.* **1956**, *9*, 379−384.

(16) Barbezat-Debreuil, S. Contribution à l'étude des paraffines normales pures de leurs mélanges binaires. *C. R. Acad. Sci.* **1958**, séance du 19 Mai, 2907−2912.

(17) Teare, P. W. The crystal structure of orthorhombic hexatriacontane. *Acta Crystallogr.* **1959**, *12*, 294−301.

(18) Ohlberg, S. M. The stable crystal structures of pure n-paraffins containing an even number of carbon atoms in the range C_{20} to C_{36}. *J. Phys. Chem.* **1959**, *63*, 248−250.

(19) Broadhurst, M. G. An analysis of the solid-phase behavior of the normal paraffins. *J. Res. Natl. Bur. Stand., A: Phys. Chem.* **1962**, *66*, 241−249.

(20) Nyburg, S. C.; Lüth, H. *n*-Octadecane: a correction and refinement of the structure given by Hayashida. *Acta Crystallogr.* **1972**, *B28*, 2992−2995.

(21) Piesczek, W.; Strobl, G. R.; Malzahn, K. Packing of paraffins chains in the four stable modifications of n-tritriacontane. *Acta Crystallogr.* **1974**, *B30*, 1278−1288.

(22) Boistelle, R.; Simon, B.; Pèpe, G. Polytypic structures of *n*-$C_{28}H_{58}$ (octacosane) and *n*-$C_{36}H_{74}$ (hexatriacontane). *Acta Crystallogr.* **1976**, *B32*, 1240−1249.

(23) Retief, J. J.; Le Roux, J. H. Crystallographic investigation of a paraffinic Fischer−Tropsch wax in relation to a theory of wax structure and behaviour. *South Afr. J. Sci.* **1983**, *79*, 234−239.

(24) Heyding, R. D.; Russel, K. E.; Varty, T. L. The normal paraffins revisited. *Powder Diffr.* **1990**, *5*, 93−100.

(25) Gerson, A. R.; Roberts, K. J.; Sherwood, J. N. X-ray diffraction studies of alkanes: unit-cell parameters of the homologous series $C_{18}H_{38}$ to $C_{28}H_{58}$. *Acta Crystallogr.* **1991**, *B47*, 280−284.

(26) Gerson, A. R.; Nyburg, S. C. Structures of two binary *n*-alkane solid solutions. *Acta Crystallogr.* **1994**, *B50*, 252−256.

(27) Clydesdale, G.; Roberts, K. J. The structural stability and morphology of even number *n*-alkanes crystallising in the homologous series $C_{18}H_{38}$ − C_{28}−H_{58}. *AIChE Symp. Ser.* **1991** *87*, 138−142.

(28) Nyburg, S. C.; Gerson, A. R. Crystallography of the even *n*-alkanes: structure of $C_{20}H_{42}$. *Acta Crystallogr., Struct. Sci.* **1992**, *B48*, 103−106.

(29) Craig, S. C.; Hastie, G. P.; Roberts, K. J.; Sherwood, J. N. Investigation into the structures of some normal alkanes within the homologous series $C_{13}H_{28}$ to $C_{60}H_{122}$ using high resolution synchrotron X-ray powder diffraction. *J. Mater. Chem.* **1994**, *4*, 977−981.

(30) Sullivan, P. K.; Weeks, J. The intensity as a function of temperature of the low angle X-ray diffraction maxima of the n-paraffins: hexatriacontane, tetratetracontane and tetranonacontane. *J. Res. Natl. Bur. Stand.* **1970**, *74*, 203−214.

(31) Zerbi, G.; Magni, R.; Gussoni, M.; Moritz, K. H.; Bigotto, A.; Dirlikov. Molecular mechanics for phases transitions and melting of *n*-alkanes: a spectroscopic study of molecular mobility of solid *n*-nonadecane. *J. Chem. Phys.* **1981**, *75*, 3175−3194.

(32) Doucet, J.; Denicolo, I.; Craievich, A. F. X-Ray study of the "Rotator" phase of the odd-numbered paraffins: $C_{17}H_{36}$, $C_{19}H_{40}$ and $C_{21}H_{44}$. *J. Chem. Phys.* **1981**, *75*, 1523−1529.

(33) Ungar, G. Structure of rotator phases in *n*-alkanes. *J. Phys. Chem.* **1983**, *87*, 689−695.

(34) Denicolo, I.; Doucet, J.; Craievich, A. F. X-Ray study of the Rotator phase of paraffins (III): even-numbered paraffins $C_{18}H_{38}$, $C_{20}H_{42}$, $C_{22}H_{46}$, $C_{24}H_{50}$ and $C_{26}H_{54}$. *J. Chem. Phys.* **1983**, *78*, 1465−1469.

(35) Doucet, J.; Denicolo, O.; Craievich, A. F.; Germain, C. X-Ray study of the rotator phase of paraffins (IV): $C_{27}H_{56}$, $C_{28}H_{58}$, $C_{29}H_{60}$, $C_{30}H_{62}$ and $C_{34}H_{70}$. *J. Chem. Phys.* **1984**, *80*, 1647−1651.

(36) Ryckaert, J. P.; Klein, M. L.; Mc Donald, I. R. Disorder at the bilayer interface in the pseudohexagonal rotator phase of solid *n*-alkanes. *Phys. Rev. Lett.* **1987**, *58*, 698−701.

(37) Kim, Y.; Strauss, H. L.; Snyder, R. G. Conformational disorder in crystalline *n*-alkanes prior to melting. *J. Phys. Chem.* **1989**, *93*, 7520−7526.

(38) Sirota, E. B.; King, J. R.; Singer, D. M.; Shao, H. H. Rotator phases of the normal alkanes: an X-ray scattering study. *J. Chem. Phys.* **1993**, *98*, 5809−5824.

(39) Espeau, P.; Roblès, L.; Mondieg, D.; Haget, Y.; Cuevas-Diarte, M. A.; Oonk, H. A. J. Mise au point sur le comportement énergétique cristallographique des n-alcanes. I. Série de C_8H_{18} à $C_{21}H_{44}$. *J. Chim. Phys.* **1996**, *93*, 1217−1238.

(40) Robles, L.; Mondieg, D.; Haget, Y.; Cuevas-Diarte, M. A. Mise au point sur le comportement énergétique cristallographique des n-alcanes II. Série de $C_{22}H_{46}$ à $C_{27}H_{56}$. *J. Chim. Phys.* **1998**, 95−111.

(41) Vand, V. Density and unit cell of n-hexatriacontane. *Acta Crystallogr.* **1953**, *6*, 797−798.

(42) Provost, E.; Balesdent, D.; Bouroukba, M.; Petitjean, D.; Dirand, M.; Ruffier-Meray, V. Phase diagram of *n*-hexacosane and *n*-octacosane: experimental determination and calculation. *J. Chem. Thermodyn.* **1999**, *31*, 1135−1149.

(43) Snyder, R. G.; Maroncelli, M.; Qi, S. P.; Strauss, H. L. Phase transitions and nonplanar conformers in crystalline *n*-alkanes. *Sciences* **1981**, *214*, 188−190.

(44) Snyder, R. G.; Strauss, H. L.; Alamo, R.; Mandelkern, L. Chain length dependence of interlayer interaction in crystalline *n*-alkanes from Raman longitudinal acoustic mode measurements. *J. Chem. Phys.* **1994**, *100*, 5422−5431.

(45) Snyder, R. G.; Maroncelli, M.; Qi, S. P.; Strauss, H. L. Phase transitions and nonplanar conformers in crystalline *n*-alkanes. *Sciences* **1982**, *214*, 6237−6245.

(46) Nozaki, K.; Higashitani, N.; Yamamoto, T.; Hara, T. Solid−solid-phase transitions in n-alkanes $C_{23}H_{48}$ and $C_{25}H_{52}$: X-ray powder diffraction study on new layer stacking in phase V. *J. Chem. Phys.* **1995**, *103*, 5762−5766.

(47) Freund, M.; Csikos, R.; Keszthelyi, S.; Mozes, G. Y. Crystal structure of paraffin waxes. *Paraffin products properties, technologies, applications;* Elsevier: Budapest, 1982.

(48) Strobl, G.; Ewen, B.; Fisher, E. W.; Piesczek, W. Defect structure and molecular motion in the fur modifications of n-tritriacontane. I Study of defect structure in the lamellar interfaces using small-angle X-ray scattering. *J. Chem. Phys.* **1974**, *61*, 5257−5264.

(49) Ewen, B.; Fisher, E. W.; Piesczek, W.; Strobl, G. R. Defect structure and molecular motion in the four modifications of *n*-$C_{33}H_{68}$. II. Study of molecular infrared spectroscopy and wide-line nuclear magnetic resonance measurements. *J. Chem. Phys.* **1974**, *61*, 5265−5272.

(50) Ewen, B.; Strobl, G. R.; Richter, D. Phase transitions in crystals of chain molecules. relation between defect structures and molecular motion in the four modifications of n-$C_{33}H_{68}$. *Faraday Discuss. Chem. Soc.* **1980**, *69*, 19−31.
(51) Sirota, E. B.; Singer, D. M. Phase transition among the rotator phases of the normal alkanes. *J. Chem. Phys.* **1994**, *101*, 10873−10882.
(52) Sirota, E. B.; King, H. E.; Shao, H. H.; Singer, D. M. Rotator phases in mixtures of n-alkanes. *J. Chem. Phys.* **1995**, *99*, 798−804.
(53) Turner, W. R. Normal alkanes, Technical Review. *Ind. Eng. Chem., Prod. Res. Dev.* **1971**, *10*, 238−260.
(54) Srivastava, S. P.; Handoo, J.; Agrawal, K. M.; Joshi, G. C. Phase-transition studies in n-alkanes and petroleum-related waxes. A Review. *J. Phys. Chem. Solids* **1993**, *54*, 639−670.
(55) Kitajgorodskij, A. I. L'empaquetage de molécules longues. *Acta Crystallogr.* **1957**, *10*, 802−802.
(56) Birdwell, B. F.; Jessen, F. W. Crystallization of petroleum waxes. *Nature* **1966**, 366−374.
(57) Killian, H. G. The non homogeneous thermodynamically autonomous and equivalent mixrophase. *Prog. Colloid Polym. Sci.* **1986**, *72*, 60−82.
(58) Killian, H. G. Crystallization in oligomer and copolymer systems comprising lattice incompatible units. *Prog. Colloid Polym. Sci.* **1988**, *78*, 161−176.
(59) Snyder, R. G.; Conti, G.; Strauss, H. L.; Dorset, D. L. Thermaly induced mixing in partially microphase segregated binary *n*-alkanes crystals. *J. Phys. Chem.* **1993**, *97*, 7342−7350.
(60) Kobayashi, M.; Sakagami, K.; Tadokoro, H. Effects of interlaminar forces on longitudinal acoustic modes of *n*-alkanes. *J. Chem. Phys.* **1983**, *78*, 6391−6398.
(61) Hsu, S. L.; Krimm, S. Longitudinal acoustic mode in polymers. *J. Appl. Phys.* **1976**, *47*, 4265−4270.
(62) McGann, M. R.; Lacks, D. J. Monte Carlo simulations of the interlamellar spacing in model *n*-alkane crystals. *J. Chem. Phys.* **1998**, *108*, 2622−2625.
(63) Mnyukh, Y. V. Laws of phase transformation in a serie of normal paraffins. *J. Phys. Chem. Solids* **1963**, *24*, 631−640.
(64) Takamizawa, K.; Ogawa, Y.; Oyama, T. Thermal behavior of *n*-alkanes from *n*-$C_{32}H_{66}$ to *n*-$C_{80}H_{162}$, synthesized with attention paid to high purity. **1982**, *14*, 441−456.
(65) Hasnoui, N.; Dellacherie, J.; Schuffenecker, L.; Dirand, M. Evolution structurale en fonction de la température des phases intermédiaires β'_1 β'_2 du système docosane nC_{22}- tétracosane nC_{24}. *J. Chim. Phys.* **1988**, *85*, 675−683.
(66) Nozaki, K.; Yamamoto, T.; Hara, T.; Hikosaka, M. Rotator phase transitions through an intermediate state in odd *n*-alkanes: in situ optical observation study. *J. Appl. Phys.* **1997**, *36*, L146−L149.
(67) Norman, N.; Mathisen, H. Crystal structure of lower n-paraffins I. *n*-octane. *Acta Chem. Scand.* **1961**, *15*, 1747−1754.
(68) Filatov, S. K.; Kotelnikoya; Aleksandrova, E. A. High temperature crystal chemistry of normal odd paraffins. *Z. Kristallogr.* **1985**, *172*, 35−43.
(69) Mnyukh, Y. V.; Belatseva, B. M.; Kitaïgorodskii, A. I. Morphology of molecular packings in linear polyesters. *Dokl. Akad. Nauk SSSR* **1960**, *133*, 1132−1135.
(70) Craievich, A.; Craievich, A.; Doucet, J.; Denicolo, I. Structure and molecular disorder in three modifications of a binary $C_{23}H_{48}$−$C_{24}H_{50}$ paraffin. *J. Phys.* **1984**, *45*, 1473−1477.
(71) Ungar, G.; Keller, A. Time-resolved synchrotron X-ray study of chain-folded crystallization of long paraffins. *Polymer* **1986**, *27*, 1835−1844.
(72) Zeng, X.; Ungar, G. Lamellar structure of noninteger folded and extended long chain *n*-alkanes by small-angle X-ray diffraction. *Polymer* **1998**, *39*, 4523−4533.
(73) Nyburg, S. C.; Potworowski. Prediction of unit cells and atomic coordinates for the n-alkanes. *Acta Crystallogr.* **1973**, *B29*, 347−351.
(74) Nyburg, S. C.; Pickard, F. M.; Norman, N. X-ray powder diagrams of certain *n*-alkanes: corrigenda and extension. *Acta Crystallogr.* **1976**, *B32*, 2289−2292.
(75) Chevallier, V.; Petitjean, D.; Ruffier-Meray, V.; Dirand, M. Correlation between the crystalline long c-parameter and the number of carbon atoms of pure *n*-alkanes. *Polymer* **1999**, *40*, 5953−5956.
(76) Chevallier, V.; Provost, E.; Bourdet, J. B.; Bouroukba, M.; Petitjean, D.; Dirand, M. Mixtures of numerous different *n*-alkanes − I Structural studies by X-ray diffraction at room temperature − Correlation between the crystallographic long c parameter and the average composition of multialkane phases. *Polymer* **1999**, *40*, 2121−2128.
(77) Chevallier, V.; Petitjean, D.; Bouroukba, M.; Dirand, M. Mixtures of numerous different *n*-alkanes − II Studies by X-ray diffraction and differential thermal analyses with increasing temperature. *Polymer* **1999**, *40*, 2129−2137.
(78) Hoffman, J. D.; Decker, B. F. Solid-state phase changes in long chain compounds. *J. Phys. Chem.* **1953**, *57*, 520−529.
(79) Piper, S. H.; Chibnall, A.; Hopkins, S. J.; Pollard, A.; Smith, J. A. B.; Williams, E. F. CCXXV. Synthesis and crystal spacings of certain long-chain paraffins, ketones and secondary alcohols. *Biochem. J.* **1931**, *25*, 2072−2094.
(80) Piper, S. H.; Malkin, T. Crystal structure of normal paraffins. *Proc. R. Soc.* **1930**, *126*, 278−286.
(81) Ställberg, G.; Stälberg-Stenhagen, S.; Stenhagen, E. Very long hydrocarbon chains. I. The synthesis of n-doctacontane and n-hectane. *Acta Chem. Scand.* **1952**, *6*, 313−318.
(82) Stenhagen, E.; Tagtström, B.; Nonatriacontane. *J. Am. Chem. Soc.* **1944**, *66*, 845−846.
(83) Ranby, B. G.; Morehead, F. F.; Walter, N. M. Morphology of *n*-alkanes linear polyethylene and isotactic polypropylene crystallized from solution. *J. Polym. Sci.* **1960**, *44*, 349−367.
(84) Francis, F.; King, A. M.; Willis, J. A. V. Long-chain carbon compounds. Tetratriacontane and hexatretracontanoic acids and their derivatives. *J. Chem. Soc.* **1937**, 999−1004.
(85) Crissman, J. M.; Passaglia, E.; Eby, R. K.; Colson, J. P. Crystal data on n−eïcosane ($C_{20}H_{42}$). *J. Appl. Crystallogr.* **1970**, *3*, 194−199.
(86) McClure, D. W. Nature of the rotational phase transition in paraffin crystals. *J. Chem. Phys.* **1968**, *49*, 1830−1841.
(87) Dreisbach, R. R. Physical properties of chemical compounds-II, comprehensive data on 476 straight-chain compounds in systematic tabular form, n° 22 of the advances in chemistry series; *The Advances in Chemistry Series*; Edited by the staff of *Industrial and Engineering Chemistry*, 1959.
(88) Lide, D. R. *CRC Handbook of Chemistry and Physics*, 76th ed.; CRC Press: Boca Raton, FL, 1995−1996.
(89) Timmermans, J. *Physicochemical constants of pure organic compounds*; Elsevier Publishing Company: Amsterdam−London−New York, 1965; Vol. 2, pp 1−61.
(90) T.R.C. Databases American National Standard, Standard Test Method for Purity of Hydrocarbons from Freezing Points, ANSI/ASTM D 1016-74; Reapproved 1979; pp 481−497.
(91) *T.R.C. Databases for Chemistry and Engineering*; *TRC Source Database;* Texas Engineering Experiment Station, Texas A & M University: 1998.
(92) Messerly, J. F.; Guthrie, G. B.; Todd, S. S.; Finke, H. L. Low-temperature thermal data for *n*-pentane, *n*-heptadecane and *n*-octadecane, revised thermodynamic functions for the n- alkanes, C_5−C_{18}. *J. Chem. Eng. Data* **1967**, *3*, 338−346.
(93) Atkinson, C. M. L.; Richardson, M. J. Phase behaviour of *n*-alkanes and polyethylene. *Trans. Faraday Soc.* **1969**, *654*, 1749−1763.
(94) Seyer, W. F.; Patterson, R. F.; Keays, J. L. The density and transition points of the n-paraffin hydrocarbons. *J. Am. Chem. Soc.* **1944**, *66*, 179−182.
(95) Finke, H. L.; Gross, M. E.; Waddington, G.; Huffman, H. M. Low-temperature thermal data for the nine normal paraffin hydrocarbons from octane to hexadecane. *J. Am. Chem. Soc.* **1954**, *76*, 333−341.
(96) Bosselet, F.; Letoffe, J. M.; Claudy, P.; Esson, S.; Valentin, P. Etude du comportement thermique des n-alcanes dans des milieux hydrocarbonés complexes par analyse calorimétrique différentielle. I. Etude du comportement thermique des n-alcanes en programmation linéaire de température. *Thermochim. Acta* **1983**, *70*, 7−18.
(97) Snow, R. L.; Ott, J. B.; Goates, J. R.; Marsh, K. N.; O'shea, S.; Stokes, R. H. (Solid + liquid) and (vapor + liquid) phase equilibria and excess enthalpies for (benzene + n-tetradecane), (benzene + n-hexadecane), cyclohexane + tetradecane) and (cyclohexane + n-hexadecane) at 293.15, 298.15 and 308.15 K comparison of G^e_m calculated from (vapor + liquid) and (solid + liquid) equilibria. *J. Chem. Thermodyn.* **1986**, *2*, 107−130.
(98) Fredricks, R. E. Thermal and thermodynamic characteristics of the hydrocarbon components of industrial paraffin waxes. *J. Am. Chem. Soc., Div. Polym. Mater. Sci. Eng.* **1986**, *54*, 634−637.
(99) Barbillon, P.; Schuffenecker, L.; Dellacherie, J.; Balesdent, D.; Dirand, M. Variation d'enthalpie subie de 260 K à 340 K par les n-paraffines comprises entre l'octadécane (*n*-C_{18}) l'hexacosane (*n*-C_{26}). *J. Chim. Phys.* **1991**, *88*, 91−113.
(100) Koleskinov, S. I.; Syunyaev, Z. I. Phase transitions in the melting and crystallization of n-$C_{18}H_{38}$ and *n*-$C_{20}H_{42}$. *J. Appl. Chem. USSR* **1986**, 2097−2101.
(101) Ksiazczak, A.; Parczewska, B. Vapour pressures of binary three-phase (solid + liquid + vapour) mixtures. I. Melting temperatures of polymorphic phases. *J. Chem. Thermodyn.* **1988**, *20*, 785−790.
(102) Maroncelli, M.; Qi, S. P.; Strauss, H. L.; Snyder, R. G. Nonplanar conformers and the phase behavior of socio *n*-alkanes. *J. Am. Chem. Soc.* **1982**, *104*, 6237−6247.
(103) Aoulmi, A.; Bouroukba, M.; Rogalski, M.; Solimando, R. Thermodynamics of mixtures formed by polycyclic aromatic hydrocarbons with long chain alkanes. *Fluid Phase Equilib.* **1995**, *110*, 299−308.
(104) Company, J. C. Mesure interprétation des équilibres de cristallisation de solutions de paraffines lourdes d'hydrocarbures aromatiques. *Chem. Eng. Sci.* **1973**, *28*, 318−323.

(105) Domanska, U. *Int. DATA Ser., Sel. Data Mixtures* **1987**, *4*, 269−276.

(106) Domanska, U. *Int. DATA Ser., Sel. Data Mixtures* **1989**, *3*, 188−192.

(107) Heitz, W.; Wirth, T.; Peters, R.; Strobl, G.; Fischer, E. W. Synthese und Eigenschaften Molekulareinheitlicher n-Paraffine bis zum $C_{140}H_{282}$. *Makromol. Chem.* **1972**, *162*, 63−79.

(108) Ksiazczak, A.; Parczewska, B. Vapour pressures of binary three-phase (solid liquid + vapour) mixtures. III. Melting temperatures of n−eïcosane phases. *J. Chem. Thermodyn.* **1989**, *21*, 1231−1236.

(109) Parks, G. S.; Todd, S. S. Heats of fusion of some paraffin hydrocarbons, industrial and engineering chemistry. *Ind. Eng. Chem.* **1929**, *21*, 1235−1237.

(110) Parks, G. S.; Huffman, H. M.; Thomas, S. B. Thermal data on organic compounds VI. The heat capacities, entropies and free energies of some saturated, nonbenzenoïd hydrocarbons. *J. Am. Chem. Soc.* **1930**, *52*, 1032−1041.

(111) Templin, P. R. Coefficient of volume expansion for petroleum waxes and pure n-paraffins. *Ind. Eng. Chem.* **1956**, 154−161.

(112) Mazee, W. M. On the properties of paraffin wax in the solid state. *J. Inst. Pet.* **1949**, *35*, 97−102.

(113) Garner, W. E.; Van Biber, K.; King, A. M. CCXI − The melting points and heats of crystallization of the normal long-chain hydrocarbons. *J. Chem. Soc.* **1931**, 1539−1541.

(114) Domanska, U.; Kniaz, K. *Int. DATA Ser., Sel. Data Mixtures, Ser. A* **1990**, *2*, 83−93.

(115) Domanska, U.; Kniaz, K. *Int. DATA Ser. Sel. Data Mixtures* **1990**, *3*, 194−206.

(116) Kern, R.; Dassonville, R. Growth inhibitors and promoters exemplified on solution growth of paraffin crystals. *J. Cryst. Growth* **1992**, *116*, 191−203.

(117) Small, D. M. *The physical chemistry of lipids. From alkanes to phospholipids*; Plenum: New York, 1986.

(118) Andon, R. J. L.; Martin, J. F. Thermodynamic properties of hexacosane. *J. Chem. Thermodyn.* **1976**, *8*, 1159−1166.

(119) Lourdin, D. Contribution à l'étude des propriétés thermophysiques des matériaux organiques; étude par analyse thermobarométrique de paraffines et de polymères (polyéthylène, polyoxyéthylène, polyvinyldifluorés). Ph.D. Thesis, University Blaise Pascal, Clermont-Ferrand, France, D.U. 375, 1991.

(120) Josefiak, C.; Würflinger, A.; Schneider, G. M. Under high pressure. *Colloid Polym. Sci.* **1977**, *255*, 170−171.

(121) Ksiazczak, A. Vapour pressures of binary three-phase (solid + liquid + vapour) mixtures. II. Melting temperatures of n−eïcosane phases. *J. Chem. Thermodyn.* **1989**, *21*, 789−792.

(122) Mazee, W. M. Thermal analysis of normal alkanes. *Anal. Chim. Acta* **1957**, *17*, 97−106.

(123) Bonsor, D. H.; Bloor, D. Phase transition of *n*-alkanes systems. Part 1: calculation of heats of transition of the order−disorder phase transtion of pure paraffins. *J. Mater. Sci.* **1977**, *12*, 1552−1558.

(124) Slowinski, E. J.; Walter, H.; Miller, R. L. On the determination of methyl content in polyethylenes. *J. Polym. Sci.* **1956**, XIX, 353−358.

(125) Ungar, G.; Stenjy, J.; Keller, A.; Bidd, I.; Whiting, M. C. The crystallization of Ultralong Normal Paraffins: The onset of chain folding. *Science* **1985**, *229*, 386−389.

(126) Jin, Y.; Wunderlich, B. Heat capacities of paraffins and polyethylene. *J. Phys. Chem.* **1991**, *95*, 9000−9007.

(127) Schaerer, A. A.; Baylé, G. G.; Mazee, W. M. The phase behaviour of *n*-alkanes. *Recueil* **1956**, *75*, 513−529.

(128) Oyama, T.; Takamizawa, K.; Urabe, Y.; Ogawa, Y. Synthesis of higher *n*-alkanes and their transition phenomena. II. Carbon number dependence of transition temperature of odd *n*-alkanes. *Kyushu Diagaku Kogaku Shuho* **1979**, *52*, 129−133.

(129) Oyama, T.; Takamizawa, K.; Ogawa, Y. Studies on phase transitions of higher odd n-alkanes. I. Effects of purity on phase transitions of higher odd *n*-alkanes. *Kobunshi Ronbunshu* **1980**, *37*, 711−715.

(130) Broadhurst, M. G. The melting temperature of the n-paraffins and the convergence temperature for polyethylene. *J. Res. Natl. Bur. Stand., A: Phys. Chem.* **1966**, *70A*, 481−486.

(131) Flory, P. J.; Vrij, A. Melting points of linear-chain homologues. The normal paraffin hydrocarbons. *J. Am. Chem. Soc.* **1963**, *85*, 3548−3553.

(132) Calange, S. Modélisation thermodynamique compositionnelle de la cristallisation des bruts paraffiniques. Ph.D. Thesis, Université de Pau et des Pays de l'Adour (France), spécialité: Sciences Physiques, 1996.

(133) Paunovic, I.; Mehrota, A. K. Liquid−solid-phase transformation of C16H34, C28H58 and C14H84 and their binary and ternary mixtures. *Thermochim. Acta* **2000**, *356*, 27−38.

(134) Lourdin, D.; Roux, A. H.; Grolier, G.; Buisine, J. M. Thermobarometric and differential Scanning calorimetric study of the polymorphism of some even and odd paraffins (C_{26}, C_{27}, C_{40}, C_{60}). *Thermochim. Acta* **1992**, *204*, 99−110.

(135) Schmidt, A. W.; Schoeller, V.; Eberlein, K. Physical data of 1-olefins and normal paraffins. *Ber.* **1941**, *74B*, 1313−1324.

(136) Verdonk, G. Calorimetrische analyse van paraffine, bijdrage tot het algemen onderverp. Calorimetrische Analyse van J. Straub en R. N. M. A. Malotaux. *Chem. Weekbl.* **1938**, *35*, 741−743.

(137) Wunderlich, B. Development towards a single-run DSC for heat capacity measurements. *J. Thermal Anal.* **1987**, *32*, 194−204.

(138) Bornstein, L. *Enthalpies of fusion and transition of organic compounds, IV, A*; Springer: 1995; ISBN 3-540-58854-X.

(139) Domanska, U.; Lachwa, J.; Morawski, P.; Malanowski, S. Phase equilibria and volumetric properties in binary mixtures containing branched chain ethers (Methyl 1,1-Dimethylethyl Ether or Ethyl 1,1-Dimethylethyl Ether or Methyl 1,1- Dimethylpropyl Ether or Ethyl 1,1-Dimethylpropyl Ether). *J. Chem. Eng. Data* **1999**, *44*, 974−984.

(140) Pak, J.; Wunderlich, B. Thermal Analysis of Paraffins as Model Compounds for Polyethylene. *J. Polym. Phys.* **2000**, *38*, 2810−2821.

(141) Asbach, V. G. I.; Killian, H. G. Zur Thermodynamik Von Mischsystemen Aus n-Paraffinen. *Ber. Bunsen-Ges.* **1970**, *74*, 814−823.

(142) Kravchenko, V. The eutectics and solid solutions of paraffins. *Acta Physicochim. URSS* **1946**, *21*, 335−344.

(143) Smith, A. E. The structure of stable ordered phases in mixed paraffins and their relation to the structure of pure n-paraffins. *Acta Crystallogr.* **1957**, *10*, 802−803.

(144) Mazee, W. M. Paraffin, seine zusammensetzung und das phasenverhalten seiner wichtigsten komponenten, der normalen alkane. *Erdöl und Kohle* **1960**, *2*, 88−93.

(145) Lüth, H.; Nyburg, S. C.; Robinson, P. M.; Scott, H. G. Crystallographic and calorimetric phase studies of the n-eicosane, $C_{20}H_{42}$: n-docosane, $C_{22}H_{46}$ system. *Mol. Cryst. Liq. Cryst.* **1974**, *27*, 337−357.

(146) Asbach, V. G. I.; Killian, H. G.; Stacke, F. Isobaric binary state diagrams of *n*-alkanes. *Colloid Polym. Sci.* **1982**, *260*, 151−163.

(147) Hasnoui, N.; Dellacherie, J.; Schuffenecker, L.; Dirand, M.; Balesdent, D. Mise en évidence par diffraction des rayons-X à 20 °C de trois phases intermédiaires orthorhombiques dans le systèmes des deux n-alcanes: docosane (*n*-C_{22})-tétracosane (*n*-C_{24}). *J. Chim. Phys.* **1988**, *85* (2), 153−160.

(148) Sirota, E. B.; King, H. E.; Hughes, G. J.; Wan, W. K. Novel phase behavior in normal alkanes. *Phys. Rev. Lett.* **1992**, *68* **(**99), 492−495.

(149) Achour, Z.; Barbillon, P.; Bouroukba, M.; Dirand, M. Détermination du diagramme de phases du systèmes docosane (*n*-C_{22})-tétracosane (*n*-C_{24}): variation de l'enthalpie des mélanges en fonction de la température. *Thermochim. Acta* **1992**, *204*, 187−204.

(150) Achour, Z.; Bourdet, J. B.; Bouroukba, M.; Dirand, M. Evolution structurale en fonction de la température des mélanges binairs *n*-C_{22}, *n*-C_{24} compris entre 20 et 48% mol en C_{24}. Détermination du diagramme de phases du système docosane-tétracosane. *J. Chim. Phys.* **1992**, *89*, 707−725.

(151) Snyder, R. G.; Srivatsavoy, V. J. P.; Cates, D. A.; Strauss, H. L.; White, J. W.; Dorset, D. L. Hydrogen/deuterium isotope effects on microphase separation in unstable crystalline mixtures of binary *n*-alkanes. *J. Phys. Chem.* **1994**, *98*, 674−684.

(152) Achour, Z.; Bourdet, J. B.; Bouroukba, M.; Dirand, M. Binary systems of even-numbered *n*-alkane (C_{2p} H_{4p+2} - C_{2p+2} H_{4p+6}, $10 \leq P \leq 12$). *J. Chim. Phys.* **1993**, *90*, 325−332.

(153) Sabour, A.; Bourdet, J. B.; Bouroukba, M.; Dirand, M. Binary phase diagram of the alkane mixtures *n*-C_{23}: *n*-C_{24} : modifications. M. *Thermochim. Acta* **1995**, *249*, 269−283.

(154) Achour-Boudjema, Z.; Bourdet, J. B.; Petitjean, D.; Dirand, M. Structural behaviour of n-tetracosane and n-hexacosane mixtures. *J. Mol. Struct.* **1995**, *354*, 197−211.

(155) Jouti, B.; Bourdet, J. B.; Bouroukba, M.; Dirand, M. Structural behavior of n- tricosane and *n*-pentacosane mixtures at 20 °C. *Mol. Cryst. Liq. Cryst.* **1995**, *270*, 159−173.

(156) Jouti, B.; Provost, E.; Petitjean, D.; Bouroukba, M.; Dirand, M. Structural evolutions of heneicosane and n-tricosane molecular alloys at 293 K. *J. Mol. Struct.* **1995**, *356*, 191−199.

(157) Achour-Boudjema, Z.; Bouroukba, M.; Dirand, M. Binary phase diagram of the consecutive even-numbered *n*-alkanes n-tetracosane, *n*-$C_{24}H_{50}$: n-hexacosane, *n*-$C_{26}H_{54}$. *Thermochim. Acta* **1996**, *76*, 243−256.

(158) Dirand, M.; Achour, Z.; Jouti, B.; Sabour, A. Binary mixtures of *n*-alkanes. Phase diagram generalization: intermediate solid solutions, rotator phases. *Mol. Cryst. Liq. Cryst.* **1996**, *275*, 293−304.

(159) Dirand, M.; Achour-Boudjema, Z. Structural evolution versus temperature of the βo phase of the n-eicosane/n-docosane system: rotator transitions. *J. Mol. Struct.* **1996**, *375*, 243−248.

(160) Dirand, M.; Achour, Z. Généralisation des diagrammes de phases binaires de n-alcanes consécutifs. *Entropie* **1997**, 202−203.

(161) Robles, L.; Mondieg, D.; Haget, Y.; Cuevas-Diarte, M. A.; Alcobe, X. Non isomorphism and miscibility in the solid state: determination of the equilibrium phase diagram n- octadecane C_{18} + *n*-nonadecane C_{19}. *Mol. Cryst. Liq. Cryst.* **1996**, *281*, 279−290.

(162) Jouti, B.; Bourdet, J. B.; Bouroukba, M.; Dirand, M. Phase diagram of n-tricosane and *n*-pentacosane mixtures at 20 °C. *Mol. Cryst. Liq. Cryst.* **1996**, 275−283.
(163) Jouti, B.; Provost, E.; Petitjean, D.; Bouroukba, M.; Dirand, M. Phase diagram of n-heneicosane and n-tricosane alloys. *J. Mol. Struct.* **1996**, *382*, 49−56.
(164) Nouar, H.; Petitjean, D.; Bourdet, J. B.; Bouroukba, M.; Dirand, M. Diagram of the n-tricosane: n-tetracosane mixtures: corrections. *Thermochim. Acta* **1997**, *293*, 87−92.
(165) Nouar, H.; Bouroukba, M.; Petitjean, D.; Dirand, M. Binary phase diagram of the system: n-docosane-n-tricosane. *J. Mol. Struct.* **1998**, 197−204.
(166) Oonk, H. A. J.; Mondieg, D.; Haget, Y.; Cuevas-Diarte, M. A. Perfect families of mixed crystals: the rotator I *n*-alkane case. *J. Chem. Phys.* **1998**, *108*, 715−722.
(167) Holder, G. A.; Winkler, J. Wax crystallization from distillate fuels. Part I. cloud and pour phenomena exhibited by solutions of binary n-paraffin mixtures. *J. Inst. Pet.* **1965**, *51*, 228−234.
(168) Denicolo, P.; Craievich, A. F.; Doucet, J. X-ray diffraction and calorimetric phase study of a binary paraffin: $C_{23}H_{48}$, $C_{24}H_{50}$. *J. Chem. Phys.* **1984**, *12*, 6200−6203.
(169) G. J.; Masic, J. Order in the rotator phase of *n*-alkanes. *J. Chem. Phys.* **1985**, *89*, 1036−1042.
(170) Maroncelli, M.; Strauss, H. L.; Snyder, R. G. Structure of the alkane binary solid n-C_{19}/*n*-C_{21} by infrared spectroscopy and calorimetry. *J. Phys. Chem.* **1985**, 5260−5267.
(171) Yamamoto, T.; Nozaki, K. Evidence of active chain diffusion in the rotator phase of *n*-alkanes: solid-state mixing of $C_{21}H_{44}$ and $C_{23}H_{48}$. *Polymer* **1994**, *36*, 3340−3342.
(172) Metivaud, V.; Rajabalee, F.; Cuevas-Diarte; Calvet, T.; Mondieg, D.; Haget, Y. The "low temperature" structural behaviour of the binary system octadecane ($C_{18}H_{38}$) + nonadecane ($C_{19}H_{40}$). Experimental equilibrium phase diagram. *An. Quim. Int.* **1998**, 396−402.
(173) Rajabalee, F.; Metivaud, V.; Mondieg, D.; Haget, Y.; Oonk, H. A. J. Structural and energetic behavior of mixed samples in the hecacosane ($C_{26}H_{54}$) + octacosane (*n*-C_{25}+H_{58}) system: solid−solid and solid−liquid equilibria. *Helv. Chim. Acta* **1999**, *82*, 1916−1929.
(174) Rajabalee, F.; Metivaud, V.; Mondieg, D.; Haget, Y.; Oonk, H. A. J. Thermodynamic analysis of solid−solid and solid−liquid equilibria in binary systems composed of *n*-alkanes: application to the system tricosane ($C_{23}H_{48}$) + pentacosane (C_{25}+H_{52}). *Chem. Mater.* **1999**, *11*, 2788−2795.
(175) Rajabalee, F.; Metivaud, V.; Mondieg, D.; Haget, Y. New insight on the crystalline forms in binary systems of *n*-alkanes: characterisation of the solid phases in the phase diagram tricosane + pentacosane. *J. Mater. Res.* **1999**, *14*, 2644−2654.
(176) Metivaud, V.; Rajabalee, F.; Mondieg, D.; Haget, Y.; Cuevas-Diarte, M. A. Solid−solid and solid−liquid equilibria in the heneicosane-docosane binary system. *Chem. Mater.* **1999**, *11*, 117−122.
(177) Haget, Y. Molecular mixed crystals: another real of alloys. *J. Chim. Phys.* **1993**, *90*, 313−324.
(178) Asbach, V. G. I.; Geiger, K.; Wilke, W. X-ray investigations of binary solid solutions of *n*-alkanes as model systems for extended chain crystals of polyethylene. *Colloid Polym. Sci.* **1979**, *287*, 1049−1069.
(179) Matheson, R. R.; Smith, P. A simple thermodynamic analysis of solid-solution formation in binary systems of homologous extended-chain alkanes. *Polymer* **1985**, *26*, 288−295.
(180) Dorset, D. L. Electron diffraction structure analysis of expitaxially crystallized n-paraffins. *Macromolecules* **1986**, *24*, 79−87.
(181) Dorset, D. L. Chain length and the cosolubility of n-paraffins in the solid state. *Macromolecules* **1990**, *23*, 623−633.
(182) Hammami, A.; Mehrotra, A. K. Liquid−solid-solid thermal behaviour of *n*-$C_{44}H_{90}$ + *n*-$C_{50}H_{102}$ and *n*-$C_{25}H_{52}$ + *n*-$C_{28}H_{58}$ paraffinic binary mixtures. *Fluid Phase Equilib.* **1995**, *111*, 253−272.
(183) Hammami, A.; Mehrotra, A. K. Non isothermal crystallization kinetics of binary mixtures of *n*-alkanes: ideal eutectic and isomorphous systems. *Fuel* **1996**, *75*, 500−508.
(184) Palatnik, L. S.; Landau, A. I. *Phase equilibria in multicomposent system*; Holt, Rhinart and Wiston: New York, 1964.
(185) Yamamoto, T.; Aoki, H.; Miyaji, S.; Nozaki, K. In situ optical observation of the chain diffusion in an *n*-alkane crystal: temperature dependence of the chain diffusivity. *Polymer* **1996**, *38*, 2643−2647.
(186) Achour-Boudjema, Z.; Bouroukba, M.; Balesdent, D.; Provost, E.; Dirand, M. Variation enthalpy of the system n-tetracosane-n-hexacosane as functions of temperature and composition. *J. Therm. Anal.* **1997**, *50*, 685−704.
(187) Achour, Z.; Sabour, A.; Dirand, M.; Hoch, M. Thermodynamic properties of the *n*-alkanes $C_{19}H_{40}$ to $C_{26}H_{54}$ and their binary phase diagrams. *J. Therm. Anal.* **1998**, *51*, 477−488.
(188) Jouti, B. M.; Bouroukba, M.; Balesdent, D.; Dirand, M. Enthalpy variation of the nine solid phases of the binary molecular alloys (n-tricosane: *n*-pentacosane) VS. temperatures. *J. Therm. Anal.* **1998**, *54*, 785−802.
(189) Srivastava, S. P.; Butz, T.; Oschmann, H. J.; Rahimian, I. Study of the temperature and enthalpy of thermally induced phase-transitions in *n*-alkanes, their mixtures and Fischer−Tropsch waxes. *Pet. Sci. Technol.* **2000**, *18*, 493−518.
(190) Dorset, D. L. Crystal structure of an n-paraffin binary eutectic solid. An electron diffraction determination. *J. Phys. Chem. B* **1997**, *101*, 4870−4874.
(191) Espeau, P.; Oonk, H.; Van der Linde, P.; Alcobe, X.; Haget, Y. Experimental binary phase diagram of pentadecane-heneïcosane. Thermodynamic analysis. *J. Chim. Phys.* **1995**, *92*, 747−757.
(192) Garkushin, I. K.; Agafonov, I. A.; Miftakhov, T. T.; Snorou, S. G. Study of the *n*-$C_{19}H_{40}$−*n*-$C_{24}H_{50}$ binary system. *Russ. J. Gen. Chem.* **1996**, *66*, 557−558.
(193) Nouar, H.; Bouroukba, M.; Petitjean, D.; Dirand, M. Ternary phase diagram n-docosane: n-tricosane: n-tetracosane molecular alloys at 293 K. *Mol. Cryst. Liq. Cryst.* **1998**, *309*, 273−282.
(194) Basson, I.; Reynhardt, E. C. Identification of defect chain motions in the low temperature orthorhombic phase of binary mixtures of *n*-alkanes by means of nuclear magnetic resonance spin lactice relaxation time measurements. *J. Chem. Phys.* **1991**, 95−107.
(195) Clavell-Grunbaum, D.; Strauss, H. L.; Snyder, R. G. Structure of model waxes: conformational disorder and chain packing in crystalline multicomponent *n*-alkane socio solutions. *J. Phys. Chem. B* **1997**, *101*, 335−343.
(196) Snyder, R. G.; Goh, M. G.; Srivatsavoy, V. J. P.; Strauss, H. L.; Dorset, D. L. Measurement of the growth kinetics of microdomains in binary *n*-alkanes solid solutions by infrared spectroscopy. *J. Phys. Chem.* **1952**, *96*, 10008−10019.
(197) Coutinho, J. A. P.; Andersen, S. I.; Stenby, E. H. Evaluation of activity coefficient models of alkane solid/liquid equilibria. *Fluid Phase Equilib.* **1995**, *103*, 23−35.
(198) Provost, E.; Chevallier, V.; Bouroukba, M.; Dirand, M.; Ruffier-Meray, V.; Behar, E. V. Experimental determination and representation of binary and ternary diagrams of n-hexacosane, *n*-octacosane and *n*-heptane. *Rev. Inst. Fr. Pét.* **1998**, *53*, 27−33.
(199) Provost, E.; Chevallier, V.; Bouroukba, M.; Petitjean, D.; Dirand, M. Solubility of some n- alkanes (C_{23}, C_{25}, C_{26}, C_{28}) in heptane, methylcyclohexane, and toluene. *J. Chem. Eng. Data* **1998**, *43*, 745−749.
(200) Ghogomu, P. M.; Dellacherie, J.; Balesdent, D. Solubility of normal paraffin hydrocarbons (C_{20} to C_{24}) and some of their binary mixtures (C_{22} + C_{24}) and (C_{23} + C_{24}) in enthylbenzene. *J. Chem. Thermodyn.* **1989**, *21*, 925−934.
(201) Ghogomu, P. M.; Dellacherie, J.; Balesdent, D. Impurity effects on the solubility of high molecular weight normal alkanes in ethylbenzene. *Thermochim. Acta* **1990**, *157*, 241−257.
(202) Ghogomu, P. M.; Schuffenecker, L.; Dellacherie, J.; Dirand, M.; Balesdent, D. Dissolution of some normal alkanes in ethylbenzene: deduction of the enthalpy of mixing two n-alkanes in the solid state. *Thermochim. Acta* **1997**, *294*, 147−155.
(203) Ghogomu, P. M.; Bouroukba, M.; Dellacherie, J.; Balesdent, D.; Dirand, M. Excess thermodynamic properties of some binary solutions of ethylbenzene + *n*-alkanes. *Thermochim. Acta* **1997**, *302*, 151−158.
(204) Ghogomu, P. M.; Bouroukba, M.; Dellacherie, J.; Balesdent, D.; Dirand, M. Calorimetric measurements of molar excess enthalpies of dilute solutions of ethylbenzene higher n-alkanes. *Thermochim. Acta* **1997**, *302*, 159−164.
(205) Ghogomu, P. M.; Bouroukba, M.; Dellacherie, J.; Balesdent, D.; Dirand, M. On the ideality of liquid mixtures of long-chain *n*-alkanes. *Thermochim. Acta* **1997**, *306*, 69−71.
(206) Chang, S. S.; Maurey, J. R.; Pummer, W. J. Solubilities of two *n*-alkanes in various solvents. *J. Chem. Eng. Data* **1983**, *28*, 187−189.
(207) Arenosa, R. L.; Menduina, C.; Diaz Pena, M. Thermodynamics of concentrated electrolyte mixtures. 5. A review of the thermodynamic properties of aqueous calcium chloride in the temperature range. *J. Chem. Eng. Data* **1985**, *30*, 120−128.
(208) Domanska, U.; Hofman, T.; Rolinska, J. Solubility and vapor pressures in saturated solutions of high-molecular-weight hydrocarbons. *Fluid Phase Equilib.* **1987**, *32*, 273−293.
(209) Domanska, U. Solubilities of n-paraffin hydrocarbons in binary solvent mixtures. *Fluid Phase Equilib.* **1987**, *35*, 217−236.
(210) Domanska, U.; Rolinska, J. Correlation of the solubility of even-numbered paraffins n$C_{20}H_{42}$, n$C_{24}H_{50}$, n$C_{26}H_{54}$, n$C_{28}H_{58}$ in pure hydrocarbons. *Fluid Phase Equilib.* **1989**, *45*, 25−38.
(211) Madsen, H. E. L.; Boistelle, R. Solubility of long-chain n-paraffins in pentane and heptane. *J. Cryst. Growth* **1976**, *Paper 5/1466*, 1078−1081.
(212) Flöter, E.; Hollanders, B.; de Loos, T. W.; de Swaan Arons, J. The ternary system (n-heptane + docosane + tetracosane): the solubility of mixtures of docosane and tetracosane in heptane and data on solid−liquid and solid−solid equilibria in the binary subsystem (docosane + teracosane). *J. Chem. Eng. Data* **1997**, *42*, 562−565.

(213) Buchowski, H.; Ksiazczak, A.; Pietrzyk, S. Solvent activity along a saturation line and solubility of hydrogen bonding solids. *J. Phys. Chem.* **1980**, *84*, 975−979.
(214) Mahmoud, R.; Solimando, R.; Rogalski, M. Solid−liquid equilibria of systems containing pyrene and long chain normal-alkanes. *Fluid Phase Equilib.* **1998**, *148*, 139−146.
(215) Mahmoud; Solimando, R.; Bouroukba, M.; Rogalski, M. Solid−liquid equilibrium and excess enthalpy measurements in binary {dibenzofurum or xanthen + normal long chain alkane} systems. *J. Chem. Eng. Data* **2000**, *45*, 433−436.
(216) Ruelle, P.; Kesselring. Application of the mobile order thermodynamics to predict the solubility of solid hydrocarbons in pure solvents and non polar binary solvent systems. *J. Mol. Liq.* **1995**, *67*, 81−94.
(217) Haulait-Pirson, M. C.; Huys, G.; Vanstraelen, E. New predictive equation for the solubility of solid n-alkanes in organic solvents. *Ind. Eng. Chem. Res.* **1987**, *26*, 447−452.
(218) Walsh, R.; Mortimer, P. V. New way to test product quality. *Hydrocarbon Process.* **1971**, *50* (9), 153−158.
(219) Reddy, S. R. A thermodynamic model for predicting n-paraffin crystallization in diesel fuels. *Fuel* **1986**, *65*, 1647−1658.
(220) Won, K. W. Thermodynamics for solid-solution-liquid-vapor-equilibria: was phase formation from heavy hydrocarbon mixtures. *Fluid Phase Equilib.* **1986**, *30*, 265−279.
(221) Hansen, J. H.; Fredenslund, A.; Pedersen, K. S.; Roningsen, H. P. A thermodynamic model for predicting wax formation in crude oils. *AIChE J.* **1988**, *34*, 1937−1942.
(222) Pedersen, K. S.; Skovborg, P.; Ronningsen, H. P. Wax precipitation from north sea crude oils. 2. Solid-Phase content as function of temperature determined by pulsed NMR. *Energy Fuels* **1991**, 5−24.
(223) Ungerer, P.; Faissat, B.; Leibovici, C.; Zhou, H.; Behar, E. High pressure-high temperature reservoir fluids: investigation of synthetic condensate gases containing a solid hydrocarbon. *Fluid Phase Equilib.* **1995**, *111*, 287−311.
(224) Coutinho, J. A. P.; Ruffier-Meray, V. Formation of paraffinic waxes in undercooled solutions: experimental determinations and thermodynamical modelling. *Ind. Eng. Chem. Res.* **1997**, *36*, 4977−4983.
(225) Lira-Galeana, C.; Firoozabadi, A.; Prausnitz, J. M. Thermodynamics of wax precipitation in petroleum mixtures. *AIChE J.* **1996**, *42*, 239−247.
(226) Srivastava, S. P.; Saxena, A. K.; Tandon, R. S.; Shekher, V. Measurement and prediction of solubility of petroleum waxes in organic solvents. *Fuel* **1997**, *76*, 625−630.
(227) Pauly, J.; Dauphin, C.; Daridon, J. L. Liquid−solid equilibria in a Decane + multi- paraffins system. *Fluid Phase Equilib.* **1998**, *149*, 191−207.
(228) Dauphin, C.; Daridon, J. L.; Coutinho, J. A. P.; Baylere, J.; Potin-Gautier, M. Wax content measurements in partially frozen parffinic systems. *Fluid Phase Equilib.* **1999**, *161*, 135−151.
(229) Kreger, D. R. Configuration and packing of chain molecules of native starch in the β-modification. *Nature* **1947**, *160*, 369−374.
(230) Kreger, D. R. Configuration and packing of the chain molecules of nature starch as derived from X-ray diffraction of part of a single starch grain. *Biochim. Biophys. Acta* **1951**, *6*, 406−425.
(231) Kreger, D. R. In *Investigations in the biological field, part H of selected topics in X-ray crystallography*; Monographs on Theoretical and Applied Physics; Bouman, J., Ed.; North-Holland Publishing Company: Amsterdam, 1951; pp 299−367.
(232) Basson, I.; Reynhardt, E. C. The structure and melting of paraffinic fischer-tropsch waxes. *Chem. Phys. Lett.* **1992**, *198*, 367−372.
(233) Le Roux, J. H.; Loubser, N. H. Nuclear magnetic resonance investigation of the mobile phase in paraffinic Fischer−Tropsch waxes. *South Afr. J. Sci.* **1980**, *76*, 157−161.
(234) Le Roux, J. H. Fischer−Tropsch waxes V: study of branching and its effect on crystallinity using an improved infrared method. *J. Appl. Chem.* **1970**, *20*, 203−207.
(235) Le Roux, J. H. Fischer−Tropsch waxes IV: qualitative and quantitative investigation of chain branching. *J. Appl. Chem.* **1969**, *19*, 230−234.
(236) Le Roux, J. H.; Fischer−Tropsch waxes III: indications of molecular order in molten wax. *J. Appl. Chem.* **1969**, *19*, 209−212.
(237) Dorset, D. L. The crystal structure of waxes. *Acta Crystallogr.* **1995**, *B51*, 1021−1028.
(238) Dorset, D. L. Crystallography of waxes an electron diffraction study of refined and natural products. *J. Phys. D: Appl. Phys.* **1997**, *30*, 451−457.
(239) Dorset, D. L. Development of lamellar structures in natural waxes-an electron diffraction investigation. *J. Phys. D: Appl. Phys.* **1999**, *32*, 1276−1280.
(240) Dorset, D. L. Chain length distribution and the lamellar crystal structure of a paraffin wax. *J. Phys. Chem. B* **2000**, *104*, 8346−8350.
(241) McCrorie, J. W. Some physical properties of dental modelling waxes and of their main constituents. *J. Oral Rehabil.* **1974**, *1*, 29−45.
(242) Retief, J. J.; Engel, D. W.; Boonstra, E. G. Lattice parameters of solid solutions of long- chain *n*-alkanes. *J. Appl. Crystallogr.* **1985**, *18*, 156−158.
(243) Dirand, M.; Chevallier, V.; Provost, E.; Bouroukba, M.; Petitjean, D. Multicomponent paraffin waxes and petroleum solid deposits: structural and thermodynamic state. *Fuel* **1998**, *77*, 1253−1260.
(244) Chevallier, V.; Petitjean, D.; Bouroukba, M.; Dirand, M.; Emeraux. J. P.; Ruffier-Meray, V.; Daridon, J. L. Etudes thermodynamiques et structurales de mélanges n-aires de n-alcanes et de leur cristallisation dans le tétradécane. *Entropie* **2000**, *224/225*, 38−41.
(245) Chevallier, V.; Bouroukba, M.; Petitjean, D.; Dirand, M.; Pauly, J.; Daridon, J. L.; Ruffier-Meray, V. Crystallization of a multi-paraffinic wax in normal tetradecane. *Fuel* **2000**, *79*, 1743−1750.
(246) Chevallier, V.; Briard, A. J.; Petitjean, D.; Hubert, N.; Bouroukba, M.; Dirand, M. Influence of the distribution general shape of *n*-alkane molar concentrations on the structural state of multi-alkane mixtures. *Mol. Cryst. Liq. Cryst.* **2001**, *350*, 273−291.
(247) Bosselet, F.; Letoffe, J. M.; Claudy, P.; Esson, S.; Valentin, P. Etude du comportement thermique des n-alcanes dans des milieux hydrocarbonés complexes par analyse calorimétrique différentielle. III. Etude en programmation discontinue de température. *Thermochim. Acta* **1983**, *70*, 35−47.
(248) Craig, S. R.; Hastie, G. P.; Roberts, K. J.; Roberts, K. J.; Gerson, A. R.; Sherwood, J. N.; Tack, R. D. Investigation into the structures of binary-, tertiary- and quinternary- mixtures of *n*-alkanes and real diesel waxes using high-resolution synchrotron X-ray powder diffraction. *J. Mater. Chem.* **1998**, *4*, 859.
(249) Hahn, T. *International Tables for Crystallography. The International Union of Crystallography*; D. Reidel Publishing Company: Dordrecht, Holland/Boston, 1983.
(250) American National Standard, Standard test method for purity of hydrocarbons from freezing points, A.N.S.I./A.S.T.M. D 1016-74; reapproved 1979; Vol. 974, pp 481−497.langmuir@fhi-berlin.mpg.de
(251) Domalski, E. S.; Hearing, E. D. Heat capacities and entropies of organic compounds in the condensed phase. Volume II. *J. Phys. Chem. Ref. Data* **1990**, *19*, 881−1009.
(252) Byrd, R. H.; Nocedal, J.; Zhu, C. *SIAM J. Sci. Comput.* **1995**, *16*, 1190−1208.
(253) Zhu, C.; Byrd, R. H.; Lu, P.; Nocedal, J. Tech. Report, NAM-11; EECS Department, Northwestern University: 1994.
(254) Flechter, R. *Practical methods of optimisation*; Academic Press: London, 1991.
(255) Bonsor, D. H.; Bloor, D. Phase transition of *n*-alkanes systems. Part II: melting and solid-state transition of binary mixture. *J. Mater. Sci.* **1977**, *12*, 1559−1564.
(256) Dorset, D. L. Crystal structure of lamellar paraffin eutectics. *Macromolecules* **1986**, *19*, 2965−2973.
(257) Dorset, D. L. Crystal structure of n-paraffin solid solutions: an electron diffraction study. *Macromolecules* **1988**, *18*, 2158−2163.
(258) Nouar, H.; Petitjean, D.; Bouroukba, M.; Dirand, M. Isothermal sections of ternary mixtures: n-docosane + n-tricosane + n-tetracosane. *Mol. Cryst. Liq. Cryst.* **1999**, *326*, 381−394.
(259) Wyckoff, H. W. X-ray and related studies of quenched, drawn and annealed polypropylene. *Polymer* **1962**, *62*, 83−114.

Received for review January 17, 2001. Accepted October 16, 2001. We are indebted to Centre National de la Recherche Scientifique, Institut Français du Pétrole, Gaz de France, and TOTAL-FINA-ELF for their financial support under the A.R.C. convention (petroleum fluid thermodynamics) of the ARTEP program.

JE0100084